1-1-2005

The role of transverse faults in Great Basin extension: Transfer faults or N-S extension?

Tandis S Bidgoli
University of Nevada, Las Vegas

THE ROLE OF TRANSVERSE FAULTS IN GREAT BASIN EXTENSION: TRANSFER FAULTS OR N-S EXTENSION?

by

Tandis S. Bidgoli

Bachelor of Science
San Francisco State University
2002

A thesis submitted in partial fulfillment
of the requirements for

Master of Science Degree in Geoscience
Department of Geoscience
College of Sciences

Graduate College
University of Nevada, Las Vegas
August 2005

UNLV
UNIVERSITY OF NEVADA LAS VEGAS

Thesis Approval

The Graduate College
University of Nevada, Las Vegas

June 24, 20 05

The Thesis prepared by

Tandis S. Bidgoli

Entitled

The Role of Transverse Faults in Great Basin Extension: Transfer Faults or N-S Extension?

is approved in partial fulfillment of the requirements for the degree of

Master of Science in Geoscience

Wanda J. Taylor
Examination Committee Chair

Dean of the Graduate College

Examination Committee Member

Examination Committee Member

Graduate College Faculty Representative

1017-53

ABSTRACT

The Role of Transverse Faults in Great Basin Extension: Transfer Faults or N-S Extension?

by

Tandis S. Bidgoli

Dr. Wanda J. Taylor, Examination Committee Chair
Professor of Geology
University of Nevada, Las Vegas

New geologic map data (1:24,000 scale), geometric analyses, and kinematic analyses in the vicinity of the Crescent Spring fault zone (CSFZ), an E-W-striking fault zone in eastern Nevada, allow the recognition of four distinct extensional episodes. The episodes are pre-volcanic (pre-27 Ma), syn-volcanic (~27-18 Ma), Miocene (?) post-volcanic, and Miocene (?) - Pliocene or Quaternary post-volcanic extension. This extensional pattern, which is consistent with other fault studies along the broadly defined Timpahute lineament, has several important aspects. (1) Transverse faults of the CSFZ are normal faults that accommodated a distinct N-S extensional event. (2) The strain field within this part of the Great Basin reoriented at least twice during the Tertiary, from E-W extension to N-S extension and back to E-W extension. (3) The dominantly south-dipping, transverse normal faults moved crustal material southward, which may explain N-S shortening during large-magnitude E-W extension at the latitude of Las Vegas. (4) The eastern part of the Timpahute lineament is a regional transfer fault system that accommodated changes in the magnitude, timing, location, and direction of extension.

TABLE OF CONTENTS

LIST OF FIGURES

ACKNOWLEDGEMENTS

This research was supported by grants from the Geological Society of America (GSA), the American Association of Petroleum Geologists (AAPG), and Nevada Earthquake Safety Council; grants from the University of Nevada, Las Vegas, Graduate and Professional Student Association (GPSA); Bernada E. French Scholarships; and funding from the University of Nevada- Las Vegas, Graduate College.

Additionally, I would like to thank my advisor, Dr. Wanda Taylor, for her expertise, mentorship, and patience through every stage of my graduate school experience. I have learned so much from you. Also, I would like to thank all of my committee members, Dr. Michael Wells, Dr. Andrew Hanson, and Dr. Abiodun Elegbede, for their time, help, support, and knowledge. Finally, I would like to thank my family and, most importantly, Chad for love and support through it all.

CHAPTER 1

INTRODUCTION

Since the early 1970's, with the recognition of shallowly dipping normal faults or detachments, studies of extended terranes commonly focused on the two-dimensional, across-strike geometry and kinematics of extension (e.g., Anderson, 1971; Proffett, 1977; Davis, 1980; Wernicke, 1981; Miller et al., 1983; Wernicke and Axen, 1988; Buck 1988; Rey et al., 2001). Although these studies greatly improved our understanding of rift architecture, long-lived continental rifts, such as the Basin and Range province, contain spatial and temporal heterogeneities that make two-dimensional extensional models incomplete. Understanding rifts is inherently a three-dimensional problem that requires the examination of transverse faults, faults that form approximately perpendicular to the structural grain of a region. These faults are documented in most extended terranes, including the Basin and Range province; however, the geometry, kinematics, timing, and relationship of many individual transverse faults to regional extension remains unresolved.

Transverse faults within the Basin and Range province are commonly part of major east-west-trending lineaments or zones of aligned geologic features (e.g., the Timpahute, Pritchards Station, and Warm Springs lineaments) (Fig. 1a). These lineaments are defined by topographic, aeromagnetic and gravitational anomalies, and coincide with the

locations of transverse faults, volcanic centers and mining districts (Fig. 1a) (Ekren et al., 1976; Rowley et al., 1978; Rowley, 1998). The kinematic and structural role of these east-west-trending lineaments is questionable and has been modeled or interpreted in several different ways. Models include: (1) major crustal structures that penetrate to depths near or greater than the brittle-ductile transition zone (e.g., Ekren et al., 1976; Rowley et al., 1978; Rowley, 1998); (2) transfer faults that are physical and kinematic links between normal fault systems (Fig. 2a) (e.g., Duebendorfer and Black, 1992; Faulds and Varga, 1998); (3) accommodation zones that lack a fault and transfer strain between overlapping systems of normal faults (Fig. 2b) (e.g., Faulds et al., 1990; Faulds and Varga, 1998); (4) barrier faults that terminate propagating normal faults (e.g., Bartley and Taylor, 1992; Overtoom and Bartley, 1996; Williams, 2000); and (5) normal faults that are younger or older than the faults that end at them, reflecting changes in regional stresses (Fig. 2c) (e.g., Overtoom and Bartley, 1996; Taylor and Switzer, 2001). Here, I examine the Crescent Spring fault zone (CSFZ), one of several transverse fault zones that make up the broadly defined Timpahute lineament (Figs. 1a and 3) to test the hypothesis that the CSFZ accommodated north-south extension.

This thesis presents the results of new detailed geologic mapping (1:24,000 scale), geometric analyses and kinematic analyses of CSFZ and other faults in the Mount Irish and Timpahute ranges, eastern Nevada. These data and analyses are used to address several questions. (1) What is the structural role of the CSFZ and how does it interact with other extensional faults? (2) Does the CSFZ correlate to other transverse faults documented along the Timpahute lineament? (3) What are the roles of the CSFZ and Timpahute lineament in regional extension?

Based on cross-cutting relations, four Cenozoic extensional episodes are evident: prevolcanic (pre-27 Ma), synvolcanic (~27-18 Ma), postvolcanic Miocene (?), and postvolcanic Miocene (?)-Pliocene or Quaternary extension. This four-phase extensional pattern is consistent with other fault studies along the Timpahute lineament (e.g., Taylor and Switzer 2001; Taylor, 2002).

The timing, orientations, and kinematics of faulting, combined, imply that the stress field in the Great Basin reoriented at least twice during the Cenozoic, from east-west extension to north-south extension and back to east-west extension. Importantly, faults of the CSFZ are transverse normal faults that accommodated this distinct north-south extensional event. North-south-directed extension during the Miocene is problematic because (1) most recognized extension in the Basin and Range is oriented approximately E-W and (2) present models for the central Basin and Range, near the latitude of Las Vegas, propose a component of north-south shortening during large-magnitude E-W extension (Fig. 1b) (e.g., Wernicke et al., 1988; Cakir and Aydin, 1990; Anderson and Barnard, 1993; Anderson et al., 1994).

In this thesis, I present a new model for extension in the region. I suggest that N-S-directed extension along dominantly south-dipping transverse faults drove crustal material into the central Basin and Range and produced apparent constriction south of the Timpahute lineament. The transverse faults that accommodated N-S extension are concentrated near the top of a topographic and potential energy step that developed as a result of spatial and temporal heterogeneities in extension and magmatism across the Timpahute lineament. In addition, available geologic data from extensional systems north and south of the lineament (e.g., Bartley et al., 1988; Axen et al., 1990; Guth, 1990;

Taylor and Bartley, 1992; Axen et al., 1993) suggest that the Timpahute lineament persisted through time as a major transverse or transfer zone that accommodated changes in the magnitude, timing, location, and direction of extension between the northern and central Basin and Range (Fig. 1b).

This study is significant for three main reasons. (1) This study documents N-S-directed extension and regional shifts in the stress field during Miocene to Quaternary time. N-S-directed extension during this time interval conflicts with current extensional models for the central Basin and Range, which propose a component of N-S shortening during large-magnitude E-W extension (Fig. 1b) (e.g., Wernicke et al., 1988; Cakir and Aydin, 1990; Anderson and Barnard, 1993; Anderson et al., 1994). A new extensional model, presented here, may resolve this paradoxical relationship. (2) This study demonstrates that extension is heterogeneous in magnitude, timing, location and direction; therefore, holistic approaches to modeling extension must examine the geometry, kinematics, and role of transverse structures in extended terranes. (3) Most of the well-studied transverse structures and zones (e.g., East African rifts) are in extended regions that lack some of the complications associated with long-lived, tectonically complex rifts such as the Basin and Range province. This study demonstrates some aspects of the wide range of kinematic and structural roles of transverse structures in regional extension.

In addition to a structural and tectonic significance, this study may have broad economic implications. Transverse faults can influence the accumulation and trapping of hydrocarbons, the development of mineral deposits, and the distribution and flow of groundwater (e.g., Morley et al., 1990; Gawthorpe and Hurst, 1993; Grabb, 1994; Faulds

and Varga, 1998; Rowley, 1998). Transverse faults influence the accumulation and trapping of hydrocarbons by (1) forming structural traps; (2) controlling patterns of synextensional sedimentation, which may impact the location and extent of source and reservoir rocks; and (3) controlling the migration of fluids (Morley et al., 1990; Gawthorpe and Hurst, 1993; Grabb, 1994). Transverse faults are also zones of groundwater recharge and discharge, and commonly serve to direct or divert groundwater (Gawthorpe and Hurst, 1993, Faulds and Varga, 1998). Similarly, transverse faults act as natural conduits for mineralizing solutions (Rowley, 1998). Increased understanding of transverse faults, through this case study of the CSFZ, may aid in exploring for such resources.

CHAPTER 2

REGIONAL GEOLOGY

Structural and Tectonic Background

In the eastern Great Basin extensional structures overprint contractional structures. Mesozoic contractional structures form two north-trending belts in the central and eastern Great Basin: the central Nevada thrust belt and the Sevier orogenic belt (Fig. 1c). The Mount Irish and Timpahute ranges lie within the dominantly east-vergent central Nevada thrust belt (CNTB), the age of which is bracketed loosely between the Permian and Cretaceous (Fig. 1c) (Taylor et al., 1993, 2000). The CNTB comprises a series of north-striking thrusts with steeply-dipping ramps and associated upper plate and footwall folds (Taylor et al., 1993, 2000). CNTB structures in these ranges are part of the Garden Valley thrust system and include the Mount Irish and Monte Mountain thrusts (Taylor et al., 1993, 2000). The east-vergent folds and thrusts of the Jurassic to Eocene Sevier orogenic belt lie ~200 km east of the study area (Fig. 1c) (Allmendinger, 1992). Extensional overprinting of contractional structures began in the late Mesozoic to Eocene and continued episodically through the Quaternary.

In the northern Basin and Range, space and time patterns of volcanic centers indicate that volcanism, active between the Eocene and Miocene times, was concentrated along east-west-trending belts that become progressively younger towards the south (Fig. 1d)

(e.g., Best and Christiansen, 1991; Armstrong and Ward, 1991; Best et al., 1993). Volcanism occurred in the region north of the Mount Irish and Timpahute ranges from 31-22 Ma, forming the Central Nevada and Indian Peak caldera complexes (Fig. 3) (Best et al., 1993; Overtoom and Bartley, 1996). By the earliest Miocene, the locus of volcanism had migrated south, forming the Caliente and Kane Springs Wash caldera complexes, which were active from ~23-11 Ma (Fig. 3) (Best et al., 1993; Rowley et al., 1995; Scott et al., 1995).

Eocene to Miocene volcanism in the northern Basin and Range resulted in the eruption of regionally extensive ash-flow tuffs. These ash-flow tuffs provide timing constraints on extension; therefore, extensional faults can be categorized according to their relation to volcanism in a particular region (i.e., prevolcanic, synvolcanic, or postvolcanic). However, because volcanism swept southward through the region, extension that is synvolcanic in the north may be prevolcanic to the south of the volcanic belt.

Prevolcanic extension in the northern Basin and Range occurred during two time intervals: the late Mesozoic to Eocene and the late Eocene to Oligocene. During the earlier of these two intervals, extensional events affected parts of northeastern Nevada, northwestern Utah and southeastern Idaho (e.g., Pequop, Raft River, and Black Pine Mountains) (e.g., Wells et al., 1990, 1998; Wells, 1992; Camilleri, 1996; Nutt, 1996). These extensional fault systems are thought to have formed in response to gravitational collapse of the overthickened Sevier orogen. Extension during the late Eocene to Oligocene time interval occurred in two ~north-trending belts in the northern Basin and Range (Fig. 1e) (Axen et al., 1993). The eastern belt is defined by the east-directed

Snake-Stampede detachment system, which comprises the Snake Range decollement, Stampede detachment and Seaman breakaway fault (Figs. 1e and 3) (Miller et al., 1983; Taylor and Bartley, 1992; Axen et al., 1993). Prevolcanic normal faults, interpreted to be minor footwall faults to this system, were documented east of the study area in the Hiko Range (Fig. 3) (Taylor and Switzer, 2001). The western belt, however, is defined mostly by stratigraphic evidence of extensional basin development and scattered prevolcanic faults (e.g., the Badger Mountain fault; Jayko, 1990) (Axen et al., 1993).

Synvolcanic extension occurred along both north-south-striking (e.g., North Pahroc and Highland ranges) and east-west-striking (e.g., Golden Gate and Hiko ranges) normal faults (Fig. 3) (Taylor et al., 1989; Taylor, 1990; Overtoom and Bartley, 1996; Taylor and Switzer, 2001). Synvolcanic, north-south-striking faults (e.g., Highland Peak detachment) that accommodated east-west-directed extension are a typical feature of the Basin and Range; however, east-west-striking normal faults that accommodated north-south-directed extension are less common (Fig. 3). Two proposed models, the caldera collapse model (Best and Christiansen, 1991) and the tectonomagmatic rift model (Bartley, 1989; Overtoom and Bartley, 1996), explain the temporal and genetic link between crustal extension, volcanism, and the formation of east-west-striking normal faults (Figs. 4 and 5). In the caldera collapse model, synvolcanic east-west-striking faults are confined to the area near a caldera and are concentric and/ or radial to it (Fig. 4). In contrast, the tectonomagmatic rifting model suggests that east-west-striking normal faults develop in response to a shift in the regional stress field that is associated with thermal uplift related to the southward migration of mid-Tertiary volcanism and related plutonism (Fig. 5) (Bartley, 1989; Overtoom and Bartley, 1996). The thermally driven uplift and

weakening of the crust occurs as the east-west-trending belt of volcanism migrates into and occupies a region (Fig. 5) (Bartley, 1989; Overtoom and Bartley, 1996).

Postvolcanic, east-west-directed extension during the Miocene is generally attributed to stresses generated at or near the plate margin (e.g., transtension models, back-arc extension models, etc.) (Severinghaus and Atwater, 1990; Bohannon and Parsons, 1995; Dokka and Ross, 1995). Less understood is the phase of postvolcanic north-south-directed extension that occurred in parts of the Great Basin. For example, Taylor and Switzer (2001) recognized postvolcanic, east-west-striking normal- and oblique-slip faults in the central Hiko Range (Fig. 3). Similarly, Taylor (2002) identified postvolcanic, east-west-striking normal- and oblique-slip faults in the western Timpahute Range (Fig. 3). The relationship of these individual transverse faults to the Miocene regional extensional framework is difficult to resolve, particularly because present extensional models invoke a component of north-south contraction during large-magnitude, east-west extension in the central Basin and Range (e.g., Wernicke et al., 1988; Cakir and Aydin, 1990; Anderson and Barnhard, 1993; Anderson et al., 1994).

The most recent extension in the region is postvolcanic and Miocene (?)-Pliocene to Quaternary in age. For example, the Pliocene (?) to Quaternary Hiko fault zone bounds the west-side of the Hiko Range, ~10 km east of the map area (Fig. 3). Pliocene to Quaternary east-west-directed extension is widespread and is responsible for the linear, north-trending topography of the Great Basin (e.g., Stewart, 1978; Eaton, 1982; Axen et al., 1993).

East-West-Trending Lineaments

Transverse faults in the Great Basin tend to be concentrated along east-west-trending lineaments or zones whose roles in regional extension are unclear (Figs. 1a and 3). The lineaments were first identified by Ekren et al. (1976) based on the alignment of a variety of features (e.g., topography, structures, mineralized zones, etc.) (Figs. 1a and 3). Some of the lineaments have since been described and interpreted by a number of workers (e.g., Stewart et al., 1977; Rowley et al., 1978; Bartley, 1989; Overtoom and Bartley, 1996; Axen, 1998; Hudson et al., 1998; Rowley, 1998; Williams, 2000; Rowley and Dixon, 2001; Taylor and Switzer, 2001).

The Timpahute lineament, which contains the CSFZ, is a broadly defined, ~25 km wide zone that extends from the northern Groom Range, eastward to the eastern edge of the Caliente caldera complex, and possibly eastward into Utah (Fig. 3) (Ekren et al., 1976). Presently, the lineament lies just north of a north-south gradient or east-west oriented step in regional elevations and gravitational potential energy (Figs. 3, 6, and 7) (Jones et al., 1996). Basin elevations north of the lineament are approximately 300-600 m (1000-2000 ft) higher than basin elevations to the south. The change in gravitational potential energy also dramatically increases north of the Timpahute lineament (Fig. 7) (Jones et al., 1996).

The topographic and potential energy gradients across the Timpahute lineament reflect physical differences within the crust and mantle. For example, surface heat flow is on average higher in the northern Basin and Range than in the central and southern Basin and Range (Lachenbruch and Sass, 1978; Mabey et al., 1978; Blackwell, 1983). The high heat flow of the northern Basin and Range probably reflects a greater degree of

thinning and removal of mantle-lithosphere beneath the region, and subsequent replacement by hot, upwelling asthenosphere (Jones et al., 1992). In contrast, mantle-lithosphere thickness is interpreted to be greater in the relatively cool central Basin and Range (Jones et al., 1992). Crustal thickness estimates based on seismic profiles vary. Some workers suggest that the crust is of uniform thickness across the Basin and Range province (e.g., Jones et al., 1992). Others suggest that, in general, northern Basin and Range crust is thinner than central and southern Basin and Range crust (Prodehl, 1970).

The physical differences across the Timpahute lineament are also manifest in active deformation and Quaternary faulting. The Timpahute lineament parallels and partly coincides with a west-trending belt of small to moderate, shallow earthquakes that is a branch of the Intermountain Seismic Belt (Smith and Sbar, 1974; Ekren et al., 1976; Smith and Arabasz, 1991). Although the kinematic role of this seismically active zone is not clear, the earthquakes may accommodate some of the physical differences across the Timpahute lineament. In addition, the Basin and Range province north of the Timpahute lineament is more seismically active than the central and southern Basin and Range, and contains a greater number of Quaternary faults (Thenhaus and Barnard, 1998, Bennett et al., 1999; Thatcher et al., 1999). This observation, however, may be biased by a greater number of settlements, geologic studies, and seismic stations in central and northern Nevada, and western Utah. Current studies of Quaternary to Holocene faults in the vicinity of Las Vegas and better distribution of recording stations may challenge this perception of the central Basin and Range in the future.

Data from extensional systems to the north and south of the Timpahute lineament suggest that the lineament has been separating regions with contrasting amounts, styles,

locations, and directions of extension since the late Eocene to Oligocene and possibly earlier (e.g., Bartley et al., 1988; Axen et al., 1990; Guth, 1990; Taylor and Bartley, 1992; Axen et al., 1993; Taylor and Switzer, 2001). For example, the lineament forms the southern boundary of the Snake-Stampede detachment system and separates the highly extended region north of the lineament from the area to the south, which remained unextended until the early Miocene (Fig. 3) (Bartley et al., 1988; Taylor et al., 1989; Taylor, 1990; Taylor and Bartley, 1992). The lineament also forms a boundary to the Highland, Mormon Peak and Tule Spring detachment systems, which initiated in the middle to late Miocene (Fig. 3) (Bartley et al., 1988; Taylor et al., 1989; Axen et al., 1990; Taylor, 1990).

Transverse faults that are part of the Timpahute lineament have been studied to the east and west of the CSFZ and, thus far, have provided somewhat contradictory information. For example, transverse faults in the western Timpahute and Hiko ranges are primarily normal and oblique-slip faults (Taylor and Switzer, 2001; Taylor, 2002, Sandru and Taylor, 2003). Farther east, the lineament contains transverse strike- and oblique-slip faults (Ekren et al., 1976; Rowley and Shroba, 1991; Rowley et al., 1994, Hudson et al., 1998). The CSFZ is ideal for a case study because it is the last remaining segment of the Timpahute lineament that is needed to be examined in detail, and it may provide the key to understanding the disparate data to the east and west.

CHAPTER 3

STRATIGRAPHY

The well-defined stratigraphy in the region (Byers et al., 1961; Tschanz and Pampeyan, 1970; Best and Christiansen, 1991; Best et al., 1993, Scott et al., 1995; Chamberlain and Warme, 1996) facilitates mapping and documenting complex structural relationships. The Mount Irish and Timpahute ranges expose Paleozoic shelf strata that are unconformably overlain by Tertiary volcanic and sedimentary rocks (Figs. 8 and 9; Plates 1 and 2). Quaternary alluvial and fluvial deposits fill Tikaboo Valley, which lies between the two ranges (Figs. 3 and 9; Plate 1). Detailed descriptions of these units are provided on Plate 1. In the following brief synopsis of regional and local stratigraphic relations, the stratigraphic nomenclature of Byers et al. (1961), Tschanz and Pampeyan (1970) and Best et al. (1993) are combined.

Paleozoic Stratigraphy

Most of the Paleozoic strata exposed in the southern Mount Irish and eastern Timpahute ranges lie in the Mount Irish thrust plate (Fig. 10; Plates 1 and 2). The exposed strata consist of uppermost Cambrian through Mississippian carbonates, and subordinate quartz sandstones, siltstones, and shales (Fig. 8; Plate 1) (Tschanz and

Pampeyan, 1970). These rocks are part of a shallow-water, marine shelf succession containing a few disconformities.

Sub-Tertiary Unconformity

Paleozoic rocks in the region are unconformably overlain by Tertiary ash-flow tuffs or freshwater conglomerate and limestone (Figs. 9 and 10; Plates 1 and 2). The sub-Tertiary unconformity is a regional marker that is important for restoring cross sections to their prevolcanic configuration and for determining paleotopographic patterns in the area. Based on outcrop patterns and cross-section constructions, the following relations about the sub-Tertiary unconformity were recognized. (1) In most of the map area, late Oligocene-age tuffs unconformably overlie folded and tilted Ordovician through Devonian strata; however, locally, Tertiary limestone and conglomerate unconformably overlie the Ordovician Ely Springs Dolomite or the Devonian Guilmette Formation (Fig. 10; Plate 1). In addition, the limestone and conglomerate are interpreted to overlie Mississippian units in some cross sections (Plate 2). (2) The unconformity is angular (~30°-40°) and dips gently to moderately east (Figs. 10 and 11; Plates 1 and 2). (3) Tertiary unit thickness variations and exposures of the unconformity reveal several paleotopographic lows and highs. For example, a buttress unconformity is exposed in the western part of the mapped area where an ~800 ft (~245 m) thick section of the Shingle Pass Tuff (lower cooling unit) thins to ~150 ft (~45 m) (Figs. 10 and 12; Plates 1 and 2). In addition, the upper part of a paleohill of Ordovician units surrounded by Tertiary tuffs is exposed in the central part of the mapped Mount Irish Range (Fig. 10; Plates 1 and 2).

Tertiary Stratigraphy

Tertiary lacustrine limestone and conglomerate are the oldest terrestrial deposits in the area (Figs. 9 and 10; Plate 1). The limestone occurs as both massive and algal-laminated limestone that typically overlies cobble-conglomerate that consists wholly of clasts derived from the Paleozoic section (e.g., Scotty Wash Quartzite and Pogonip Group) (Fig. 13). Most of the limestone is sandwiched between the lower and upper cooling units of the Monotony Tuff (Fig. 10; Plates 1 and 2). Based on this relationship, the age of the lacustrine limestone and conglomerate is estimated to be ~27 Ma.

Most of the ash-flow tuffs in the Mount Irish and Timpahute ranges erupted from the Central Nevada caldera complex, which was active between about 31 and 22 Ma (Fig. 3). The youngest tuff, the Hiko Tuff (18.5 Ma), is the exception (Best et al., 1993; Scott et al., 1995). It was erupted from the Caliente caldera complex (Fig. 3). Ash-flow tuffs erupted from the Central Nevada caldera complex include: (1) two cooling units of the Monotony Tuff (27.3), a dacitic ash-flow tuff that was erupted from a source in the southern Pancake Range, northwest of the study area; (2) the Shingle Pass Tuff (26.0-26.7 Ma), a rhyolitic tuff that erupted from a caldera in the Quinn Canyon Range, west of the Timpahute Range; (3) the tuff of Hancock Summit (26.78 ± 0.15 Ma; Appendix II), a distinctive phenocryst-rich rhyolitic ash-flow tuff between lower and upper cooling units of the Shingle Pass Tuff; and (4) the Pahranagat Tuff (22.6 Ma), a rhyolitic ash-flow tuff thought to have been erupted from a source in the Kawich Range (Figs. 3 and 9) (Best at al., 1993, 1995; Scott et al., 1995).

CHAPTER 4

METHODS

Standard geologic techniques (e.g., Compton, 1985) were used to map ~35 km^2 in the Mount Irish and Timpahute ranges at 1:24,000 scale. The geologic data were placed onto portions of the Crescent Spring, Mount Irish, Mount Irish SE, Monte Mountain, and Tempiute Mountain SE, USGS 7.5 minute quadrangle, topographic base maps. Aerial photos at ~1:24,000-scale were used to map the surficial geology and aid in geologic interpretations. In addition, this study incorporates new geologic map data from the eastern Mount Irish range (Fig. 10; Plate 1) (Taylor, W.J., Mrozek, S., and Livingston, T., unpublished data).

Three major techniques were used to analyze the geologic map data (Appendix I). (1) Stereoplots of faults, folds and other structural orientation data were created using the stereonet program for Windows of Allmendinger (2002a). (2) Fault orientations and geometries not measured in the field were calculated using the three-point and structure-contour methods. (3) Retrodeformable cross-sections were constructed using standard line-length balancing techniques (e.g., Dahlstrom, 1969; Nunns, 1991; Groshong 1994; Kerr and White, 1994). However, because many of the cross-sections violate the two-dimensional criterion of cross-section balancing, the cross-sections were made retrodeformable as a network of cross-sections. The cross-sections were adjusted

iteratively until all sections matched the map data and all intersected cross-sections. Thus, area was conserved in a cross-section grid. The cross-sections aided in analysis of the type and amount of fault movement, subsurface bedrock structure, and three-dimensional distribution of strain.

CHAPTER 5

FAULT DESCRIPTIONS

A total of 82 faults were mapped in the eastern Timpahute and western Mount Irish ranges (Fig. 10; Plate 1). An additional 31 faults were mapped by W.J. Taylor, S. Mrozek, and T. Livingston (unpublished data) in the eastern Mount Irish Range (Fig. 10; Plate 1). Faults that are part of this unpublished data are not included in fault totals or stereoplots of poles to fault surfaces presented in the following sections. In the field, faults were identified by offset features, omission or repetition of stratigraphy, fault breccia, and fault surfaces. The mapped faults and their cross-cutting relations reveal three Cenozoic extensional episodes: synvolcanic (~27-18 Ma), postvolcanic Miocene (?), and postvolcanic Miocene (?)-Pliocene or Quaternary extension. These extensional episodes are defined by ~east-west-striking and ~north-south-striking faults (Figs. 14 and 15).

~East-West-Striking Faults

Fifty-three ~east-west-striking faults were recognized in the area (Fig. 14). The faults may be divided into two sets based on their relation to Tertiary volcanic units. The first set consists of synvolcanic east-west-striking faults, which cut some, but not all volcanic units (Fig. 15). The second set comprises postvolcanic east-west-, east-northeast-, and

northeast-striking faults (Fig. 15). These faults cut Paleozoic and Tertiary units, including the youngest exposed tuff, the 18.5 Ma Hiko Tuff (Fig. 10; Plate 1).

Synvolcanic East-West-Striking Faults

Three synvolcanic east-west-striking faults are exposed in the eastern Timpahute range (labeled (d), (e), and (f) on Fig. 10 and Plate 1). The faults are planar and dip between 45° to 70° north and south. Two of the synvolcanic faults cut lower units of the tuff of Hancock Summit, but are overlain by middle to upper units of this formation (labeled (d) and (e) on Fig. 10 and Plate 1). The faults have minor (<10 m) normal- and/ or oblique-slip displacements (Figs. 10 and 15; Plate 1). Another synvolcanic fault juxtaposes the Shingle Pass Tuff (lower cooling unit) against the tuff of Hancock Summit, but is overlapped by the ~26.7 Ma Shingle Pass Tuff (upper cooling unit) (labeled (f) on Fig. 10 and Plate 1). The stratigraphic separation across this fault is apparent normal and may be as much as 245 m (816 ft.). The slip sense is not known because kinematic indicators were not observed on this fault.

Postvolcanic Miocene (?) ~East-West-Striking Faults

Most of the faults in the area are postvolcanic east-west-, east-northeast- and northeast-striking faults that make up the Crescent Spring fault zone (CSFZ) (Fig. 10; Plate 1). The CSFZ contains 37 faults, prominent in the southern half of the map area (Figs. 3 and 10; Plate 1). In the Mount Irish Range, faults of the CSFZ are concentrated along two domains: one lies near Crescent Spring and the other lies ~2 km south of Crescent Spring (Fig. 10; Plate 1). In the eastern Timpahute range, the two domains spread to form a single more broadly distributed zone of faults (Fig. 10; Plate 1).

The CSFZ cuts Paleozoic and Tertiary rocks, including the youngest exposed tuff, the 18.5 Ma Hiko Tuff. The faults anastamose along strike and are both planar and nonplanar with depth based on differences between the dips of the hanging wall and footwall strata (Fig. 10; Plates 1 and 2). The faults dip moderately to steeply (45°-90°) to the north or south; however, most of the faults in the CSFZ dip south (Figs. 10 and 14; Plates 1 and 2). The separation across the faults is apparent right-lateral on south-dipping faults, and apparent left-lateral on north-dipping faults (Fig. 10; Plate 1). The stratigraphic separation across most of the faults ranges from 30 to 150 m (100 to 500 ft) (Plate 2). Kinematic indicators, including fault grooves and mullions and fault striae, are exposed along several of the CSFZ faults (Plate 1). The kinematic indicators have rakes ranging from ~63°E to 90°, indicating dominantly dip-slip fault motion.

The Crescent Spring fault is the main fault in the zone and is inferred to extend across the entire map area (Fig. 10; Plate 1). The mean fault plane strikes N81°E and dips 71° south; however, the fault surface is irregular along strike and dips vary from 52° to vertical (Figs. 10 and 16a; Plate 1). The stratigraphic separation across the fault is apparent normal and ranges from ~600 to 900 m (2000 to 3000 ft) (Fig. 10; Plates 1 and 2). Slickenlines and fault grooves and mullions measured along the fault have rakes that range from 76°W to 87°E (Fig. 16b). The kinematic data, combined with the information on the fault's geometry and stratigraphic separation, indicate normal slip along the fault.

Poor exposure leaves uncertainty about the relation between volcanism and motion along several of the east-west-striking faults. It is unclear whether these faults are overlapped by or cut the 27.3 Ma Monotony Tuff (Fig. 10; Plate 1). The Monotony Tuff is poorly to moderately welded and tends to crumble and/ or powder near faults. I favor

the interpretation that the faults are postvolcanic in age because most of the east-west-striking faults in the area with similar orientations and geometries are postvolcanic Miocene-age faults. This interpretation, however, does not preclude prevolcanic extension in the region. Stratigraphic relations and regional structural relations suggest that prevolcanic extension may have affected the area (discussed in following sections).

~North-South-Striking Faults

Twenty-nine ~north-south-striking faults were documented in the area (Fig. 14). The faults are divided into two sets based on their relation to east-west-striking faults in the area. The first set consists of postvolcanic north-south- and north-northwest-striking faults that cut Paleozoic and Tertiary units, including the 18.5 Ma Hiko Tuff, and end at postvolcanic east-west-striking faults (Figs. 10 and 15; Plate 1). The second set, comprises north-south-striking faults that cut Paleozoic rocks, Tertiary rocks, and postvolcanic Miocene (?) east-west-striking faults (Figs. 10 and 15; Plate 1).

Postvolcanic Miocene (?) North-South-Striking Faults

Twenty-five postvolcanic Miocene (?) ~north-south-striking faults end at ~east-west-striking faults. Faults in this set are mostly planar and dip between 45° and 70° to the east or west (Figs. 10 and 14; Plates 1 and 2). The stratigraphic separation is, in general, less than 180 m (600 ft) (Plate 2). Small stratigraphic separations of around 45 m (150 ft) are common on many of the faults in this set (Plate 2). The separation across the faults is apparent normal; however, some of the faults show apparent left- and right-lateral separations (Fig. 10; Plate 1). Because no kinematic indicators were identified, the slip directions along these faults is not known.

Postvolcanic Miocene (?) to Pliocene or Quaternary North-South-Striking Faults

Four ~north-south-striking, moderately-dipping (50°-70°) faults are exposed in the western Mount Irish Range (Fig. 10; Plates 1 and 2). These faults cut the Crescent Spring fault and several other postvolcanic Miocene (?) east-west-striking faults (Fig. 10; Plate 1). The separation across the faults is apparent normal and apparent right-lateral. The stratigraphic separations are small (~100 m; 350 ft) (Fig. 10; Plates 1 and 2). Slickenlines, and grooves and mullions were measured at two locations along one of the faults. The kinematic indicators have rakes of 55° and 65° (Plate 1).

One of the ~north-south-striking faults in this set and a southward splay that are exposed on the west side of the Mount Irish Range may be divided into geometric sections. The sections are defined by changes in fault strike (i.e., bends in the fault). The northern portion of the fault strikes N8°E (Fig. 10; Plate 1). South of Crescent Spring, the fault strike bends to north-northeast (N10°E-N27°E) (Fig. 10; Plate 1). The southernmost section of the fault strikes N15°W (Fig. 10; Plate 1). The changes in orientation between the northern and southern sections form a salient near a transverse fault (near F1 on Figure 10; Plate 1). Consequently, the salient and the transverse faults define a geometric and structural section boundary. Air photos show that several other bends and section boundaries may exist along the fault to the south.

In addition to these faults, a north-south-striking fault with ~1500 m (4900 ft) displacement was placed in the subsurface, near the Mount Irish range-front (Fig. 10; Plates 1 and 2). The fault is geometrically required to properly balance cross sections (Plate 2). The fault is probably equivalent to the Mount Irish Range fault (MIRF) mapped by Ekren et al. (1977) and Dohrenwend et al. (1996). The MIRF is 11 km in

length and extends from west of Logan Pass south to northwest of Hancock Summit (Fig. 3). The fault is divided into northern and southern segments that are separated by a right step near the center of the fault trace (Dohrenwend et al., 1996). Photogeologic mapping by Dohrenwend et al. (1996) indicates fault scarps that cut Pleistocene-age deposits near the step. No fault scarps or secondary features (e.g., fissures) were noted in late Tertiary or Quaternary deposits in the map area. Consequently, the northern MIRF may have become inactive sometime in the Miocene or Pliocene, while the southern segment remained active into the Quaternary.

In addition to north-south-striking faults, 28 north-south-striking, steeply-inclined to vertical fractures were measured in the western Mount Irish Range (Fig. 17). The fractures are concentrated in jasperoid breccia that formed along the trace of the Crescent Spring fault just north of Crescent Spring (Fig. 17; Plate 1). The fractures have consistent north-south orientations and a systematic ~30-50 cm spacing (Fig. 17). Plumose structure or hackle plumes were observed on several of the fracture surfaces.

CHAPTER 6

FOLD DESCRIPTIONS

The east-west-striking and north-south-striking faults in the map area cut three map-scale (wavelengths of ~2 km) and several smaller (wavelengths of 1-2 m) folds that are exposed within Paleozoic rocks (Fig. 10; Plates 1 and 2). In their present orientation, the folds are mostly north- to northwest-trending, gently (~18°-25°) northwest-plunging, steeply inclined, open folds (Fig. 10; Plate 1). The folds are unconformably overlain by Tertiary sedimentary and volcanic rocks (Fig. 10; Plates 1 and 2). In addition to these folds, folds not exposed at the surface were geometrically required to properly balance and restore cross sections (Plate 2).

The most prominent fold in the area is the Mount Irish anticline, which lies in the Mount Irish thrust plate (Fig. 10; Plates 1 and 2). The anticline is well exposed north of Logan Pass (Taylor et al., 1993; 2000); however, to the south the anticline is partly masked by volcanic and sedimentary cover (Plates 1 and 2). The anticline is a north-trending, steeply inclined, open and broad-hinged fold (Plate 2). The eastern limb of the fold is short, gently (~15°) east-dipping, and is truncated by the Mount Irish thrust (Plates 1 and 2). The western limb is longer and dips 20°W (Plates 1 and 2). Restoring the 10°-20° of eastward tilt recorded in the Tertiary volcanic rocks shows that the anticline

originally had an almost horizontal eastern limb and a moderately- to steeply-dipping western limb (Plates 1 and 2).

CHAPTER 7

STRUCTURAL AND TECTONIC INTERPRETATIONS

The documented deformational episodes in the Mount Irish and eastern Timpahute ranges include Mesozoic contraction and four phases of extension: prevolcanic (pre-27 Ma) (explained below), synvolcanic (~27-18 Ma), postvolcanic Miocene (?), and postvolcanic Miocene (?) - Pliocene or Quaternary extension. This deformational pattern is consistent with regional tectonic patterns. Studies in nearby ranges (e.g., Hiko, North Pahroc, and Pahranagat ranges) documented similar styles and timing of extension (e.g., Jayko, 1990; Taylor and Bartley, 1992; Taylor and Switzer, 2001; Taylor, 2002) implying that structures in the Mount Irish and eastern Timpahute ranges are likely related to regional structural and tectonic events. Below, the new data are related to these other data and models to develop a larger picture of tectonism in space and time.

Mesozoic Contraction

Contractional structures in the Mount Irish and Timpahute ranges, which include the Mount Irish thrust, Mount Irish anticline, and a few other north- to northwest-trending folds, are related to the Central Nevada thrust belt (CNTB). The Mount Irish thrust and anticline are CNTB structures that are well-documented north of Logan Pass (Armstrong and Bartley, 1993; Taylor et al., 1993; Taylor et al., 2000). However, CNTB structures

only have been inferred for the area south of Logan Pass, where Tertiary normal faults (east-west- and north-south-striking), and volcanic and sedimentary cover obscure structural relations. Mapping for this study and by W.J. Taylor, S. Mrozek, and T. Livingston (unpublished data), as well as cross section constructions show that both the Mount Irish thrust and anticline are present south of Logan Pass. The recognition of these CNTB structures to the south confirms the interpretation of Taylor et al. (2000) that the Mount Irish thrust continues southward to correlate with the Pahranagat thrust in the Pahranagat Range.

Prevolcanic Extension

Although no indisputable prevolcanic normal faults are exposed in the area of Figure 10, field relations suggest that prevolcanic extension may have affected the area. The primary evidence for possible prevolcanic extension is late Oligocene-age basin-fill deposits that unconformably overlie folded Paleozoic strata (Figs. 9, 10, and 13; Plates 1 and 2). The deposits of lacustrine limestone and conglomerate are interpreted here to have formed in a closed (?) basin during regional Eocene to Oligocene-age extension. This interpretation is supported by (1) the wide distribution of basin-fill strata of similar age and rock types (e.g., Tschanz and Pampeyan, 1970; Ekren et al., 1977; Jayko, 1990; Guth, 1990; Prothro and Drellack, 1997); (2) regional variations in Tertiary section thickness, which suggest that the eastern Timpahute and western Mount Irish ranges contained a paleotopographic low relative to the area near the Mount Irish range crest south of Logan Pass and the adjacent Hiko Range; and (3) documented prevolcanic extension in nearby ranges.

Deposits similar in age and rock types to the basin-fill strata exposed in the map area have been described elsewhere in eastern Nevada (Fig. 18). For example, Taylor and Bartley (1992) describe the formation of Rattlesnake Spring in the North Pahroc Range, which unconformably overlies Paleozoic strata, and consists of conglomerate and lacustrine limestone interbedded with mafic flows (Fig. 18) (Taylor and Bartley, 1992). The formation of Rattlesnake Spring is estimated to be Oligocene in age based on relations with the overlying 30.6 Ma Cottonwood Wash Tuff and provenance data from the upper half of the conglomerate, which contains clasts that have been correlated to a ~32.9 Ma porphyry stock in the Schell Creek Range (Taylor and Bartley, 1992). Similar basin-fill deposits and relations also have been noted in the Desert, Pintwater, and Spotted ranges; in the Jumbled, Buried, and Fallout hills; and south of Frenchman Flat (Fig. 18) (Tschanz and Pampeyan, 1970; Ekren et al., 1977; Jayko, 1990; Guth, 1990; Prothro and Drellack, 1997). The widespread distribution of these basin-fill deposits may indicate deposition in either a single broad basin or in several smaller basins.

Variations in the thickness of Tertiary deposits aid in reconstructing regional paleotopographic patterns and identifying areas of possible prevolcanic basin development. An important assumption here is that the tops of ash-flow tuffs form with a nearly horizontal upper surface that slopes gently away from the vent area, but may drape paleotopographic highs. Thus, tuffs form thick accumulations in paleotopographic lows or basins and a thin covering across paleotopographic highs. The thickness of ash-flow tuff, however, also is strongly influenced by proximity to calderas, volume and direction of eruptions, prevailing winds, and later erosion. In the Timpahute and western Mount Irish ranges, the total Tertiary section is approximately 1350 m (4500 ft) thick (Fig. 9).

The Tertiary section in the Hiko Range, 10 km east of the study area, is by comparison thin (~270 m; 900 ft) (Switzer, 1996; Taylor and Switzer, 2001). At least some of this difference in thickness may be attributed to the proximity of the ranges to caldera sources (e.g., the Mount Irish and Timpahute ranges lie closer to source vents in the central Nevada caldera complex); however, the Hiko Tuff, whose source area is the Caliente Caldera complex, relatively close to the Hiko Range, is at least double the thickness in the Mount Irish Range as in the Hiko Range (Fig. 3) (cf., Switzer, 1996; Taylor and Switzer, 2001). This may imply that the eastern Timpahute and western Mount Irish ranges contained a paleotopographic low or basin that lay west of a paleotopographic high in the vicinity of the Mount Irish range crest south of Logan Pass (Plate 2) and in the Hiko Range. This interpretation is supported by the presence of the basin-fill deposits (i.e., Tertiary lacustrine limestone and conglomerate) in the area and their absence east of the Mount Irish Range crest and in the Hiko Range (Switzer, 1996; Taylor and Switzer, 2001).

The relationship between the basin development documented in these ranges and tectonism is not clear. One possible interpretation is that the Tertiary deposits are infilling paleorelief related to Mesozoic contraction; however, the large time gap (>30 m.y.) between activity in the CNTB and the age of the basin-fill deposits render this scenario unlikely. An alternative and preferred interpretation is that the limestone and conglomerate infill paleorelief related to regional late Eocene to Oligocene-age extension.

Evidence for late Eocene to Oligocene-age extension and basin development is abundant in the region (e.g., Bartley et al., 1988; Taylor et al., 1989; Taylor, 1990; Jayko,

1990; Taylor and Bartley, 1992; Axen et al., 1993). Extensional systems of this age define two ~north-trending belts in the northern Basin and Range (Fig. 1e) (Axen et al., 1993). The eastern belt is defined by the east-directed Snake-Stampede detachment system (Axen et al., 1993). The hanging wall, and consequently most of the faults related to this system, lie east of the White River Valley, where the Seaman breakaway is buried (Fig. 3) (Taylor and Bartley, 1992). The western belt is interpreted to extend from the northern Death Valley region northeast nearly to the Nevada-Idaho state line (Axen et al., 1993). The belt is mostly defined by stratigraphic evidence for Oligocene-age extensional basins and scattered prevolcanic faults (Axen et al., 1993).

Although structural evidence for the western extensional belt is poor, a few prevolcanic normal faults have been documented in the Pahranagat Range, Spotted Range, Pintwater Range, Jumbled Hills, and Fallout Hills (Tschanz and Pampeyan, 1970; Ekren et al., 1977; Guth, 1990; Jayko, 1990). Paleorelief in the map area may be related to activity along one such fault, the Badger Mountain fault; a northwest-striking, west-dipping, prevolcanic normal fault exposed in the Pahranagat Range (Fig. 3) (Jayko, 1990). This interpretation is favored for two main reasons. (1) The Badger Mountain fault is the nearest structure of appropriate age; exposures of the fault lie ~10-15 km along strike to the south of the study area (Fig. 3). (2) Conglomerate and lacustrine limestone similar to the basin-fill strata in the map area formed in the hanging wall of the fault. These basin-fill deposits also are overlain by the ~27 Ma Monotony Tuff.

Synvolcanic Extension

Synvolcanic extension in the northern Basin and Range province has been documented along both north-south-striking (e.g., North Pahroc and Highland ranges) and east-west-striking faults (e.g., Hiko Range, Golden Gate Range, and Dry Lake Valley area) (Taylor et al., 1989; Taylor, 1990; Overtoom and Bartley, 1996; Taylor and Switzer, 2001). Synvolcanic north-south-striking faults are not surprising because the bulk of extension in the Basin and Range province occurred along ~north-south-striking faults that accommodated approximately east-west extension. More problematic are synvolcanic east-west-striking faults that accommodated north-south-directed extension. Synvolcanic faults documented here fall into this category.

Two different models have been suggested to explain the development of east-west-striking normal faults during peak Tertiary volcanism. Best and Christiansen (1991) suggested that synvolcanic faults in the region form as the result of instability and collapse of erupting calderas. In this model, the faults develop as the result of local perturbations to the stress-field and are limited to the area near a collapsed caldera (Fig. 4). In contrast, Bartley (1989) and Overtoom and Bartley (1996) suggest a tectonomagmatic model for the formation of synvolcanic east-west-striking faults that are part of the Warm Springs lineament in the Golden Gate and Seaman ranges (Fig. 5). In this model, the faults develop in response to a shift in the regional stress field that is associated with the southward migration of the mid-Tertiary volcanic belt (Fig. 5) (Bartley, 1989; Overtoom and Bartley, 1996). As the volcanic belt migrates into and occupies the area of the lineament, it thermally uplifts and weakens the crust, generating

conditions that favor north-south extension (Fig. 5) (Bartley, 1989; Overtoom and Bartley, 1996).

The synvolcanic faults that accommodated north-south extension in the Mount Irish and Timpahute ranges are interpreted here to have formed by tectonomagmatic rifting associated with the migration of the mid-Tertiary volcanic belt into the area of the Timpahute lineament. This interpretation is favored because the study area lies far from any caldera sources (Fig. 3); therefore it is unlikely that the faults formed in relation to caldera collapse. Also, synvolcanic north-south-directed extension is documented elsewhere along the Timpahute lineament (e.g. Hiko Range, east of the study area), which implies that the faults formed in response to a regional, not a local, stress field (Switzer, 1996; Taylor and Switzer, 2001).

Synvolcanic extension in the Mount Irish and Timpahute ranges appears to have been minor because synvolcanic faults are rare and have relatively small displacements (<10 m). Best and Christiansen (1991) and numerous other studies that examined the spatial and temporal association of volcanism and extension in the region came to a similar conclusion (e.g., Bartley et al., 1989; Taylor et al., 1989; Taylor, 1990; Axen et al., 1993). In fact, it appears that most of the extension in the region predates or postdates peak volcanism. These observations suggest that the relationship between extension and volcanism may not be simple. Humphreys (1995) suggests that buckling or removal of the Farallon slab beneath western North America may have been a principle control on the timing and location of extension and magmatism in the Basin and Range. Consequently, dynamic models (e.g., active vs. passive rifting models) that have been

proposed for the Basin and Range province (e.g., Sengor and Burke, 1978) may not apply to this region.

Postvolcanic Miocene (?) Extension

Most of the documented postvolcanic Miocene-age extensional systems in the northern Basin and Range accommodated east-west-directed extension (e.g., Stewart, 1978; 1998; Taylor et al., 1989; Best and Christiansen, 1991). However, postvolcanic ~east-west-striking and ~north-south-striking faults that end at east-west-striking faults in these parts of the Mount Irish and Timpahute ranges appear to have accommodated north-south-directed extension. The east-west-striking faults are transverse to prevolcanic extensional faults documented in the region (e.g., faults of Snake-Stampede detachment system and Badger Mountain fault) and to postvolcanic Miocene (?) to Pliocene or Quaternary faults documented in the study area (e.g., Mount Irish Range fault and Hiko fault).

P (shortening) and T (extension) axes derived from kinematic data collected along the Crescent Spring fault provide a qualitative assessment of the regional kinematic axes for this fault (Fig. 19). Two important observations emerge from the qualitative assessment. First, the data produce a subhorizontal, north-south extension direction for the Crescent Spring fault (Fig. 19). Second, the data yield a subvertical shortening axis (Fig. 19). These regional kinematic axes are consistent with normal faulting along the Crescent Spring fault. More quantitative kinematic and/or paleostress calculations could not be performed because in most cases fault slip-sense data were lacking, and because such

analyses require large numbers (n >30) of contemporaneous faults (e.g., Angelier et al., 1985; Michel-Noel et al., 1990; Marrett and Allmendinger, 1990).

The north-south-striking faults that end at east-west-striking faults are interpreted to be kinematically linked to the postvolcanic east-west-striking faults. This interpretation is supported by several observations. (1) The north-south-striking faults that end at east-west-striking faults do not correlate across the latter faults (Figs. 10; Plate 1). (2) The displacement across the north-south-striking faults is commonly small (~45 m; 150 ft) (Fig. 10; Plates 1 and 2). (3) Many of the north-south-striking faults have short traces (< 600 m) and occur in the hanging walls of east-west-striking faults, where the stratigraphic separation across east-west-striking faults is at a maximum (Fig. 10; Plate 1). The frequency of these faults decreases where the stratigraphic separation across east-west-striking faults is less (Fig. 10; Plate 1). This implies that the north-south-striking faults accommodate differences in strain along the east-west-striking faults. (4) In places, a north-south-striking fault both ends at and appears to cut east-west-striking faults (e.g., faults labeled g, h and i on Fig. 10 and Plate 1). Seemingly contradictory relations such as these may imply that the north-south-striking and east-west-striking faults were active generally synchronously.

Postvolcanic Miocene-age transverse faults that accommodated north-south extension were documented elsewhere along the Timpahute lineament, in the Hiko Range, northern Mount Irish Range, and western Timpahute Range (Taylor, 2000; Taylor and Switzer, 2001; Sandru and Taylor, 2003). The faults record a regional change from east-west-directed extension during the Eocene to Oligocene to north-south-directed extension during the Miocene. This change in extension direction is difficult to explain because

unlike synvolcanic faults in the area, which can be readily explained by a tectonomagmatic model, these faults appear to postdate volcanism in the area (Taylor and Switzer, 2001). The faults cut the youngest exposed tuffs in these ranges, the ~18.5 Ma Hiko Tuff in the Mount Irish and Timpahute ranges and the 14.7 Ma Sunflower Tuff in the Hiko Range (Fig. 10; Plate 1) (Taylor and Switzer, 2001). However, the change in extension direction may be explained if tectonomagmatic rifting occurs along the trailing edge of the migrating volcanic belt and is accompanied by a decrease in plate boundary and other stresses. Taylor and Switzer (2001) used this modified tectonomagmatic model to explain postvolcanic north-south-directed extension in the Hiko Range.

North-south-directed extension along the Timpahute lineament postdates major eruptions from the Caliente and Kane Springs Wash caldera complexes, which occupied the southeastern end of the Timpahute lineament from ~23-11 Ma (Best and Christiansen, 1991; Best et al., 1993; Rowley et al., 1995; Harding et al., 1995). One could argue that tectonomagmatic rifting seems unlikely if the southward-sweeping volcanic belt had already migrated away from the lineament by the time extension initiated. However, thermal models of solidifying magma chambers demonstrate that a body with a 10 km radius may take ~1 m.y. to cool to near country rock temperatures (Spera, 1980). Variables such as depth of emplacement, magma body size and shape, and properties of the surrounding rocks can either increase or decrease the cooling times (Spera, 1980; Henry et al., 1997). Thus, it is possible that the thermal anomaly associated with large and long-lived systems like the Caliente and Kane Springs Wash caldera complexes outlasted eruptions.

Taylor and Switzer (2001) suggest that extension directions in the region are largely controlled by plate boundary interactions. In the Basin and Range province, these plate boundary stresses generate dominantly east-west-directed extension. Consequently, stresses added by the migrating volcanic belt or tectonomagmatic rifting only influence the area when plate boundary stresses are sufficiently weak (Taylor and Switzer, 2001). This may explain several important observations: (1) north-south directed extension along both the Timpahute and Warm Springs lineaments (Fig. 1a) occurred after prevolcanic east-west-directed extension ended, (2) no east-west-directed extensional systems appear to have been active during synvolcanic north-south-directed extension along either the Timpahute or Warm Springs lineaments, and (3) no significant east-west-directed extensional system in the region appears to have been active during postvolcanic north-south-directed extension along the Timpahute lineament (Overtoom and Bartley, 1996; Taylor and Switzer, 2001). Although plate boundary stresses are clearly an important control on extension directions, large differences in extensional strain north and south of the Timpahute lineament appear to have also played an important role in the development of postvolcanic north-south-directed extension (see discussion; Chapter 8).

Postvolcanic Miocene (?) to Pliocene or Quaternary Extension

In the Mount Irish and Timpahute ranges, postvolcanic Miocene (?) to Pliocene or Quaternary extension is documented by north-south-striking faults that accommodated ~east-west-directed extension. East-west-directed extension is also documented by Mode I fracture data collected along the Crescent Spring fault in the Mount Irish range (Fig. 17). The north-south-striking fractures, concentrated within jasperoid breccia that

formed along the trace of the faults, record an east-west least principal stress direction (Fig. 20).

Additional evidence for east-west-directed extension is the 10° to 20° of eastward tilt of the Mount Irish and Timpahute ranges (Fig. 10; Plates 1 and 2). Cross-section constructions indicate that the tilt occurred after or during movement along the Mount Irish Range fault (MIRF) (Plate 2). Movement along the MIRF ceased sometime in the Miocene (?) to Pliocene because the fault cuts Miocene-age tuffs and is covered by Pliocene (?) to Quaternary sedimentary deposits (Fig. 10; Plates 1 and 2). The east tilt of the ranges is likely related to movement on the Hiko fault zone, a Pliocene to Quaternary fault that bounds the west side of the Hiko range, ~10 km east of the study area (Fig. 3) (Switzer, 1996; Taylor and Switzer, 2001). This interpretation is favored because: (1) the Hiko fault zone is the nearest north-south-striking fault of appropriate age, (2) it dips west and lies east of the map area, consistent with the east tilt of these ranges, and (3) stratigraphic evidence from the Pahranagat Valley support a tilted half-graben model for the hanging wall of the fault (Fig. 3) (Switzer, 1996; Taylor and Switzer, 2001).

The faults, fractures and 10° to 20° of eastward tilt record a change in the regional stress field, from north-south-directed extension back to east-west-directed extension. This return to east-west-directed extension is probably related to a decrease in the tectonomagmatic stresses, as well as a possible increase in plate boundary stresses.

CHAPTER 8

DISCUSSION

Regional Transverse Zone

The Timpahute lineament, which contains the CSFZ and other transverse faults, is one of several east-west-trending lineaments or zones that are defined by the alignment of topography, geophysical anomalies, transverse faults, volcanic centers and mining districts (Fig. 1a) (Ekren et al., 1976, 1977). The role of east-west-trending lineaments, systems, and zones in the Basin and Range is contentious. The Timpahute lineament is no exception and has been interpreted in a variety of ways. The earliest interpretation of the lineament is as a deep-seated crustal structure (Ekren et al., 1976). More recent interpretations suggest that at least part of the lineament is a diffuse left-lateral transfer zone (Hudson et al., 1998; Axen, 1998). In this section, I review available data from extensional systems to the north and south of the Timpahute lineament and suggest that the lineament not only accommodated north-south-directed extension during the Miocene, but is a long-lived transverse zone that has been accommodating differences in the magnitude, timing, location, and direction of extension since the Late Eocene to Oligocene and possibly earlier.

The earliest Cenozoic structural role of the Timpahute lineament was during the late Eocene to Oligocene. During this time, the lineament formed the southern boundary of

the east-directed Snake-Stampede detachment system, and separated highly extended crust north of the lineament from the relatively unextended crust to the south (Fig. 21a) (Bartley et al., 1988; Taylor et al., 1989; Taylor, 1990; Taylor and Bartley, 1992). The geometry and kinematics of the lineament at this time are not well-known. In Figure 21a, the Timpahute lineament is represented as a rift margin-style, transfer fault. Axen et al. (1993) and Axen (1998) present several other possible configurations, including an east-west-trending zone of fault tips and a tear fault.

In the early Miocene, the east-west-trending belt of volcanism, which previously occupied the area north of the lineament, migrated to the southeastern part of the Timpahute lineament and formed the Caliente and Kane Springs Wash caldera complexes (Figs. 21b and 21c) (Best et al., 1993; Rowley et al., 1995; Scott et al., 1995). The volcanic belt remained in this region from ~23 to 11 Ma, during which the lineament served several important roles (Best and Christiansen, 1991; Best et al., 1993). (1) In the Timpahute, Mount Irish, and Hiko ranges, synvolcanic pre-18.5 Ma east-west-striking faults formed along the lineament and accommodated minor north-south-directed extension (Fig. 21c) (Taylor and Switzer, 2001; Taylor, 2002). (2) From ~18 to 15 Ma the lineament formed the southern boundary of the west-directed Highland detachment system and separated regions with contrasting amounts of extension (Fig. 21d) (Bartley et al., 1988; Taylor et al., 1989; Taylor, 1990). The net extension across this system is not known, but was probably greater than 10 km (Bartley et al., 1988). (3) During eruption of the ~18.5 Ma Hiko and younger tuffs, northwest-striking normal-, oblique-, and strike-slip faults formed within the Caliente caldera complex (Fig. 21d) (Michel-Noel et al., 1990). Michel-Noel et al. (1990) suggest that the faults locally accommodated as much

as 100 % extension in an east-northeast direction. (4) At ~17 Ma, west-directed detachment systems south of the Timpahute lineament initiated (Fig. 21e). The Mormon Peak detachment accommodated ~23 km of extension (Axen et al., 1990). The younger and structurally lower Tule Springs detachments accommodated ~7 km of extension (Axen et al., 1990). Activity on these detachment systems outlived eruptions from volcanic centers along the lineament, but ceased prior to deposition of the 8.5-5.8 Ma Muddy Creek Formation (Wernicke et al., 1988; Axen et al., 1990).

In the late Miocene after 11 Ma, the western part of the Timpahute lineament accommodated north-south-directed extension along east-west-striking faults, and southward gravitationally-driven middle to lower crustal flow (explained in following section) (Fig. 21f) (Taylor and Switzer, 2001; Taylor, 2002; Sandru and Taylor, 2003). The east-west-striking faults and southward crustal flow worked to reduce large contrasts in potential energy between the northern and central Basin and Range.

The latest Miocene to Quaternary role of the lineament is not clear. One option is that the lineament may be acting as a barrier to the propagation of younger faults. Several late Tertiary and/or Quaternary faults appear to end in the vicinity of the Timpahute lineament (Fig. 3). For example, the Hiko and Stumble faults end near the northern margin of the lineament (Fig. 3). Similarly, the Dry Lake, Pahroc, and Penoyer faults end near the boundaries of the Timpahute lineament (Fig. 3). Several authors draw a southern continuation of the Dry Lake fault along the western margin of the Delamar Valley, and connect the fault to the Maynard Lake fault of the Pahranagat shear zone (e.g., Axen, 1998); however, this interpretation is not well-supported by published geologic data.

Although the earliest Cenozoic structural role of the Timpahute lineament was during Snake-Stampede time, Taylor and Switzer (2001) suggest a possible Devonian or earlier control for the location of the Timpahute lineament. Those authors point out that the Devonian to Mississippian Antler orogenic belt is east-west-trending near the latitude of the Timpahute lineament (e.g., Stewart, 1980). The orientation of this belt may have influenced trends in stratigraphic thickness and lithofacies type within the Devonian and younger units (Poole and Sandberg, 1991; Johnson et al., 1991). One option that has been suggested is that the Timpahute lineament is the site of a pre-existing transform or transverse fault related to the Precambrian rifting of North America (Taylor and Switzer, 2001).

The eastern part of the Timpahute lineament corresponds to the central part of the Caliente Enterprise zone (CEZ) of Axen (1998) and Hudson et al. (1998) (Fig. 3). Both authors describe the middle to late Miocene history of the CEZ as a broad and diffuse left-lateral transfer zone with ~40 km of total offset. The faults within the central and eastern parts of this diffuse zone are mostly northwest-striking right-lateral and oblique-slip faults (Ekren et al., 1976; Michel-Noel et al., 1990; Rowley and Shroba, 1991; Rowley et al., 1994). The left-lateral Pahranagat shear zone composes most of the western segment of this transfer zone (Fig. 3) (Jayko, 1990; Axen, 1998; Hudson et al., 1998). Regional paleomagnetic data show that the eastern and central part of the CEZ underwent significant (~50° to 95°) counterclockwise vertical axis rotations (Hudson et al., 1998).

The evidence for both strike-slip deformation in the CEZ and dip-slip in the Timpahute, Mount Irish and Hiko ranges is strong, and thus, the along-strike differences

need to be reconciled. The left-lateral transfer zone interpretation of Hudson et al. (1998) and Axen (1998) explains vertical axis rotations and strike-slip faults along the eastern part of the Timpahute lineament. However, the model does not explain the topographic and potential energy gradients across the zone, nor does it explain east-west-striking normal faults documented by this and other studies (e.g., Taylor and Switzer, 2001; Taylor, 2002; Sandru and Taylor, 2003).

The structural variations along the length of the Timpahute lineament may be reconciled in several ways. It's possible that normal-, strike- and oblique-slip faults all worked in concert to move crustal material from the area north of the lineament to areas to the south and southeast. Another option is that the vertical axis rotations and strike-slip deformation along the eastern Timpahute lineament (central and eastern CEZ) reflect deformation along the east-west-trending part of the transition zone between the Basin and Range province and Colorado Plateau. The geometry of the stable Colorado Plateau may be forcing lateral and oblique slip along faults near the boundary. This is consistent with observations that the greatest rotations and majority of northwest-striking right-lateral and oblique-slip faults occur near this boundary. The rotations dramatically decrease west of this margin. Alternatively, the along strike variations in the geometry and kinematics the Timpahute lineament/ CEZ may simply reflect different aspects of the structural and tectonic development of the region. Figure 21f shows that east-west-striking normal faults are concentrated along the western part of the Timpahute lineament. Unlike the eastern part of the lineament, which accommodated temporally and spatially distinct extensional and volcano-magmatic episodes, no major extensional

system disrupted the area immediately north or south of the western Timpahute lineament.

Data from this study do not allow me to discern which of the above interpretations, or some combination thereof, is correct. Additional data on the timing of deformation along the length of the lineament and on the role of the Colorado Plateau on the development of the eastern Timpahute lineament (central and eastern CEZ) are needed to make such an interpretation.

In summary, the Timpahute lineament is a long-lived, composite feature. Different parts of the lineament developed and operated at different times, and accommodated temporally and spatially distinct deformations. The lineament may have operated as a left- and/ or right-lateral transfer zone for some or all of its history; however, the lineament also accommodated differences in extensional strain and magmatism as a zone of north-south-directed extension. Consequently, simple transverse fault models (e.g., transfer zones, in which most fault within the zone are kinematically similar and active synchronously) that have been applied to many continental rifts do not fully describe the wide range of kinematic and structural roles of the Timpahute lineament.

Implications of N-S Extension

Miocene-age north-south-directed extension in the Basin and Range province is significant, not only because most of the documented extensional systems in the region accommodated east-west-directed extension, but because north-south-directed extension conflicts with existing models for extension south of the Timpahute lineament. Most of the existing models suggest that large-magnitude extension at the latitude of Las Vegas

was accompanied by north-south contraction (e.g., Wernicke et al., 1988; Cakir and Aydin, 1990; Anderson and Barnard, 1993; Anderson et al., 1994). Consequently, any models for middle- to late-Miocene extension in the region must reconcile these apparently incompatible strain fields. Here I review the evidence for north-south contraction, summarize published extensional models for the central Basin and Range, and present a new kinematic and dynamic model for extension along the Timpahute lineament and to the south.

N-S Contractional Structures and Previous Models

The central Basin and Range, south of the Timpahute lineament, experienced rapid, large-magnitude east-west extension from ~16 to 10 Ma (e.g., Wernicke et al., 1988; Duebendorfer et al., 1990; Wernicke, 1992). Extension was accommodated by several west-directed detachments (e.g., Tule Springs, Saddle Island and Sheep Range detachments) and two large strike-slip faults: the Las Vegas Valley shear zone (LVVSZ) and the Lake Mead fault system (LMFS) (Bohannon, 1984; Duebendorfer et al., 1990; Guth, 1990; Rowland et al., 1990; Duebendorfer and Black, 1992). In addition to these faults, several east-west-trending folds and east-west-striking reverse faults are documented in the western Lake Mead area (Duebendorfer and Simpson, 1994; Anderson et al., 1994; Cakir et al., 1998). The contractional structures are concentrated near the eastern end of the LVVSZ and have been interpreted in various ways (e.g., Wernicke et al., 1988; Cakir and Aydin, 1990; Anderson and Barnhard, 1993; Anderson et al., 1994; Duebendorfer and Simpson, 1994; Cakir et al., 1998).

Wernicke et al. (1988) suggested that at least some of the middle- to late-Miocene extension in the central Basin and Range may have been accompanied by north-south

shortening. The strain field, consequently, was overall constriction during extension. Wernicke et al. (1988) suggests that constrictional strain may be related to significant differences in extension between the northern and central Basin and Range. The differences create a potential energy gradient between the two subprovinces. The potential energy gradient induces gravitational-driven crustal flow from areas of high potential energy (thick, moderately-extended to unextended domains) to areas of low potential energy (thin, highly extended domains).

Several other workers also proposed models invoking overall constriction of the crust during extension. For example, Anderson et al. (1994) propose that strike-slip, extensional and contractional structures in the Lake Mead area relate to southward flow of crustal blocks north of the LVVSZ and LMFS. They suggest that the southward flow of these crustal blocks was obstructed where contractional structures are present, and was compensated by the westward displacement (tectonic escape) of a triangular slice of crust that was bounded by the LVVSZ and southwestern end of the LMFS (Anderson et al., 1994).

Cakir and Aydin (1990) and Cakir et al. (1998) suggest a kinematic model for the development of the extensional, strike-slip and contractional structures documented in the Lake Mead area. The model approximates a two-dimensional system in which far-field north-south compression during the Miocene generates east-west-trending contractional structures, and east-west tension generates extensional structures (Cakir and Aydin, 1990; Cakir et al., 1998). In the model, development of east-west-trending contractional structures is enhanced by fault interactions near the junction of the LVVSZ and the LMFS (Cakir and Aydin, 1990; Cakir et al., 1998).

Duebendorfer and Simpson (1994) suggest that north-south contractional structures in the Lake Mead area may be explained by the southward flow of crustal material from relatively stable areas north of the LVVSZ into the highly extended region to the south. The model is much like that presented by Wernicke et al. (1988) except, in this model contraction is not synchronous with major extension or activity along the LVVSZ, it postdates it. The LVVSZ acts as the boundary between the differentially extended domains. Contrasts in the magnitude of extension across this boundary generate a potential energy gradient (Duebendorfer and Simpson, 1994). The north-south contractional structures form as southward crustal flow attempts to reduce differences in potential energy across the boundary (Duebendorfer and Simpson, 1994).

Another interpretation is that the contractional structures are local features related to the geometry and kinematics of strike-slip faults in the area. Such a model has been suggested by Campagna and Aydin (1991) for the area north of Lake Mead. However, this alternative is not considered here because at least some of the contractional structures appear to post-date movement along strike-slip faults (explained below) (Duebendorfer and Simpson, 1994).

All these proposed models attempt to explain the complex array of structures documented in the Lake Mead area. The new data on north-south-directed extension along the Timpahute lineament presented here require the consideration of additional alternatives. North-south-directed extension is apparently incompatible with the proposed north-south compression in these models. In addition, some models attempt to find a genetic link between extensional, strike-slip and contractional structures. However, Duebendorfer and Simpson (1994) show that contractional structures postdate

the bulk of the E-W-directed extension and basin development, and the main phase of activity along the LVVSZ. They document east-west-trending folds and east-west-striking faults that deform the informally named red sandstone unit of Bohannon (1984), which was deposited during ~11.9-8.5 Ma extension (Duebendorfer and Simpson, 1994). Some of the documented reverse faults also cut early deposits of the 8.5-5.8 Ma Muddy Creek Formation (Duebendorfer and Simpson, 1994). However, activity along major extensional systems and the LVVSZ is inferred to have ceased by 8.5 Ma because the LVVSZ in the western Lake Mead area is overlapped by the Muddy Creek Formation (Duebendorfer and Simpson, 1994). Given the new data on north-south extension and the timing of contraction, a new model or variation of existing models is needed to explain the relations along the Timpahute lineament and relations in the central Basin and Range.

Regional Tectonic Model

Any model for deformation in the region must consider the following: (1) differences in the magnitude and timing of extension between the northern and central Basin and Range, the latter interpreted to be greater and to have peaked at ~13-10 Ma after extension to the north had largely shut-down (Wernicke et al., 1988; Wernicke, 1992); (2) documented north-south-directed extension along the Timpahute lineament following major eruptions from the southward migrating volcanic belt, which ceased at ~11 Ma; (3) recognized north-south contractional structures in the Lake Mead area that postdate ~12-10 Ma movement along the LVVSZ and extensional faults like the Saddle Island detachment (Duebendorfer and Simpson, 1994); and (4) the return to dominantly east-west-directed extension in the late Miocene to Pliocene that is documented along the

Timpahute lineament and other parts of the northern Basin and Range (e.g., Taylor and Switzer, 2001). As a result, a model that includes all of the data must also evaluate the relative roles of crustal thinning, heat supplied from regional magmatism, and plate boundary stresses in governing strain in the region.

I propose a model whereby north-south-directed extension along the dominantly south-dipping CSFZ and other east-west-striking normal faults along the Timpahute lineament drove or allowed movement of crustal material into the central Basin and Range and produced apparent constriction south of the lineament. The transverse faults are concentrated near the top of a topographic and gravitational potential energy gradient that formed as a result of differences in extensional strain and magmatism across the Timpahute lineament (Figs. 6 and 7). This model views both postvolcanic north-south extension and north-south contractional structures in the Lake Mead area as a manifestation of differences across this boundary.

North-south-directed extension along the Timpahute lineament initiated certainly after ~18.5 Ma and probably around 10 Ma, after major eruptions from caldera complexes in the region had ceased. By this time a significant potential energy gradient existed between the region north of the lineament and the central Basin and Range. The gradient was in part generated by the southward sweep of volcanism through the northern Basin and Range, which functioned in two ways: (1) heat advected by upwelling mantle during volcanism thermally elevated and weakened the crust and (2) magmatic additions or underplating acted to thicken the crust. In contrast, much of the central Basin and Range was "amagmatic", or at least lacked volcanism, during this time (Best and Christiansen, 1991; Armstrong and Ward, 1991). The lack of volcanism may imply that

either melt was never generated beneath the region or had difficulty penetrating to shallower levels of the crust.

Temporal and spatial differences in extension also provided gravitational potential energy. Large-magnitude extension (~250 km) in the central Basin and Range peaked between 13-10 Ma, during which extension in the northern Basin and Range is interpreted to have been moderate to inoperative (Wernicke et al., 1988; Wernicke, 1992). The northern Basin and Range probably extended a distance comparable to the central Basin and Range (Wernicke et al., 1988; Wernicke 1992). However, as Wernicke et al. (1988) point out, the difference in the widths of the two subprovinces indicates that crustal thinning was probably greater in the central Basin and Range. Significant crustal thinning by ~10 Ma is consistent with new $\delta^{18}O$ data that suggest the central Basin and Range has lowered 1-2 km since the early Miocene (Horton, 2004).

Tectonomagmatic rifting in the wake of the migrating volcanic belt initiated north-south-directed upper crustal extension in the area of the Timpahute lineament at around 10 Ma. But because a large gradient in potential energy had developed between the region north of the lineament and the central Basin and Range, north-south-directed extension was probably accompanied by southward flow of the middle to lower crust, as proposed by Wernicke et al. (1988), Wernicke (1992), and Duebendorfer and Simpson (1994). The southward flow acts to reduce contrasts in gravitational potential energy by driving material from the thick, moderately extended domain north of the lineament into the thinned central Basin and Range (Fig. 22). A mid- to lower crustal flow mechanism may help to explain why upper crustal north-south-directed deformation was modest and only affected a narrow region along the lineament and near the LVVSZ, and why the

intervening ~150 km went largely undeformed (Fig. 22). Such collapse regimes have been described by Rey et al. (2001) and modeled by other workers (e.g., Buck, 1988; Block and Royden, 1990; Wdowinski and Axen, 1992).

North-south-directed extension along the Timpahute lineament and southward crustal flow into the central Basin and Range are interpreted to have ended at ~8 Ma. This interpretation is supported by plate reconstructions, which show that by ~8 Ma the direction of relative motion between the Pacific and North American plates shifted from west-northwest to north-northwest (Atwater and Stock, 1998). This change in plate boundary conditions is reflected in the style and locus of deformation, which transitioned from detachment systems of the central Basin and Range to strike-slip and oblique-slip faults of the western Great Basin (e.g., Reheis, 1993; Reheis and Sawyer, 1997). By 5 Ma, a significant amount of deformation in the region was accommodated by right-lateral shear and transtension along faults of the eastern California shear zone and Walker Lane belt (Snow and Wernicke, 2000). This may imply that by ~8 to 5 Ma plate boundary conditions exerted increasing control on the stress system and extension directions. The return to plate boundary driven stresses is documented in the area of the Timpahute lineament by ~north-south-striking faults and fractures that cut the ~east-west-striking CSFZ. The strong influence from the plate boundary may explain why southward crustal flow is not obviously operating today, where a strong north-south gradient in topography, heat flow, and potential energy exists across the northern and central Basin and Range (Figs. 6 and 7).

The proposed model helps to explain several issues not addressed by previous models. For example, in the Wernicke et al. (1988) model, crustal thickness variations

across the subprovinces generates southward flow. However, workers have shown that crustal thickness variations must be accompanied by other buoyancy sources (e.g., mantle buoyancy) in order to drive deformation (Sonder and Jones, 1999; Liu, 2001). In this model, buoyancy is enhanced by thermal and crustal input from the mid-Tertiary volcanic-magmatic belt. The model is similar to the Duebendorfer and Simpson (1994) model; however, the new observations and interpretations presented here suggest that the potential energy gradient across the Timpahute lineament would have been greater than that which may have existed across the LVVSZ. Nonetheless, the gradient across the LVVSZ probably helped to focus and localize shortening structures in that region.

In summary, tectonomagmatic rifting in the wake of the southward migrating volcanic belt may have been able to generate north-south-directed extension along the Timpahute lineament, but could not have altered the stress field in a wide enough area to generate contractional structures in the Lake Mead area. However, the close timing of formation of these structures and their similar orientations suggests that they may be connected by regional processes. Therefore, north-south-directed extension along the Timpahute lineament was probably accompanied by southward gravitationally-driven flow in the middle to lower crust. This flow was induced by a marked contrast in gravitational potential energy across the Timpahute lineament, generated by differences in extensional strain and magmatism between the northern and central Basin and Range.

CHAPTER 9

SUMMARY AND CONCLUSIONS

The geometry, kinematics, and timing relations among faults and folds in the Mount Irish and eastern Timpahute ranges reveal several distinct deformational episodes. They include a period of Mesozoic contraction, and as many as four Cenozoic extensional episodes, including: prevolcanic (pre-27 Ma), synvolcanic (~27-18 Ma), postvolcanic Miocene (?), and postvolcanic Miocene (?)-Pliocene or Quaternary extension.

The oldest structures documented in these ranges are prevolcanic folds that are developed in Paleozoic rocks. The folds lie in the upper plate of the Mount Irish thrust, one of several north-striking, steeply dipping thrust faults that define the Mesozoic central Nevada thrust belt (CNTB). Faults and folds related to the CNTB are well documented in these ranges, as well as in ranges to the north and south.

Prevolcanic folds are unconformably overlain by Oligocene-age lacustrine limestone and conglomerate. The basin-fill deposits are interpreted to have accumulated in a closed (?) basin that formed as the result of late Eocene to Oligocene extension. This interpretation is supported by the wide distribution of basin-fill strata of similar age and stratigraphy, the great thickness of the Tertiary section in these ranges, and by documented prevolcanic extension in nearby ranges.

Rare synvolcanic faults in the map area are east-west-striking and accommodated

minor north-south-directed extension. The faults record a change in the regional stress field, from east-west-directed extension to north-south-directed extension. The faults are interpreted to have formed by the tectonomagmatic rift model (Bartley, 1989), wherein a shift in the regional stress field is related to the southward migration of the Tertiary volcanic belt.

Postvolcanic Miocene (?) faults along the Timpahute lineament are ~east-west-striking faults that accommodated north-south-directed extension. North-south-directed extension along the lineament is interpreted to have been accompanied by southward gravitationally-driven flow in the middle to lower crust. Flow was induced by a marked contrast in gravitational potential energy across the Timpahute lineament, generated by differences in extensional strain and magmatism between the northern and central Basin and Range. North-south-directed extension along the Timpahute lineament and southward crustal flow are interpreted to have ended at ~8 Ma when plate boundary conditions began to exert increasing control on the stress system and extension directions. The return to plate boundary driven stresses is documented in the Mount Irish and Timpahute ranges by Miocene (?) to Pliocene or Quaternary ~north-south-striking faults that cut the ~east-west-striking Crescent Spring fault zone.

Data from this and other studies in the region demonstrate that the Timpahute lineament is a long-lived, broadly defined transverse zone that has been accommodating differences in the magnitude, timing, location, and direction of extension since the late Eocene to Oligocene. Consequently, simple transverse structure models (e.g., transfer zone and accommodation zone) that have been applied to many continental rifts (e.g., East African rifts) fail to describe the complex history of the Timpahute lineament.

(a) E-W-Trending Lineaments

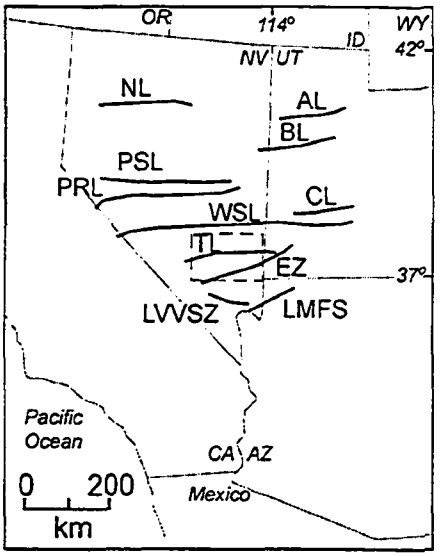

(b) Tectonic Provinces and Subprovinces

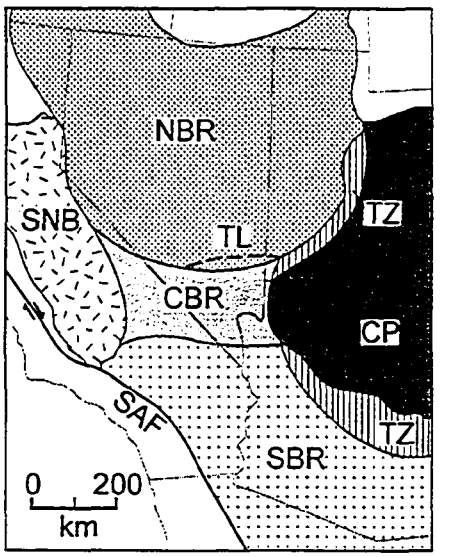

(c) Mesozoic Thrust Belts

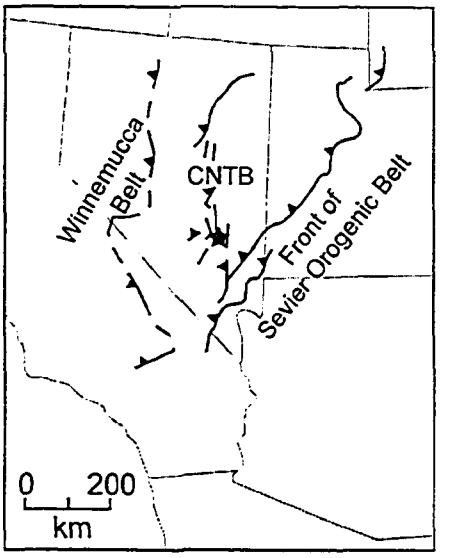

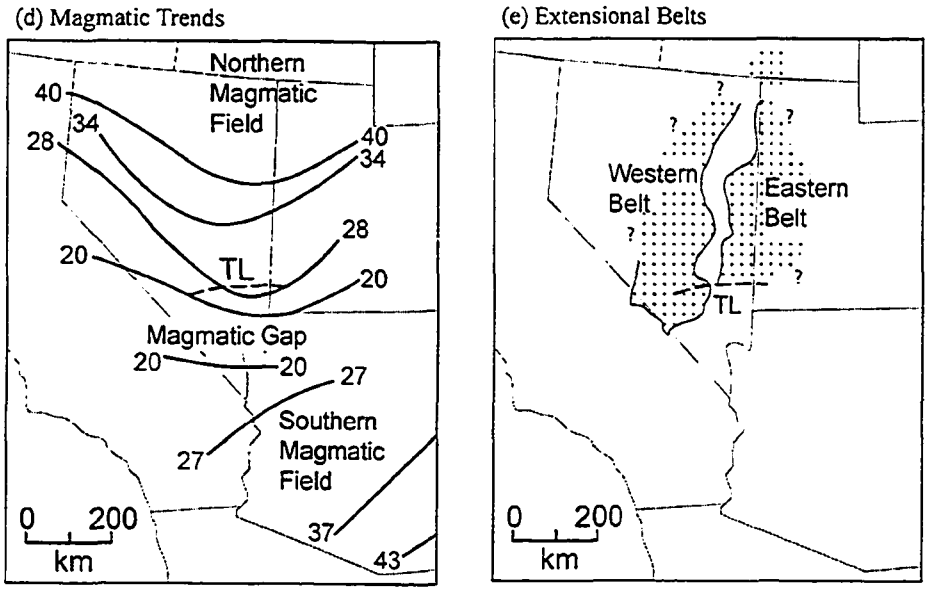

Figure 1. Tectonic setting in the vicinity of the Mount Irish and Timpahute ranges. (a) Map of Nevada and adjacent states showing the locations of major east-west-trending lineaments, zones, and systems. AL—A lineament; BL—B lineament; CL—C lineament; EZ—Escalante zone; LVVSZ—Las Vegas Valley shear zone; LMFS—Lake Mead fault system; NL—N lineament; PSL—Pritchards Station lineament; PRL—Pancake Range lineament; WSL—Warm Springs lineament; TL—Timpahute lineament. Dashed box shows the area of figure 2. Modified from Taylor and Switzer (2001). (b) Map of major tectonic provinces and subprovinces of the western U.S. Note that the Timpahute lineament (TL) lies near the transition from the northern Basin and Range to the central Basin and Range as defined by Wernicke (1992). This transition is marked by changes in topography and basinal elevations, and differences in the magnitude, timing and direction of extension. CBR—central Basin and Range; CP—Colorado Plateau; NBR—northern Basin and Range; SAF—San Andreas fault; SBR—southern Basin and Range; SNB—Sierra Nevada block; TZ—Basin and Range/ Colorado Plateau transition zones. Modified from Wernicke (1992). (c) Map showing the locations of Mesozoic thrust belts. The Mount Irish and Timpahute ranges lie at the eastern margin of the central Nevada thrust belt (CNTB). East-vergent folds and thrusts related to the CNTB crop out within these ranges. Modified from Taylor and Switzer (2001). (d) Tertiary magmatic trends (Ma). Southward and northward migration of Tertiary magmatism through the Basin and Range define two magmatic fields. These magmatic fields are separated by a magmatic gap near the latitude of Las Vegas. The Timpahute lineament lies near the southern boundary of the northern magmatic field. Figure modified from Faulds et al. (2001). (e) Late Eocene to Oligocene extensional belts in the Great Basin. From Axen et al. (1993). The eastern extensional belt is well-defined by faults of the east-directed Snake-Stampede detachment system. The western extensional belt, however, is poorly defined and is mostly inferrred by scattered prevolcanic faults and late Oligocene basin-fill strata.

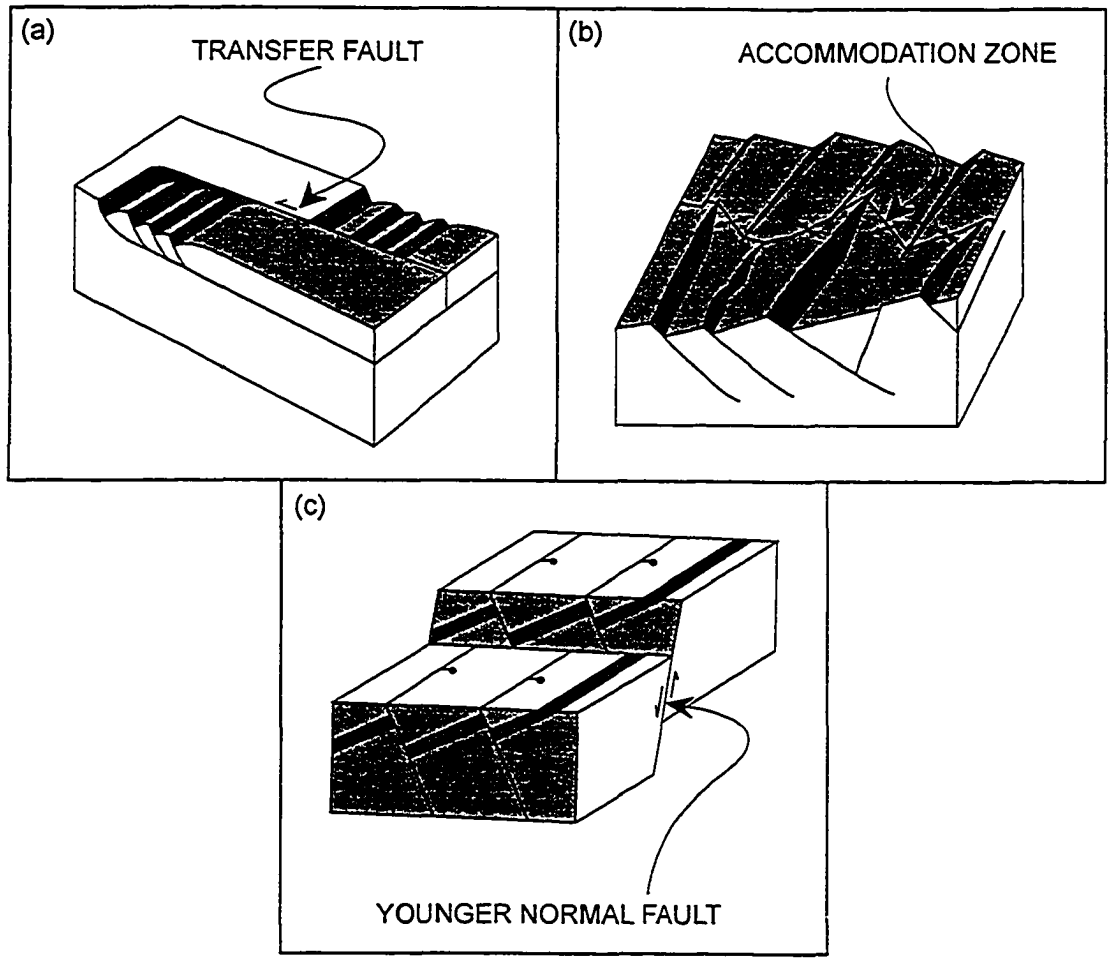

Figure 2. Three models for the development of transverse structures. (a) Transverse structures may be transfer faults. Transfer faults are physical and kinematic links between normal fault systems that shift strain across areas undergoing coeval extension. Note that the slip sense of the transfer fault is dependent on the motion of normal faults across the zone. Though transfer faults are predominantly strike-slip faults, segments may include normal, reverse, and/or oblique motion. (b) Transverse zones may be accommodation zones that lack a fault and transfer strain between overlapping systems of normal faults. Antiformal and synformal welts, and relay ramps commonly develop along the zone. (c) A normal fault cuts and offsets an older normal fault set. In this scenario, the transverse fault is younger than the faults it offsets and represents a change in extension direction. Transfer fault and accommodation zone models are modified from Faulds and Varga (1998). Normal fault model is modified from Williams (2000).

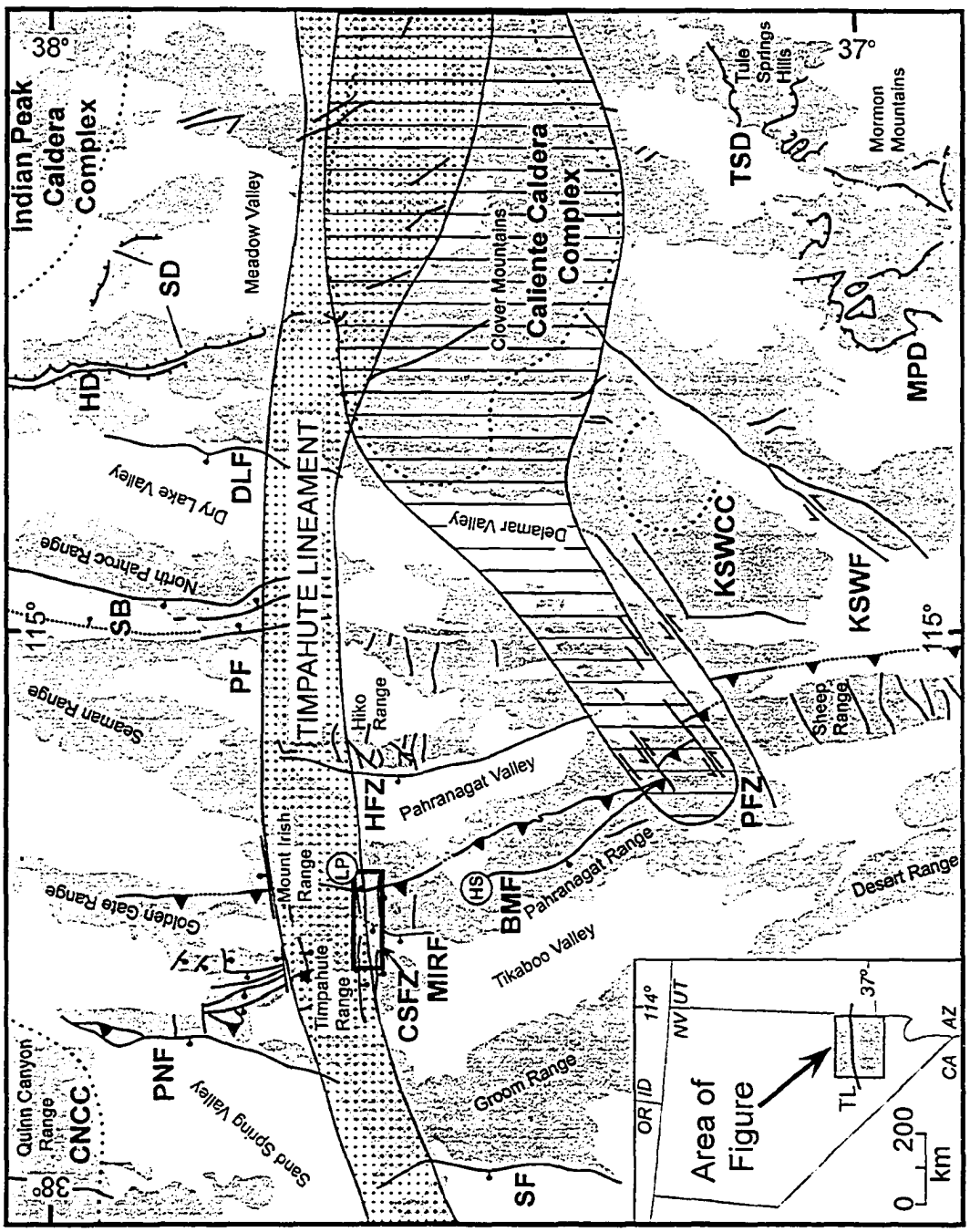

Figure 3. Location map with ranges (gray), valleys (white), and major structural elements and trends. Approximate boundaries of Tertiary calderas are dotted. Stipled area shows the Timpahute lineament boundaries as defined by Ekren et al. (1976). Ruled pattern shows western and central part of the Caliente Enterprise zone of Axen (1998) and Hudson et al. (1998). BMF—Badger Mountain fault; CNCC—Central Nevada caldera complex; HFZ—Hiko fault zone; HS—Hancock Summit; KSWF—Kane Springs Wash fault; LP—Logan Pass; PFZ—Pahranagat fault zone; PF—Pahroc fault; PNF—Penoyer fault; MIRF—Mount Irish Range fault; MPD—Mormon Peak detachment; SB—Seaman breakaway fault; SD—Stampede detachment; SF—Stumble fault; and TSD—Tule Springs detachment. Black rectangle corresponds to the approximate study area boundary and area of Figure 10.

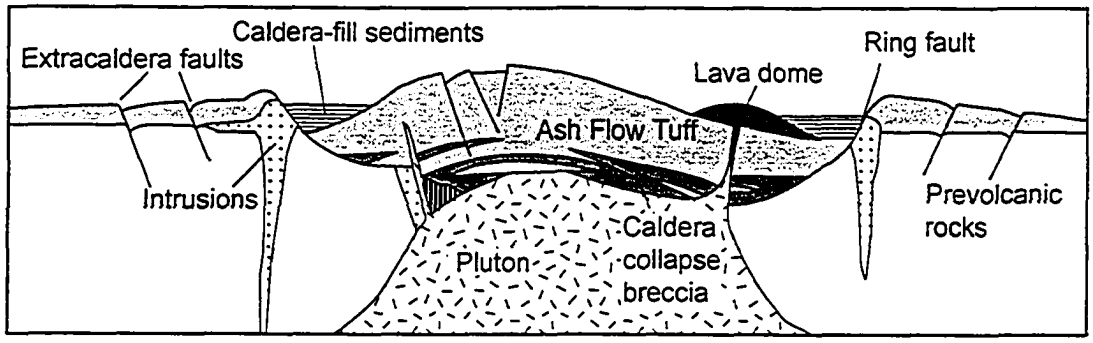

Figure 4. Schematic diagram of the major elements of a collapsed caldera. Modified from Lipman (1984). In the synvolcanic faulting model of Best and Christainsen (1991), faults that develop during caldera collapse are restricted to the area near a collapsed caldera and may have a range of orientations.

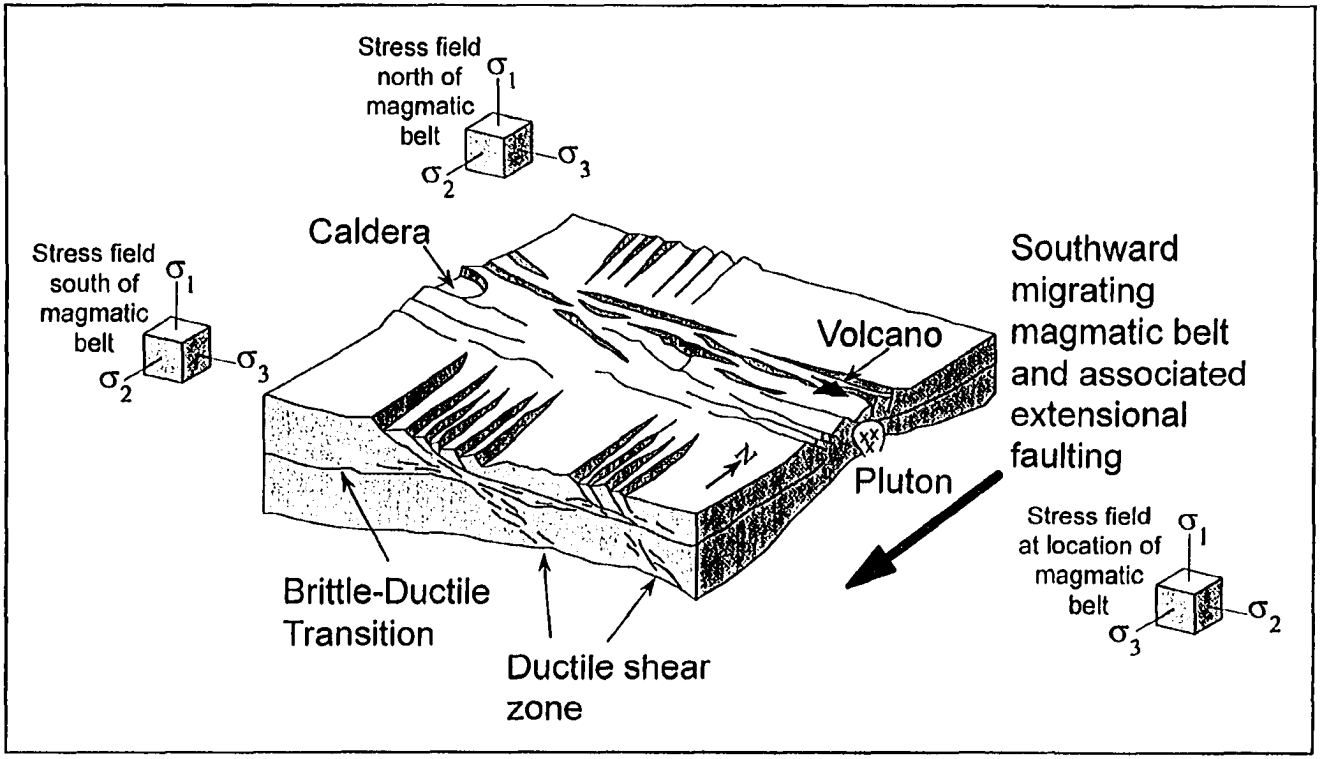

Figure 5. Tectonomagmatic rift model used to explain the development of synvolcanic faults that are approximately perpendicular to north-south-trending extensional belts (Bartley, 1989; Overtoom and Bartley, 1996). In this model, the southward migration of the mid-Tertiary magmatic belt into a region causes thermal uplift and weakening of the crust. Consequently, the area occupied by the magmatic belt experiences a regional shift in the stress field (horizontal principal stress directions rotate ~90°) and east-west-striking faults form parallel to the magmatic belt. Figure from Taylor and Switzer (2001); modified from Bartley (1989) and Overtoom and Bartley (1996).

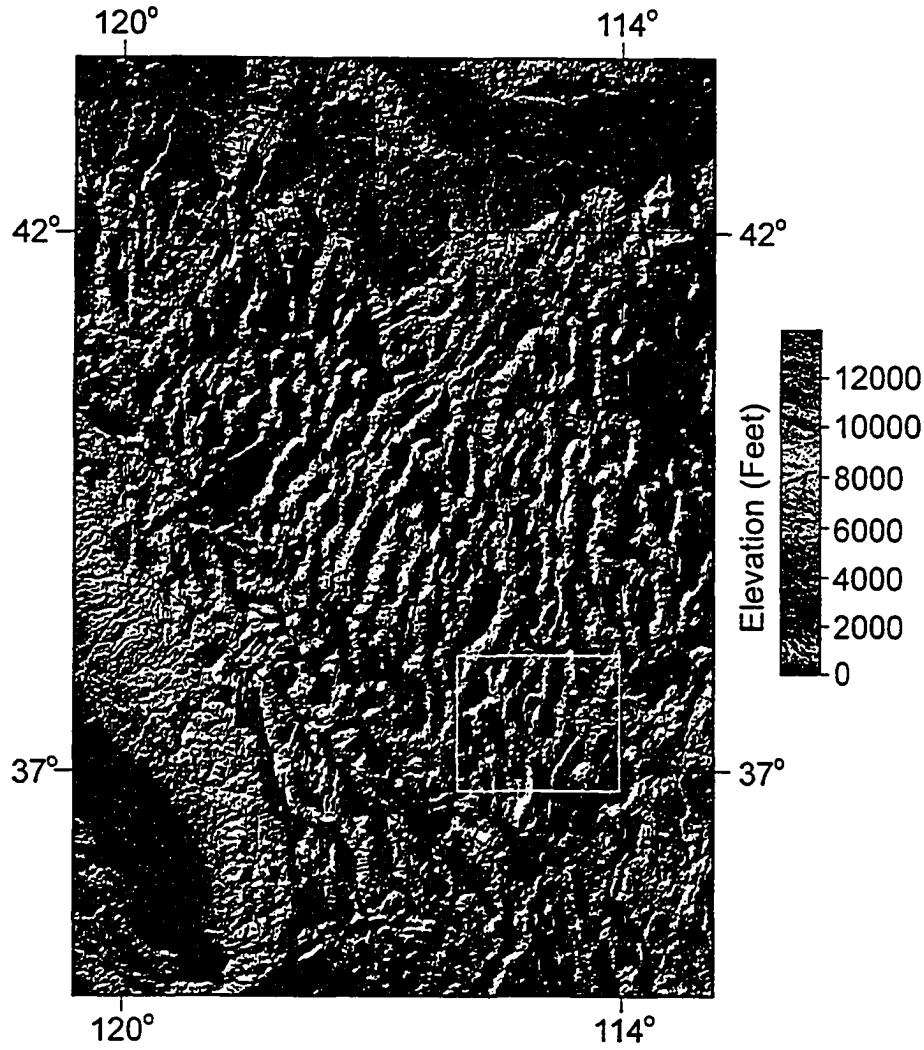

Figure 6. Digital elevation model of Nevada and adjacent states with northwest illumination showing topographic gradient south of the Timpahute lineament. White box corresponds to the area of Figure 3. Cylindrical equidistant projection, shape corrected for 37.5°N latitude. The elevation data has 1/2 arc minute horizontal resolution and 20 feet vertical resolution. Digital elevation tiles are from Sterner (1995) and digital mosaic is from Birrell (1994).

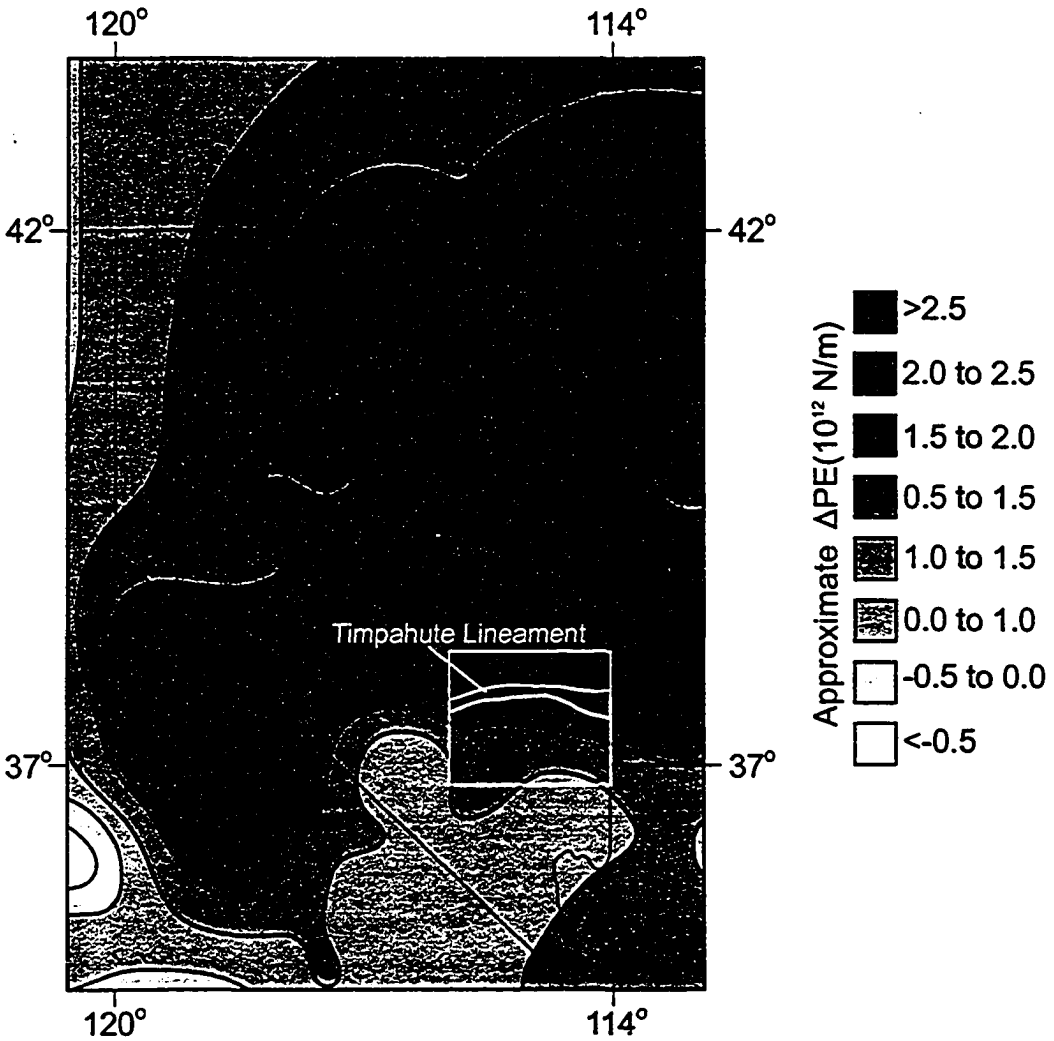

Figure 7. Change in gravitational potential energy distribution across Nevada and adjacent states. White box corresponds to the area of Figure 3. Potential energy is calculated relative to an asthenospheric reference column. The Timpahute lineament lies at the transition from high potential energy in the northern Basin and Range and relatively low potential energy to the south in the central Basin and Range. Figure modified from Sonder and Jones (1999), after Jones et al. (1996).

Figure 8. Generalized Paleozoic stratigraphy of the Mount Irish thrust plate. Stratigraphic thicknesses are based on the exposed maxiumum thickness in the study area. Where upper and/ or lower contacts are not exposed (e.g., Pogonip Group, Joana Limestone, etc.), thicknesses are based on regional studies (e.g., Tschanz and Pampeyan, 1970; Taylor et al., 2000). Standard lithologic patterns are used. Filled ovals are chert nodules.

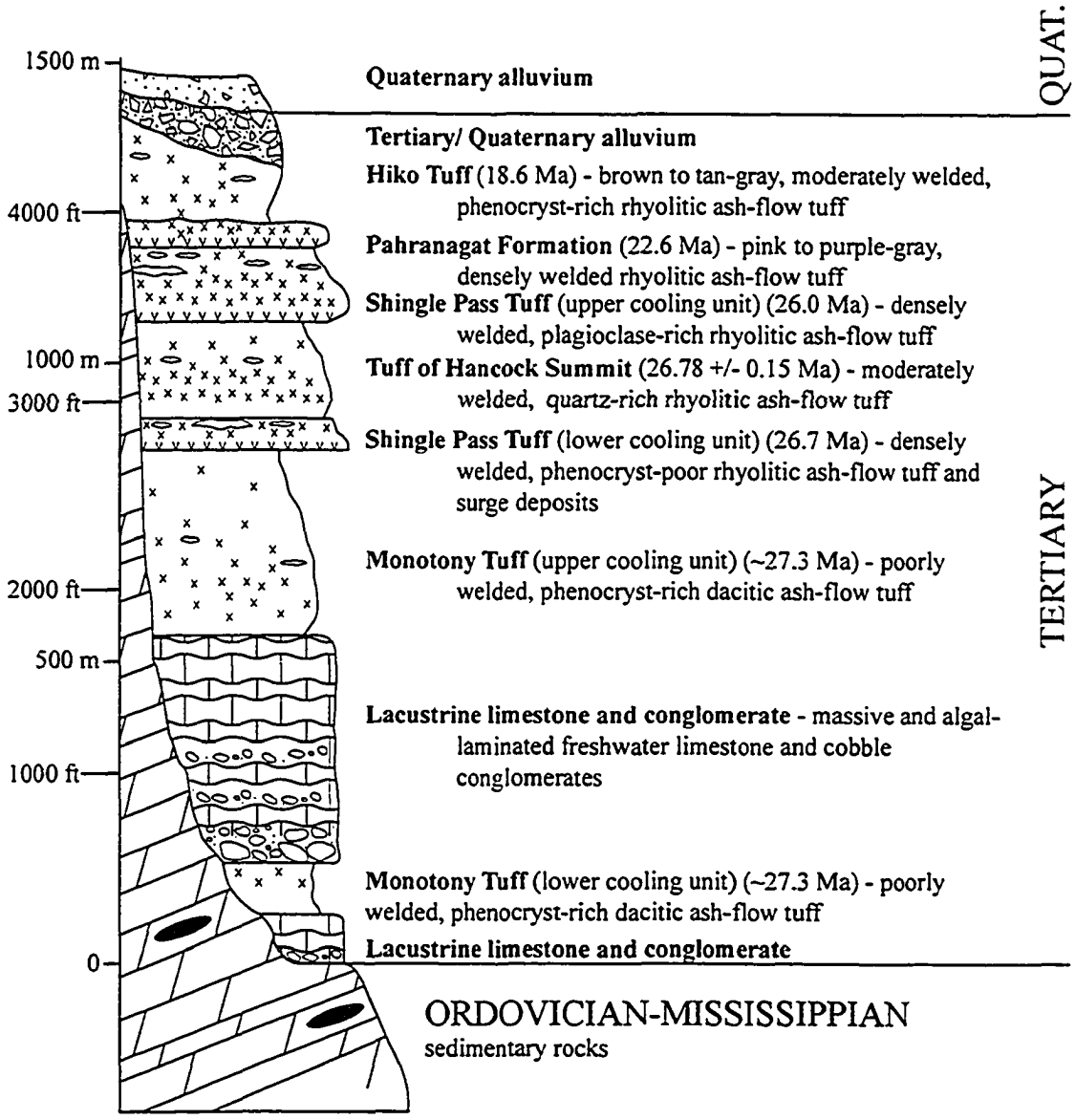

Figure 9. Generalized Cenozoic stratigraphy of the Mount Irish and Timpahute ranges. Stratigraphic thickness is based on maximum exposed thickness in the study area. Standard lithologic patterns are used for most units. Degree of welding is indicated by density of crosses in ash-flow tuff units. Irregular open ovals represent pumice fragments and fiamme. Age for the tuff of Hancock Summit is based on new $^{40}Ar/^{39}Ar$ geochronology (Appendix II). Age for the Pahranagat Formation is from Best et al. (1995). All other ages are from Best et al. (1993) and Scott et al. (1995).

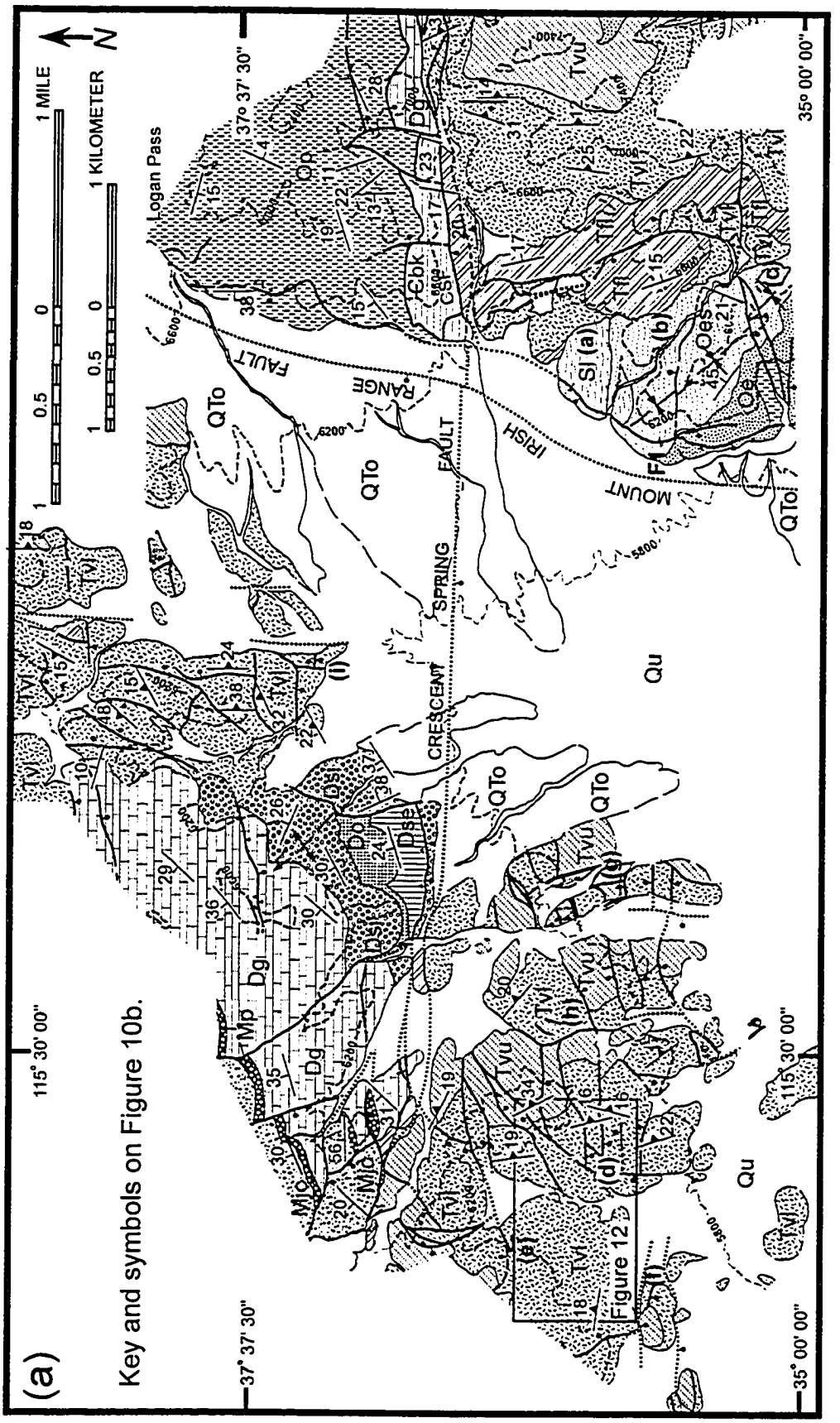

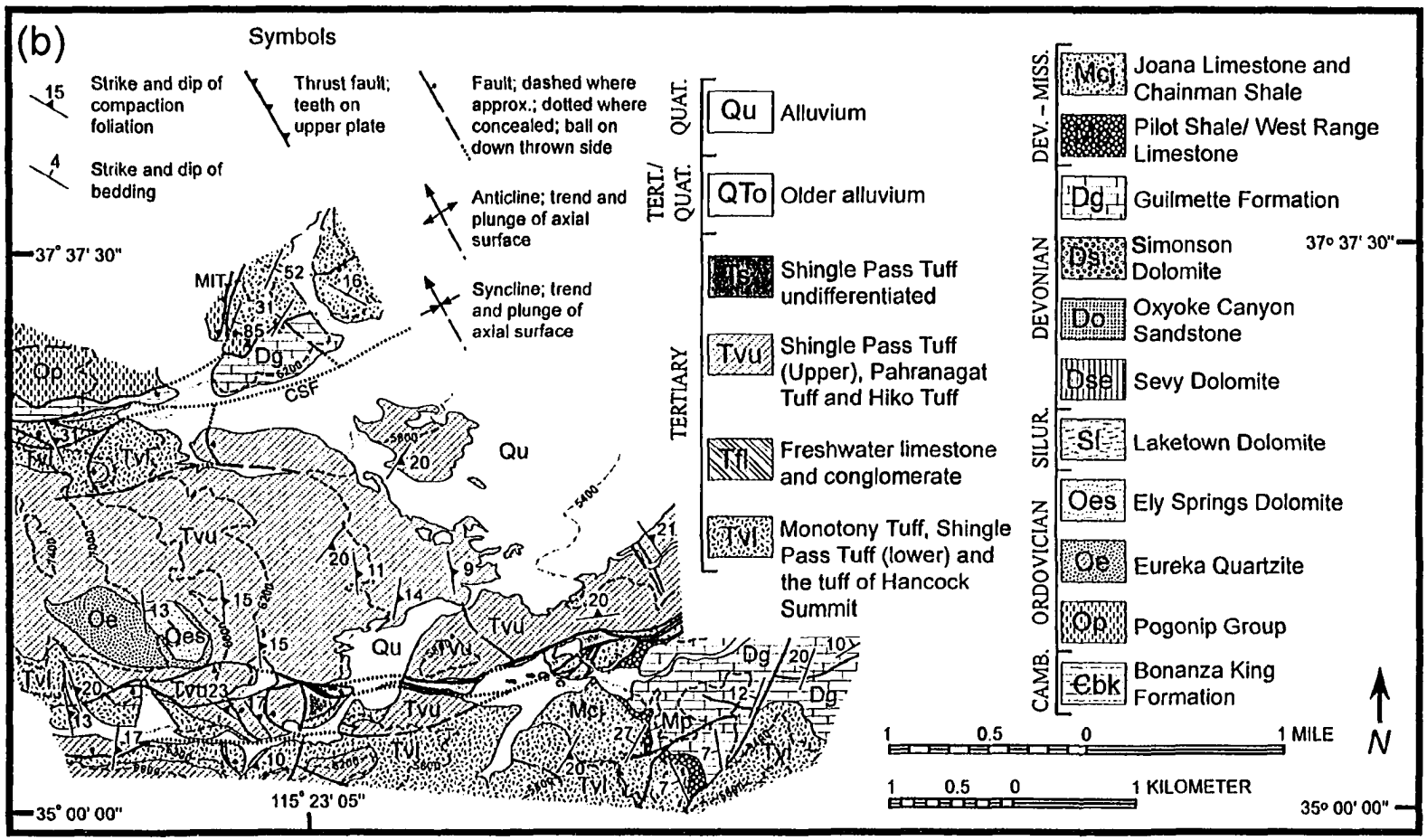

Figure 10. (a) Simplified geologic map of eastern Timpahute range and western Mount Irish range. (b) Simplified geologic map of the eastern side of the Mount Irish range. From W.J. Taylor, S. Mrozek, and T. Livingston (unpublished data). Both (a) and (b) were mapped at 1:24,000 scale. Map location on Figure 3.

Sub-Tertiary Unconformity

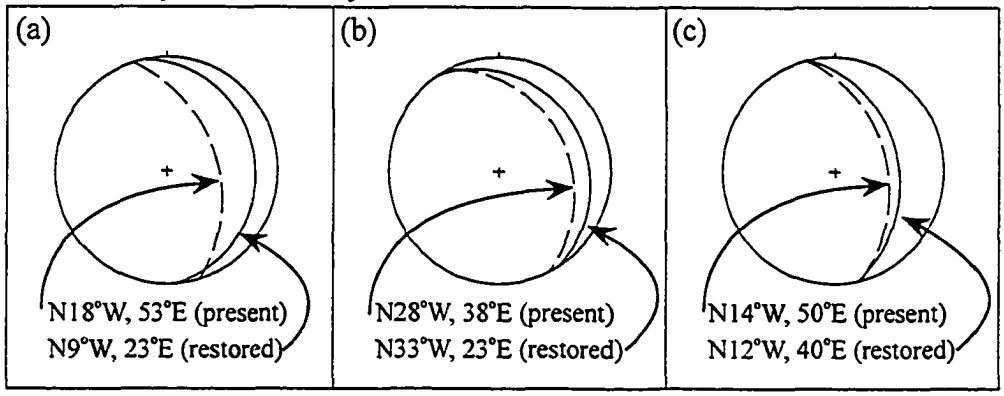

Figure 11. Stereonet plots (lower-hemisphere, equal-area projections) of the sub-Tertiary unconformity in its present (dashed) and pre-27 Ma (solid) orientations. Present unconformity geometries are based on structure contour data from three different locations in the southwestern Mount Irish Range (labeled a, b, and c on Figure 8 and Plate 1). (a) Unconformity is developed between Silurian Laketown Dolomite and the Monotony Tuff (lower cooling unit). The unconformity is rotated 31°W about a horizontal axis that trends N26°W. (b) Unconformity is developed between Ordovician Ely Springs Dolomite and Tertiary freshwater limestone and conglomerate. Unconformity was rotated 15°W about a horizontal axis that trends N19°W. (c) Unconformity developed between Ordovican Ely Spring Dolomite and the Monotony Tuff (lower cooling unit). Unconformity was rotated 10°W about a horizontal axis that trends N27°W.

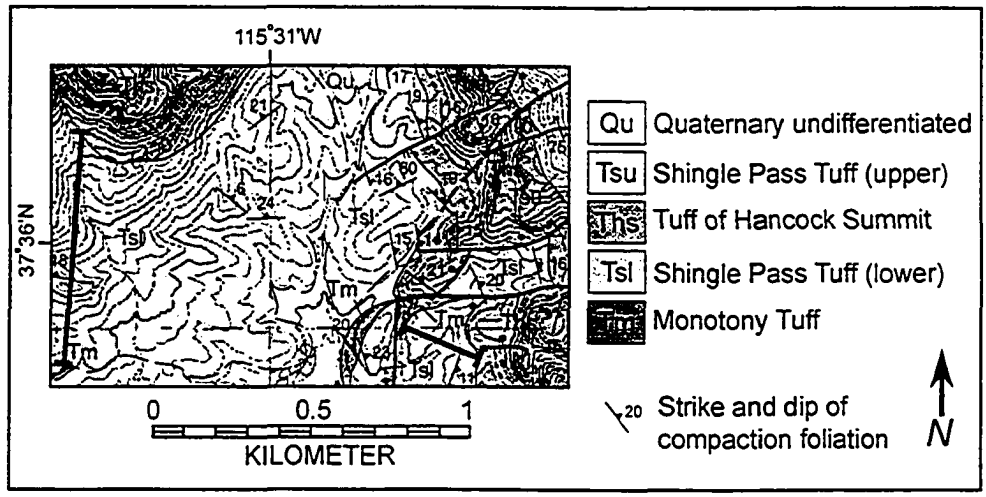

Figure 12. Geologic map of Tertiary volcanic rocks showing variation in the thickness (see heavy weight bars) of the Tertiary Shingle Pass Tuff (lower cooling unit). In the western part of this map, a thick (240 m; ~800 ft.) section of Tsl is exposed. This section thins to the east where the exposed thickness is reduced to 45 m (~150 ft). This difference in Shingle Pass Tuff thickness probably reflects paleotopography in the area. Standard geologic map symbols are used. Map area is outlined on Figure 8.

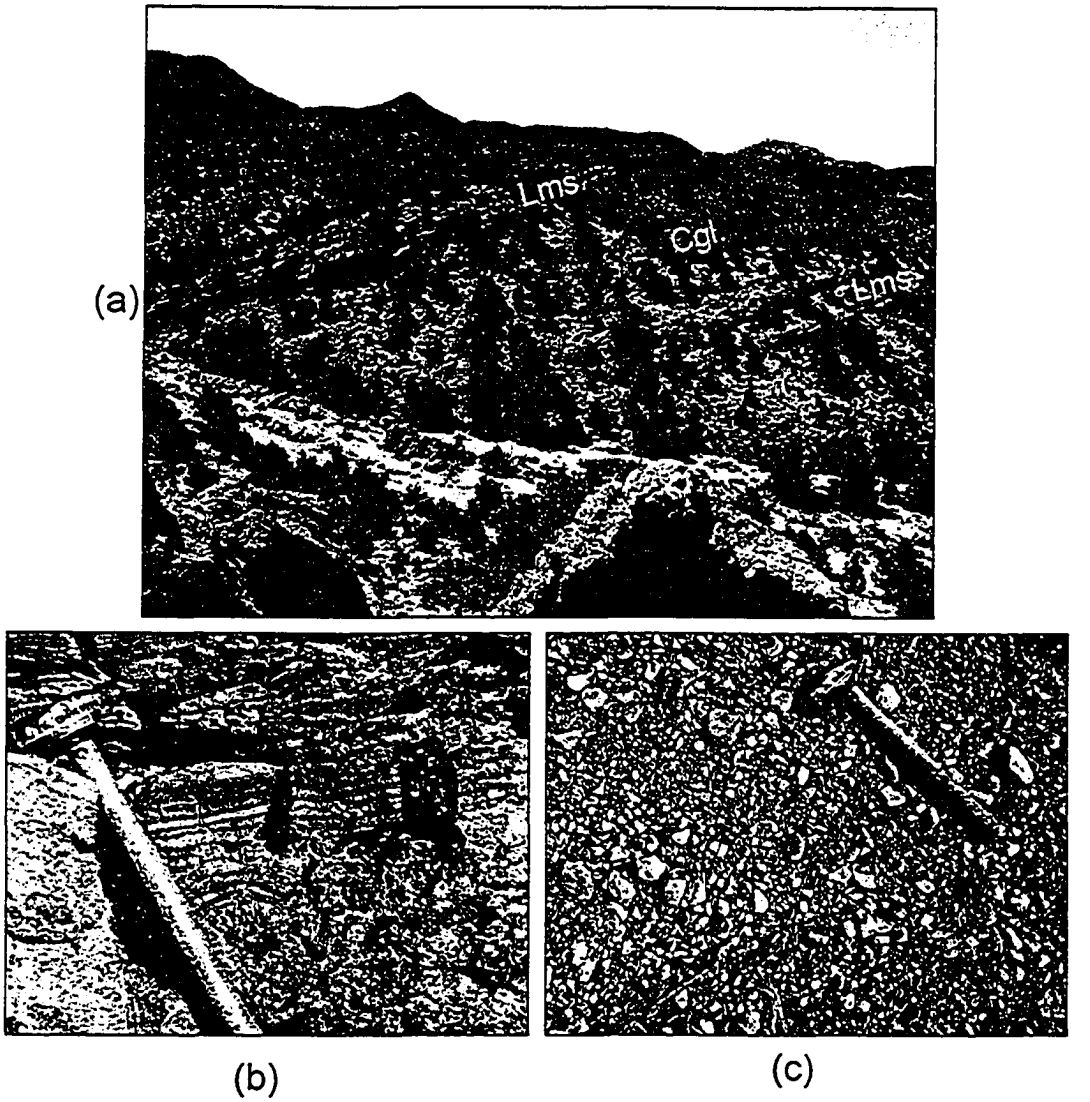

Figure 13. Tertiary basin-fill deposits. (a) View to the south-southeast of Tertiary lacustrine limestone and conglomerate. Notice that the limestone forms resistant ledges, while the conglomerate forms weak, easily eroded saddles. (b) Algal laminations and mound (low center of photo) within lacustrine limestone. (c) Pebble-conglomerate within lower part of basin-fill section.

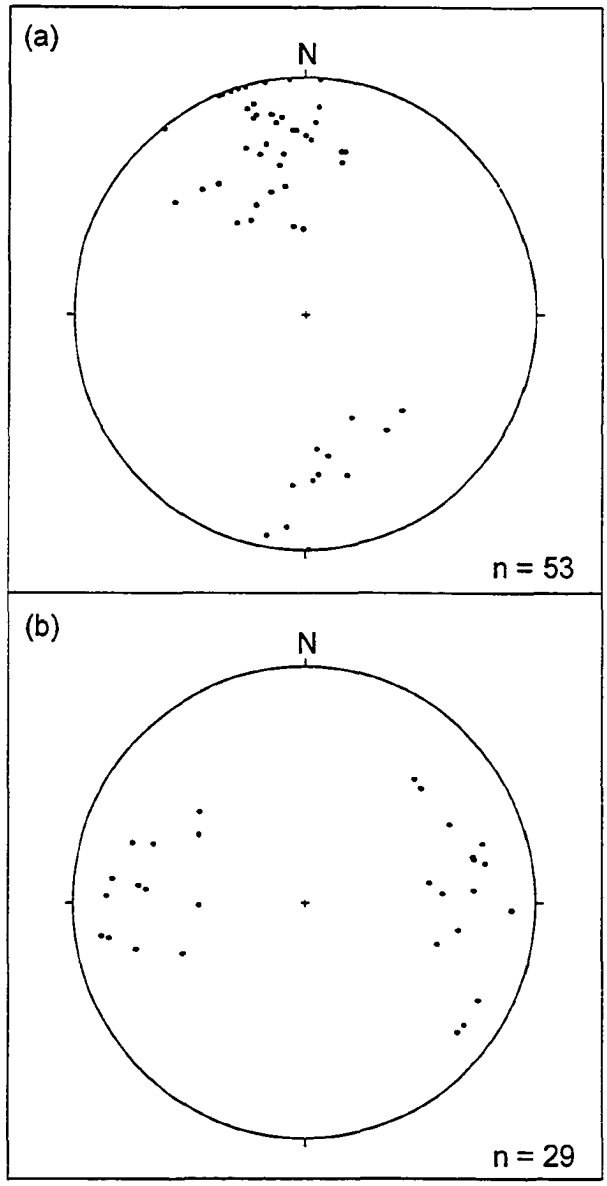

Figure 14. Lower hemisphere equal-area projections of poles to (a) ~east-west-striking and (b) north-south-striking faults. Stereoplots were made using Stereonet v. 1.2. (Allmendinger, 2002a). Structural data used to create stereoplots are listed in Table 1, Appendix II.

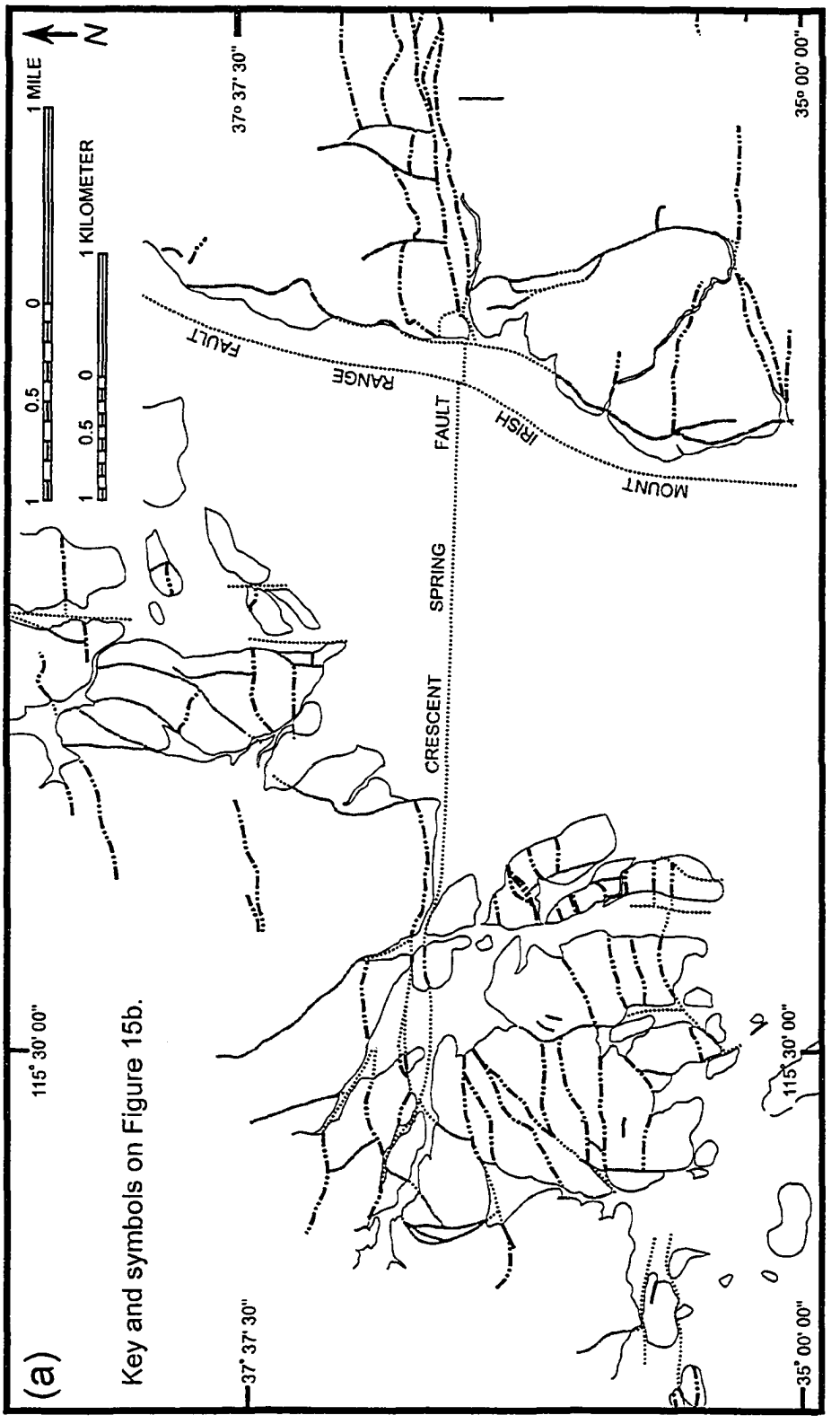

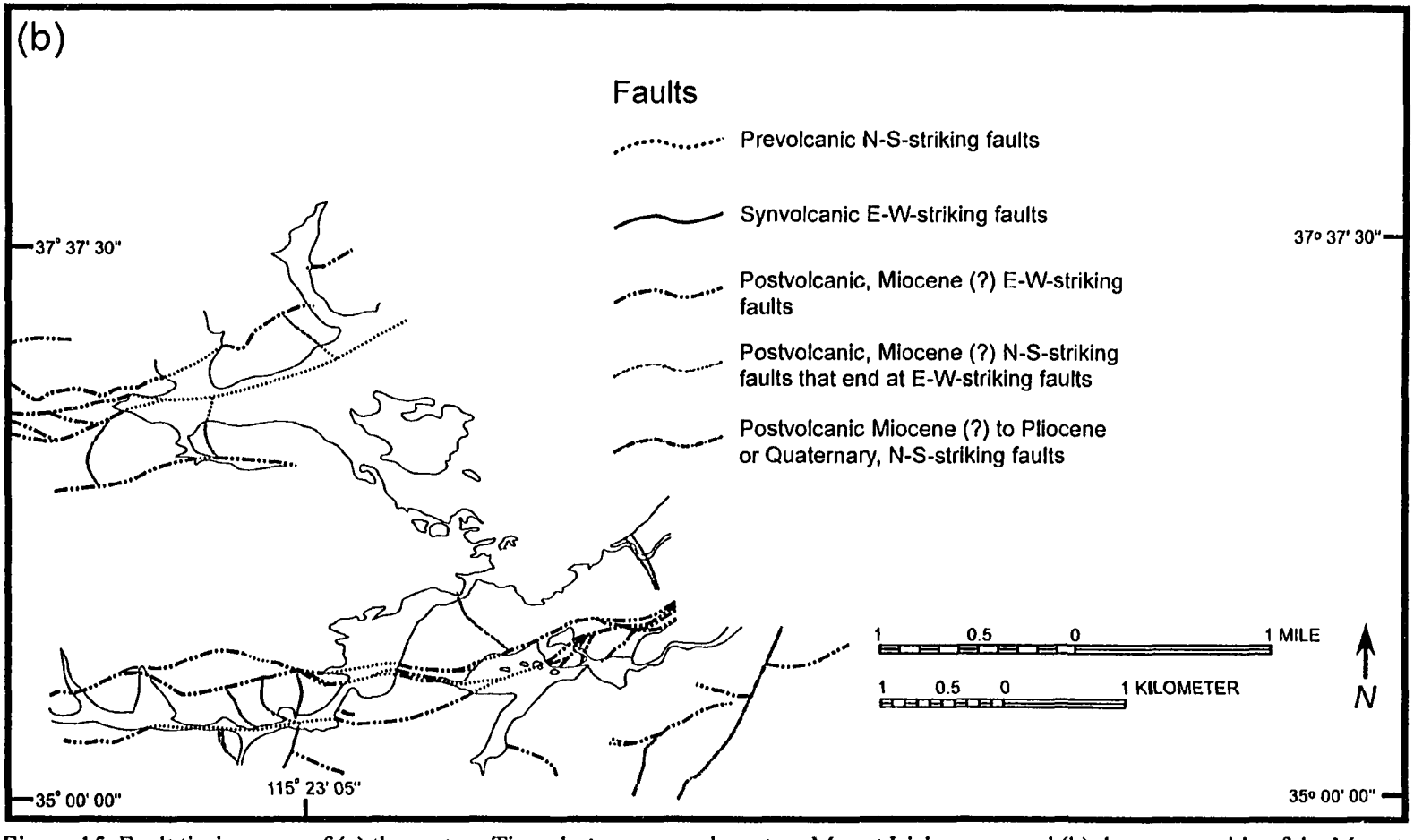

Figure 15. Fault timing map of (a) the eastern Timpahute range and western Mount Irish range, and (b) the eastern side of the Mount Irish Range.

Crescent Spring fault (CSF)

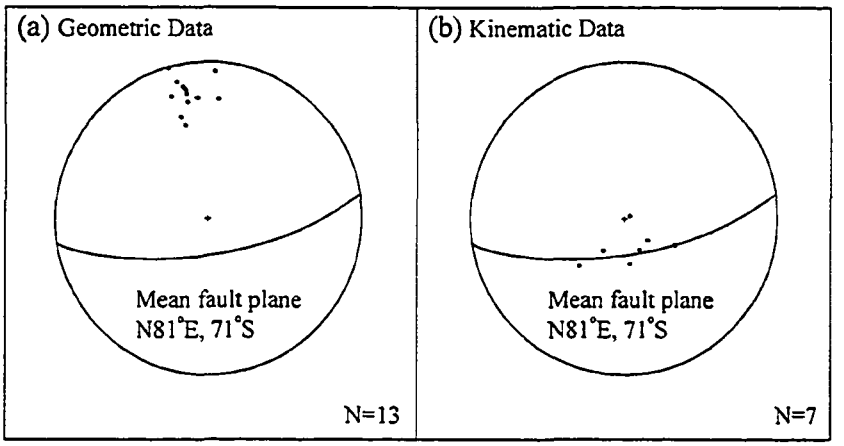

Figure 16. Lower hemisphere equal-area projections of geometric and kinematic data collected along the Crescent Spring fault (CSF) in the eastern Timpahute and western Mount Irish ranges. (a) Poles to measured fault surfaces define a mean fault plane of N81°E, 71°S for the CSF. (b) Kinematic data from the CSF indicate dominantly dip-slip fault motion. These data, combined with the stratigraphic separation across the fault, indicate the CSF is a normal fault. Data used to create stereoplots are listed in Table 1, Appendix II.

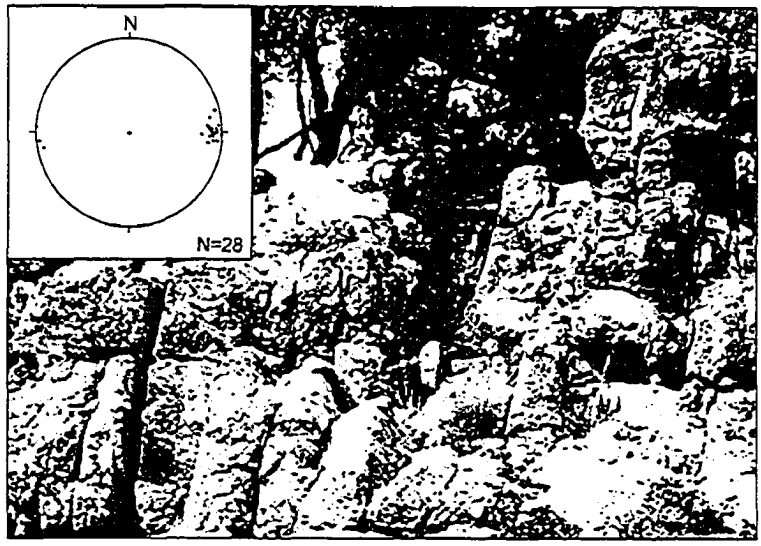

Figure 17. View to the north-northwest of Mode I fractures developed within jasperoid breccia that has formed along the Crescent Spring fault. Stereoplot shows poles to fracture surfaces. Data used to create stereoplot are listed in Table 1, Appendix II.

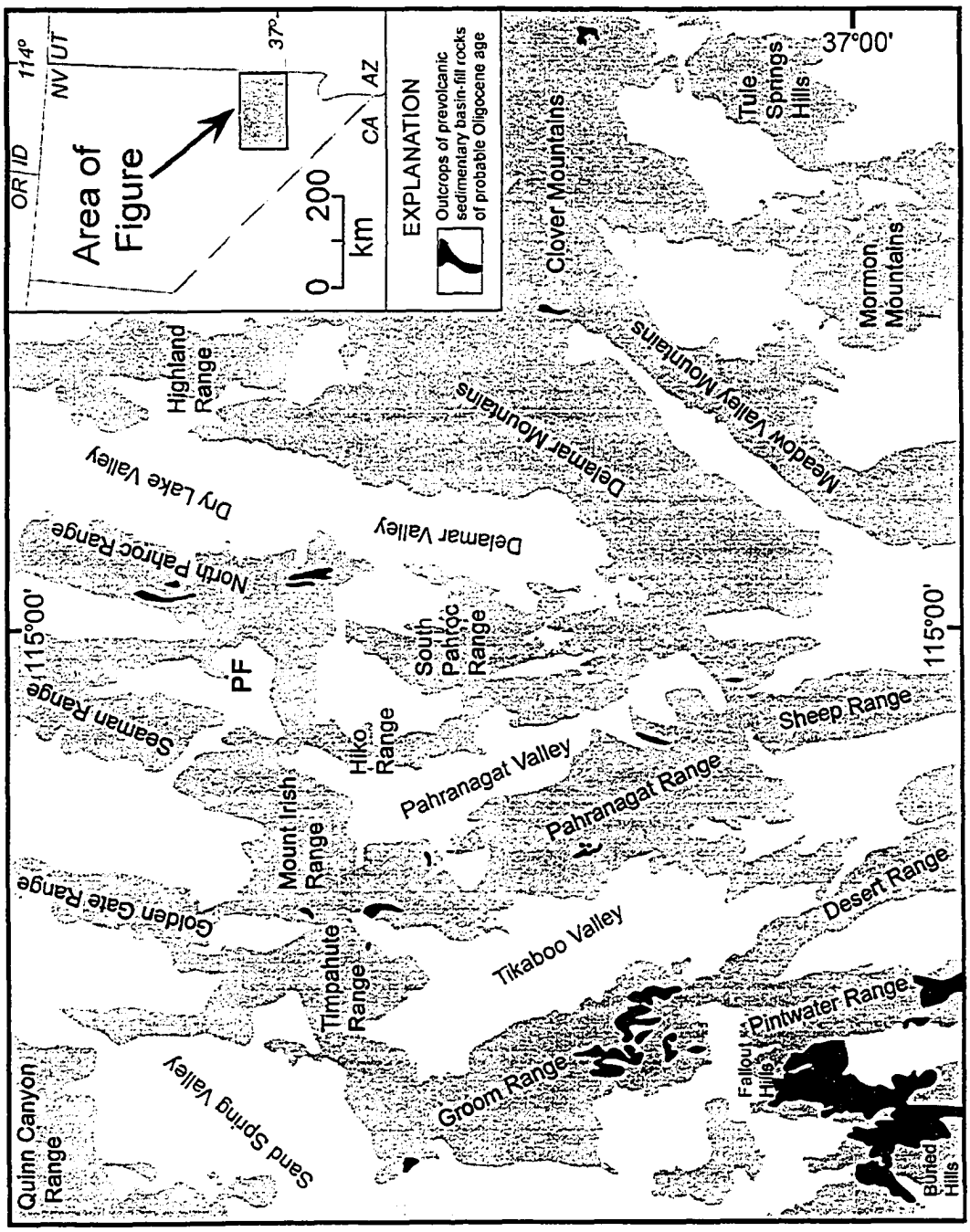

Figure 18. Outcrops of prevolcanic basin-fill deposits of probable Oligocene age. Exposed deposits primarily consist of cobble conglomerate and freshwater limestone. Adapted from Tschanz and Pampeyan (1970) and Ekren et al. (1977). Inset map of Nevada and adjacent states shows figure area.

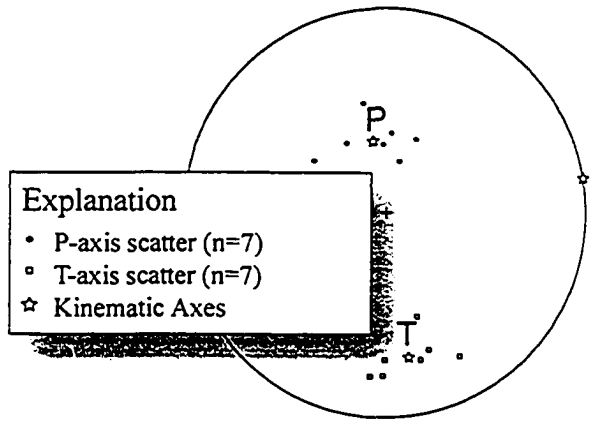

Figure 19. Lower hemsiphere equal-area projection of P (shortening) & T (extension) axes derived from CSF kinematic data. The plot, generated in FaultKin version 1.1 (Allmendinger, 2002b), provides a qualitative assessment of the regional kinematic axes for this fault. These data may imply that extension related to the CSF was in a ~N-S direction.

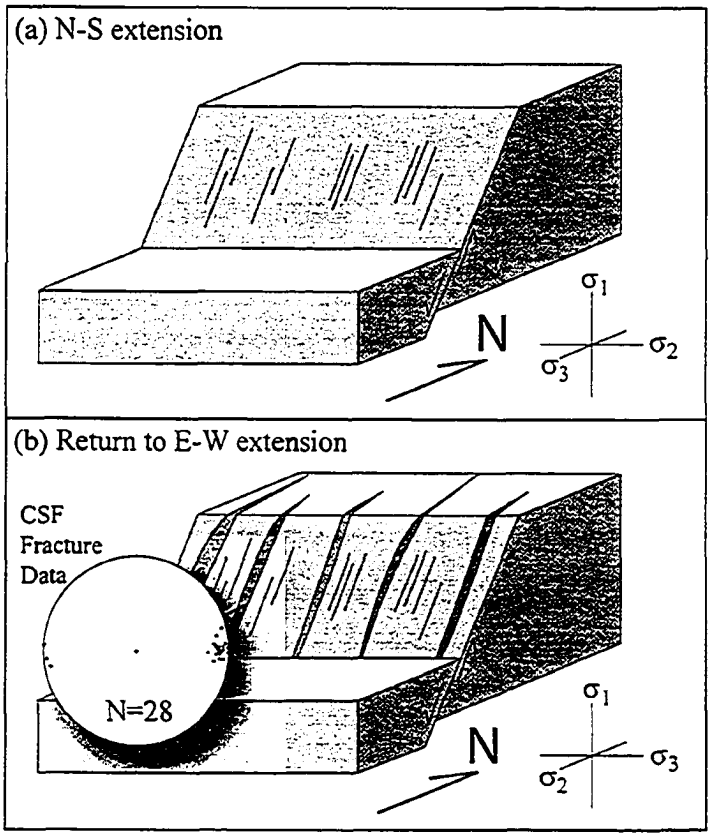

Figure 20. (a) N-S-directed extension along the CSF produces dip-slip kinematic indicators. (b) Mode I fractures concentrated in jasperoid breccia that formed along the trace of the CSF. Stereoplot shows poles to fracture surfaces measured in the western Mount Irish Range. These fractures may record a return to E-W-directed extension, following N-S-directed extension.

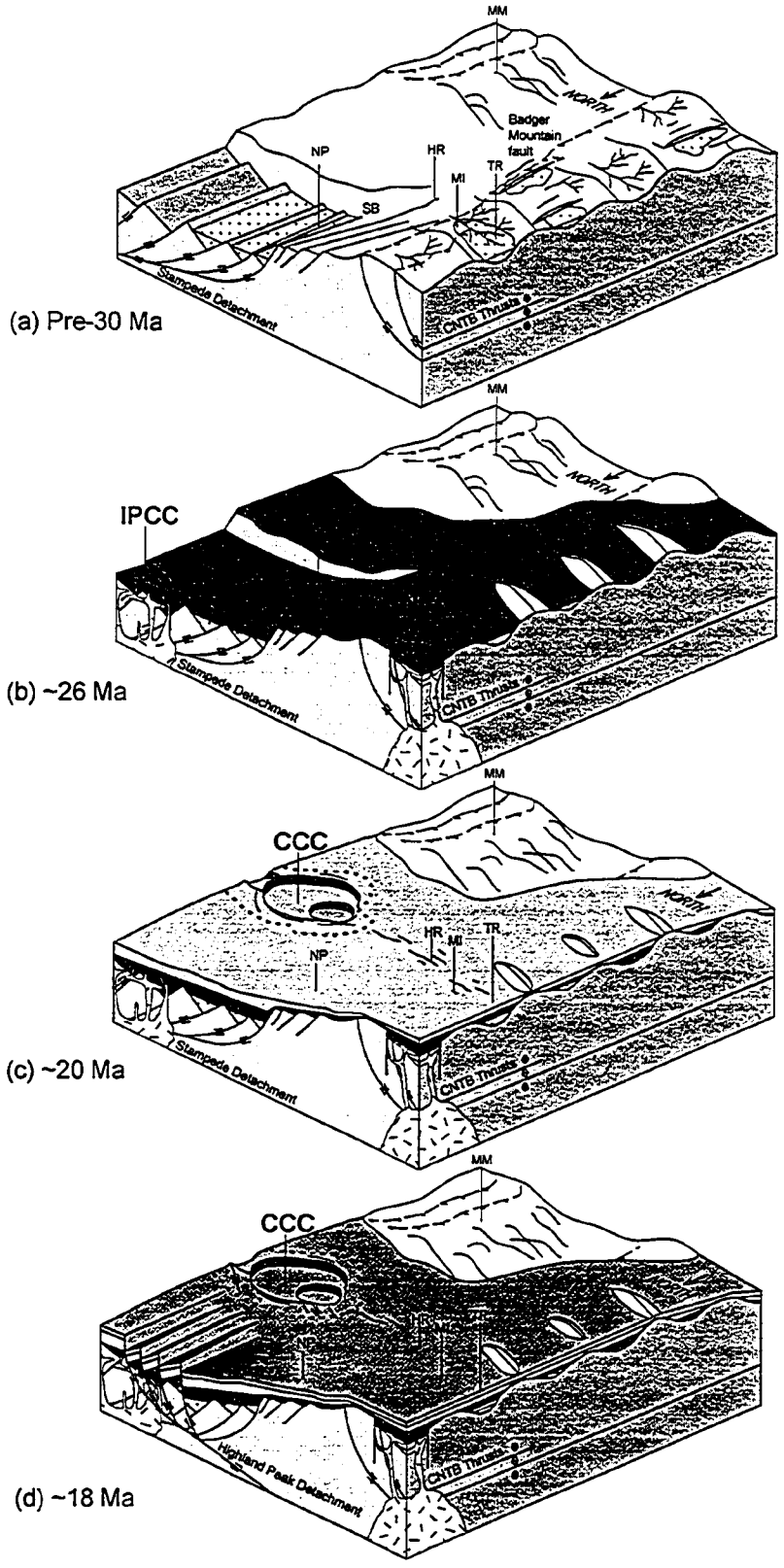

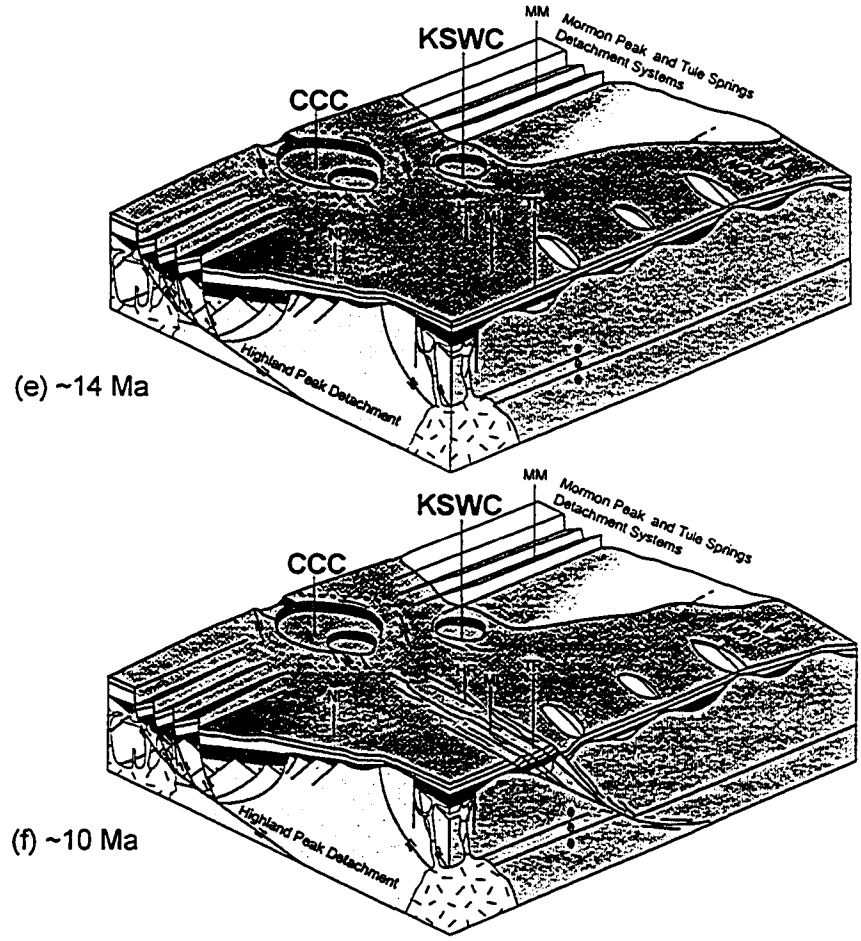

Figure 21. Schematic reconstruction of eastern Great Basin in the area of the Timpahute lineament from the late Oligocene to the late Miocene. (a) The prevolcanic (pre-30 Ma) period is characterized by activity along the Snake-Stampede detachment system and scattered prevolcanic faults (e.g., Badger Mountain fault) and related basin development. The Timpahute lineament is represented as a rift-margin transfer fault at this time. (b) Prevolcanic faults are covered by ash-flow tuffs erupted from the Central Nevada caldera complex (CNCC) and Indian Peak caldera complex (IPCC). (c) By ~20 Ma the volcano-magmatic belt migrates into the area of the Timpahute lineament forming the Caliente caldera complex (CCC). Minor synvolcanic east-west-striking faults develop along the lineament. (d) At ~18 Ma the Highland Peak detachment system extends the area north of the lineament. (e) Extension south of the lineament initiates along the Mormon Peak and Tule Springs detachment systems. The Kane Springs Wash caldera complex (KSWC) also develops at this time. (f) By 10 Ma, caldera systems along the Timpahute lineament shut down. However, a strong thermal anomaly still exists in the area and postvolcanic north-south-directed extension initiates in the Mount Irish, Timpahute and Hiko ranges. HR—Hiko Range; MI—Mount Irish Range; MM—Mormon Mountains; NP—North Pahroc Range; TR—Timpahute Range.

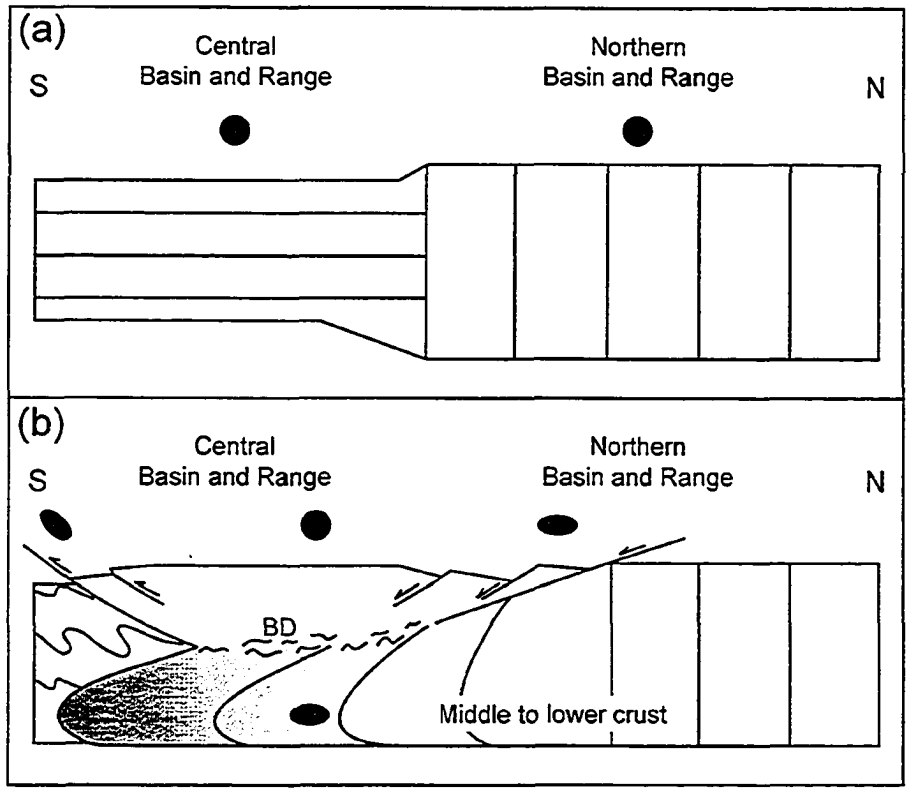

Figure 22. Regional tectonic model. Schematic cross sections across the northern and central Basin and Range (a) prior to and (b) following N-S-directed extension along the Timpahute lineament and gravitationally-driven middle to lower crustal flow. Black circles and ellipses show approximate strain field across the subprovinces. BD—Brittle-ductile transition. Figure modified from Rey et al. (2001).

APPENDIX I

METHODS

Geologic Mapping

In addition to the geologic mapping techniques presented in Chapter 4, I used Adobe Illustrator v. 10 to create a digital geologic map (Plate 1). Digital raster graphics (DRG) files of USGS standard series topographic maps were used as a digital base for the geologic map. The DRG's were made collarless and seamless in ArcMap v. 9.0. Map line weights, symbols, and colors follow the U.S. Geological Survey (USGS) publication standards (U.S. Geological Survey, 1999).

Three-Point and Structure-Contour Methods

Direct field measurement of fault surfaces was not possible in many cases because of poor preservation in certain rock types (e.g., poorly- or moderately-welded tuffs). Where fault surfaces could not be directly measured, I used the three-point and structure-contour methods to calculate fault orientations and geometries. These methods rely on the fact that a fault's orientation in space can be defined by two parameters, strike and dip. Two points of equal elevation along a fault surface trace define the strike. The fault dip or maximum inclination is perpendicular to strike. Figures 23 and 24 outline the basic elements of each technique.

Stereonet Analyses

R. Allmendinger's Stereonet v. 1.2.0 for Windows was used to generate stereonet plots, and calculate mean and mode fault orientations. Stereonets provide a convenient spherical coordinate system or grid for the analysis and graphical presentation of 3-D structural data.

R. Allmendinger's FaultKin v. 1.2.2 for Windows was used to calculate kinematic, P (shortening) and T (extension) axes and to make qualitative estimates of paleostress directions along the Crescent Spring fault. The program uses a seismological approach to fault kinematic analyses by assigning principal shortening and extension axes to each fault datum entered (Marrett and Allmendinger, 1990; Allmendinger, 2002b). The axes are then contoured to determine regional kinematic axes (Marrett and Allmendinger, 1990). The technique is a test of compatibility of faults in an established set because the fault orientations and axes are not averaged, and faults that formed under different stress regimes may produce multiple sets of kinematic axes (Marret and Allmendinger, 1990). More quantitative paleostress calculations could not be preformed because the area lacked the statistically appropriate number of contemporaneous faults ($n > 30$) and in many cases slip-sense data were unavailable (e.g., Angelier et al., 1985; Michel-Noel et al., 1990; Marrett and Allmendinger, 1990).

Cross-Section Construction

Standard line-length balancing techniques were used to construct six retrodeformable cross-sections (e.g., Dahlstrom, 1969; Nunns, 1991; Groshong 1994; Kerr and White, 1994). However, because many of the cross-sections do not meet the plane-strain

criterion of cross-section balancing (i.e., there was motion in and out of the plane of each cross-section), the cross-sections were made retrodeformable as a network of cross-sections. Subsurface information from individual cross-section lines were applied to or projected into the other cross-sections in the network. Thus, area was conserved in all cross-sections. Cross-sections aided in analysis of the type and amount of fault movement, in interpretation of the subsurface bedrock structure, and in understanding the three-dimensional distribution of strain in the region.

Point Counts

Samples of each ash-flow tuff exposed in the map area were collected for point count analyses. The point count data provide accurate estimates of the modal and volume proportions of different constituents within the tuffs, which may be used to properly correlate units to the regional stratigraphy (Table 2). The collected samples were cut into billets and made into standard petrographic thin-sections. Each thin section was counted on a mechanical stage using a fixed grid with nodes or points spaced 0.75 mm apart. This grid spacing was chosen because it is (1) close to or slightly wider than most of the phenocrysts in the thin section and (2) provided the best thin-section coverage. These two criteria help to minimize sample biases and errors. All thin sections were counted for 600 points per sample. The data were compared to data from the studies of Best et al. (1993), Scott et al. (1995), and Switzer (1996).

Geochronology

I collected a sample of the tuff of Hancock Summit for $^{40}Ar/^{39}Ar$ geochronology. The

sample was crushed and sieved to the 425 μm fraction. The 425 μm size fraction was chosen to obtain the largest number of single sanidine crystals possible. Sanidine crystals were hand picked under a binocular microscope and submitted to the Nevada Isotope Geochronology Laboratory (NIGL) for analysis.

Once at NIGL, sanidine separates were wrapped in Al foil, sealed in 6 mm diameter Pyrex vials and irradiated at the McMaster Nuclear Reactor at McMaster University, Ontario, Canada. In addition to the sample, neutron fluence monitors, K-glass and CaF_2 fragments were irradiated. The K-glass and Ca-F_2 were irradiated to correct for unwanted interference reactions. All correction factors are outlined in Table 2.

Isotope measurements were made at NIGL. Their procedure is outlined in Spell et al. (2001). The 27.9 Ma Fish Canyon Tuff sanidine flux monitor was used to calculate the sample age. All analytical data are reported at the 1 σ (standard deviation) confidence level. Isochron reliability is based on the mean square of weighted deviates (MSWD) criteria of Wendt and Carl (1991). All geochronologic data are presented in Appendix II, Table 2.

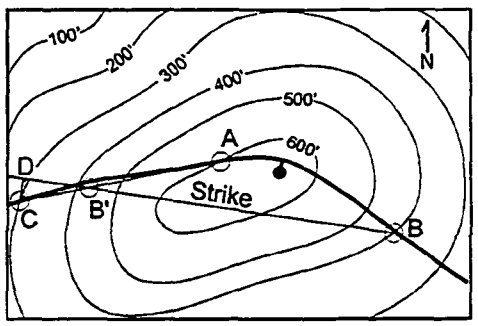

Figure 23. Example of a three-point method calculation of strike and dip on a hypothetical fault. In this method, fault orientation is determined by: (1) locating three points of different elevation along the surface trace of the fault (labeled A, B and C); (2) drawing a line connecting the highest point to the lowest point (line AC); (3) drawing a line connecting the intermediate point (B) to a point at its equivalent elevation (B') along line AC, which defines the fault strike (BB'); and (4) drawing a line perpendicular to strike that connects to the lowest elevation point (C). The location of B' is determined using the formula [(elevation of A - elevation of B) / (elevation of A - elevation of C)] * 100 = R, where R is the percentage of the line length AC measured away from A. The fault strike or azimuth can be directly measured from the map along line BB'. The fault dip can be calculated by taking the $\tan^{-1}$ of the difference in elevation between B and C divided by the horizontal map length of line CD.

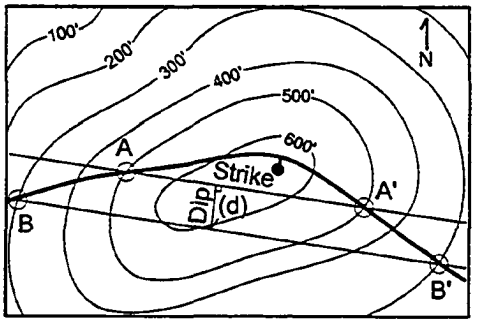

Figure 24. Structure-contour method for calculating fault orientation. In this method, fault orientation is determined by drawing structure contours or lines connecting points of equal elevation along the surface trace of a fault (e.g., lines AA' and BB'). The azimuth of the structure contour is the fault strike. The dip, which is perpendicular to strike, can be trigonometrically calculated by determing the change in elevation and the horizontal map distance (d) between structure contours and then calculating the $\tan^{-1}$ of the difference in elevation divided by (d).

APPENDIX II

ANALYTICAL DATA

Table 1. Structural data used to create stereonets within text. Structural data are presented using right hand rule (RHR).

E-W-striking faults (cf., Fig. 14a)

Fault	Azimuth	Dip (RHR)	Fault	Azimuth	Dip (RHR)
1	069	90	30	093	70
2	075	90	31	075	90
3	081	46	32	076	76
4	104	56	33	074	80
5	082	31	34	094	90
6	265	58	35	275	80
7	086	90	36	274	62
8	077	63	37	094	77
9	066	42	38	076	81
10	090	65	39	082	58
11	260	51	40	092	63
12	103	60	41	280	85
13	104	60	42	080	90
14	075	75	43	053	40
15	080	54	44	052	90
16	083	73	45	224	49
17	255	60	46	060	38
18	074	45	47	068	90
19	050	59	48	073	90
20	234	51	49	269	90
21	080	75	50	040	63
22	071	90	51	070	64
23	086	67	52	089	30
24	087	67	53	081	71
25	267	60			
26	074	60			
27	056	56			
28	245	40			
29	265	48			

Table 1. (continued)

N-S-striking faults (cf., Fig. 14)

Fault	Azimuth	Dip (RHR)
1	032	45
2	006	62
3	005	59
4	345	65
5	002	75
6	197	50
7	040	50
8	359	38
9	132	60
10	136	59
11	162	70
12	351	78
13	021	60
14	007	73
15	019	68
16	220	75
17	209	75
18	217	75
19	182	79
20	350	75
21	338	48
22	165	65
23	190	57
24	176	63
25	171	45
26	166	65
27	176	50
28	168	69
29	152	60

Fracture surfaces (cf., Figs. 17 and 20)

Fracture	Azimuth	Dip (RHR)
1	177	84
2	165	85
3	175	87
4	181	90
5	350	83
6	180	83
7	177	79
8	182	80
9	004	90
10	179	78
11	178	90
12	185	84
13	182	76
14	176	76
15	185	80
16	179	79
17	169	78
18	175	74
19	181	79
20	181	67
21	187	74
22	181	90
23	179	84
24	180	80
25	355	87
26	181	90
27	178	78
28	177	76

Table 1. (continued)

CSF Geometric Data
(cf., Figs 16 and 19)

Azimuth	Dip (RHR)
075	57
080	70
080	72
073	71
085	67
080	76
076	52
075	90
079	75
080	65
093	84
095	66
077	79

CSF Kinematic Data
(cf., Figs 16 and 19)

Azimuth	Dip (RHR)	Rake
080	70	66E
080	72	85E
073	71	60W
080	76	80E
075	90	87E
079	75	76W
095	66	85W

Table 2. Point-count data for ash-flow tuff units in the Mount Irish and Timpahute ranges. Phen=Phenocrysts; Qtz=Quartz; San=Sanidine; Plag=Plagioclase; Biot=Biotite; Amp=Amphibole; Olv=Olivine; Sph=Sphene. Modal counts were made to examine the relative abundance of each each constituent, whereas volume counts were made to examine the area occupied by each consistuent.

Unit/ Sample #	Phen	Qtz	San	Plag	Biot	Amp	Pyx	Oxides	Olv/ Sph	Pumice	Lithics	Pore-Space	Matrix	Total
Monotony Tuff Sample TR007														
Modal Counts	100	12	24	37	14	0	2	11	0	3	1	30	466	600
Modal %	16.7	2.0	4.0	6.2	2.3	0.0	0.3	1.8	0.0	0.5	0.2	5.0	77.7	100.0
Modal Phen. %		12.0	24.0	37.0	14.0		2.0	11.0						
Volume Counts	137	27	25	53	19	0	0	12	1	8	0	30	425	600
Volume %	22.8	4.5	4.2	8.8	3.2	0.0	0.0	2.0	0.0	1.3	0.0	5.0	70.8	100.0
Volume Phen. %		19.7	18.2	38.7	13.9			8.8	0.7					

Unit/ Sample #	Phen	Qtz	San	Plag	Biot	Amp	Pyx	Oxides	Olv/ Sph	Pumice	Lithics	Pore-Space	Matrix	Total
Shingle Pass Tuff (Lower) Sample TR004														
Modal Counts	50	7	14	21	0	0	1	6	1	8	0	31	511	600
Modal %	8.3	1.2	2.3	3.5	0.0	0.0	0.2	1.0	0.0	1.3	0.0	5.2	85.2	100.0
Modal Phen. %		14.0	28.0	42.0			2.0	12.0	2.0					
Volume Counts	83	10	32	34	0	0	1	4	2	44	1	25	447	600
Volume %	13.8	1.7	5.3	5.7	0.0	0.0	0.2	0.7	0.0	7.3	0.2	4.2	74.5	100.0
Volume Phen. %		12.0	38.6	41.0			1.2	4.8	2.4					

Table 2. (continued)

Unit/ Sample #	Phen	Qtz	San	Plag	Biot	Amp	Pyx	Oxides	Olv/ Sph	Pumice	Lithics	Pore-Space	Matrix	Total
Tuff of Hancock Summit TR003														
Modal Counts	111	45	35	24	4	0	0	3	0	1	3	43	442	600
Modal %	18.5	7.5	5.8	4.0	0.7	0.0	0.0	0.5	0.0	0.2	0.5	7.2	73.7	100.0
Modal Phen. %		40.5	31.5	21.6	3.6			2.7						
Volume Counts	140	60	52	18	8	0	0	2	0	2	8	62	388	600
Volume %	23.3	10.0	8.7	3.0	1.3	0.0	0.0	0.3	0.0	0.3	1.3	10.3	64.7	100.0
Volume Phen. %		42.9	37.1	12.9	5.7			1.4						

Unit/ Sample #	Phen	Qtz	San	Plag	Biot	Amp	Pyx	Oxides	Olv/ Sph	Pumice	Lithics	Pore-Space	Matrix	Total
Shingle Pass Tuff (Upper) TR002														
Modal Counts	47	4	15	22	2	0	2	2	0	5	2	4	542	600
Modal %	7.8	0.7	2.5	3.7	0.3	0.0	0.3	0.3	0.0	0.8	0.3	0.7	90.3	100.0
Modal Phen. %		8.5	31.9	46.8	4.3		4.3	4.3						
Volume Counts	56	7	16	25	3	0	2	3	0	22	5	8	509	600
Volume %	9.3	1.2	2.7	4.2	0.5	0.0	0.3	0.5	0.0	3.7	0.8	1.3	84.8	100.0
Volume Phen. %		12.5	28.6	44.6	5.4		3.6	5.4						

Table 2. (continued)

Unit/ Sample #	Phen	Qtz	San	Plag	Biot	Amp	Pyx	Oxides	Olv/ Sph	Pumice	Lithics	Pore-Space	Matrix	Total
Pahranagat Formation														
TR009														
Modal Counts	38	10	13	9	3	1	0	2	0	4	2	3	553	600
Modal %	6.3	1.6	2.1	1.5	0.5	0.0	0.0	0.3	0.0	0.6	0.3	0.5	92.1	100.0
Modal Phen. %		26.3	34.2	23.6	7.8	2.6		5.2						
Volume Counts	80	24	27	22	4	2	0	1	0	9	2	7	502	600
Volume %	13	4.0	4.5	3.6	0.6	0.3	0.0	0.1	0.0	1.5	0.3	1.2	83.6	100.0
Volume Phen. %		30.0	33.7	27.5	5.0	2.5		1.25						

Table 3. $^{40}Ar/^{39}Ar$ age data for sample TBTR08 of the Tuff of Hancock Summit

Crystal	T (C)	t (min.)	^{36}Ar	^{37}Ar	^{38}Ar	^{39}Ar	^{40}Ar	$\%^{40}Ar^*$	Ca/K	$^{40}Ar^*/^{39}ArK$	Age (Ma)	1s.d.
1	1600	6	0.092	0.515	2.207	176.162	1584.70	98.5	0.017845946	8.8741	26.81	0.18
2	1600	6	0.066	0.354	1.311	100.933	912.861	98.2	0.021409921	8.8901	26.86	0.18
3	1600	6	0.144	0.305	1.272	102.182	945.346	95.8	0.01822091	8.8764	26.82	0.18
4	1600	6	0.070	0.433	1.640	129.245	1162.270	98.5	0.02045121	8.8684	26.79	0.18
5	1600	6	0.049	0.248	1.024	81.517	734.046	98.4	0.01857155	8.8691	26.79	0.18
6	1600	6	0.062	0.395	0.779	62.159	569.485	97.3	0.038791805	8.9165	26.94	0.18
7	1600	6	0.056	0.344	1.295	102.233	916.908	98.2	0.020540557	8.8168	26.64	0.18
8	1600	6	0.038	7.024	0.070	5.782	58.511	82.4	7.429765316	8.2158	24.83	0.39
9	1600	6	0.076	0.265	1.002	79.317	725.226	96.9	0.020395035	8.8681	26.79	0.18
10	1600	6	0.095	0.271	1.288	102.137	927.688	96.3	0.017094306	8.8248	26.66	0.18
11	1600	6	0.211	0.372	1.493	115.570	1094.930	93.7	0.02073784	8.9572	27.06	0.18

Mean ± s.d. =	26.63	0.58
Mean ± s.d. (omit 8, 11) =	26.79	0.09
Wtd mean (omit 8, 11) =	26.78	0.15
Isochron age (omit 11) =	26.81	0.16

J = 0.001687 ± 0.56%
4 amu discrimination = 1.01159 ± 0.26%
40/39K = 0.0001 ± 100.0%
36/37Ca = 0.000267 ± 3.83%
39/37Ca = 0.00070 ± 0.63%
Note isotope beams in mV released; errors in reported ages include J error; ^{36}Ar through ^{40}Ar are measured beam intensities that have been corrected for decay in the age calculations; all analytical errors are reported at the 1σ (standard deviation) confidence-level.

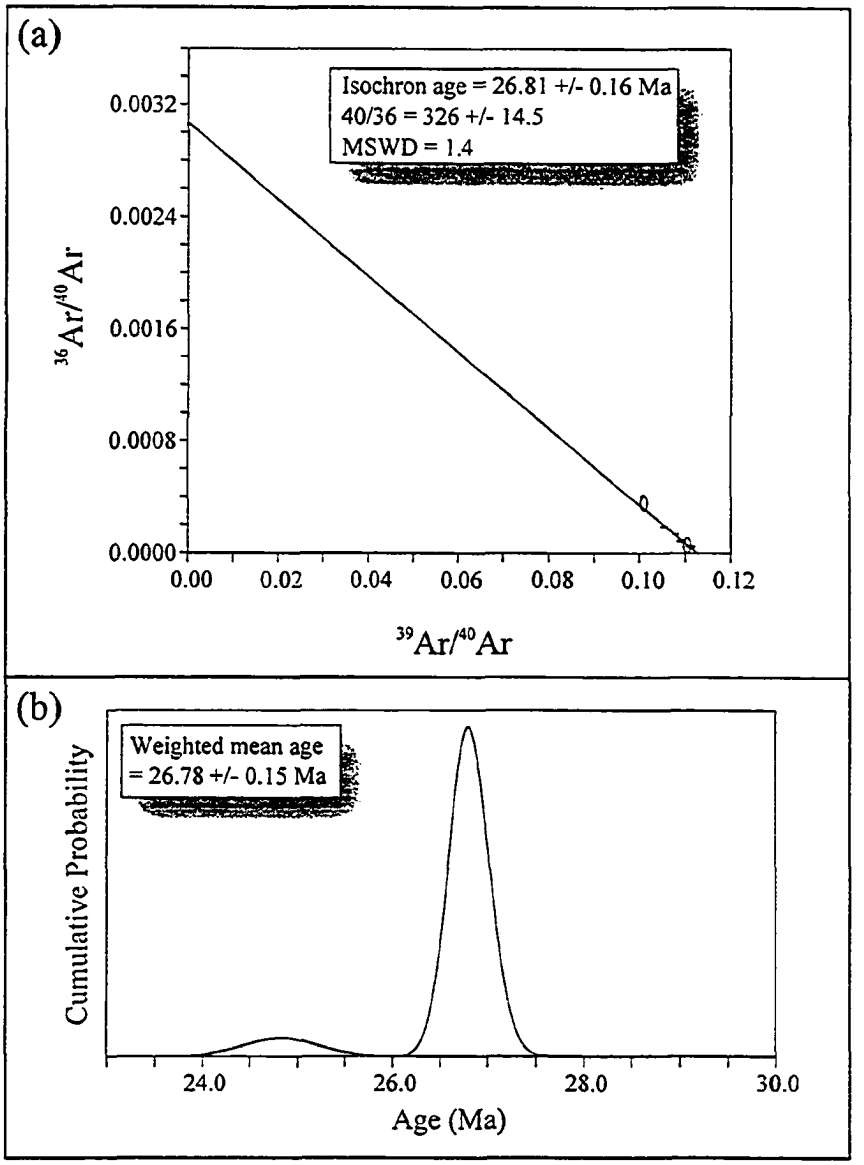

Figure 25. Geochronologic data. (a) Isochron for sample TBTR08 of the tuff of Hancock Summit. The isochron is based on 10 single crystals out of the 11 measured and has a mean square of weighted deviates (MSWD) of 1.4. Note that nearly all of the ^{40}Ar measured was radiogenically produced, leaving the upper end of the isochron poorly constrained. Although this isochron is statistically valid, this relationship indicates that the weighted mean age may be a better estimate of the age of the sample. (b) $^{40}Ar/^{39}Ar$ age probability curve for sample TBTR08 of the tuff of Hancock Summit. The weighted mean age is based on 9 out of 11 single crystals. All analytical errors are reported at the 1σ (standard deviation) confidence-level.

REFERENCES

Allmendinger R.W., 1992, Fold and thrust tectonic of the western United States exclusive of the accreted terranes, *in* Burchfield, B.C., et al., eds., The Cordilleran orogen: Conterminous U.S.: Boulder, Colorado, Geological Society of America, Geology of North America, v. G-3, p. 583-608.

Allmendinger, R.W., 2002a, StereoWin for Windows, v. 1.2.0, copyrighted software.

Allmendinger, R.W., 2002b, FaultKin for Windows, v. 1.2.2, copyrighted software.

Anderson, R.E., 1971, Thin-skinned distension in Tertiary rocks of south-eastern Nevada: Geological Society of America Bulletin, v. 82, p. 43-58.

Anderson, R.E. and Barnard, T.P., 1993, Aspects of three-dimensional strain at the margin of the extensional orogen, Virgin River depression area, Nevada, Utah, and Arizona: Geological Society of America Bulletin, v.105, p. 1019-1052.

Anderson, R.E., Barnard, T.P., and Snee, L.W., 1994, Roles of plutonism, midcrustal flow, and horizontal collapse in shaping the Miocene strain field of the Lake Mead area, Nevada and Arizona: Tectonics, v. 13, p. 1381-1410.

Anglier, J., Collette, B., and Anderson, R.E, 1985, Neogene paleostress changes in the Basin and Range: A case study at the Hoover Dam, Nevada-Arizona: Geological Society of America Bulletin, v. 96, p. 347-361.

Armstrong, P.A., and Bartley, J.M., 1993, Displacement and deformation associated with a lateral thrust termination, southern Golden Gate Range, southern Nevada, U.S.A.: Journal of Structural Geology, v. 15, p. 721–735.

Armstrong, R.L. and Ward, P., 1991, Evolving geographic pattern of Cenozoic magmatism in the North American Cordillera: The temporal and spatial association of magmatism and metamorphic core complexes: Journal of Geophysical Research, v. 96, p. 13201-13224.

Atwater, T. and Stock, J. M., 1998, Pacific-North America plate tectonics of the Neogene Southwestern United States: An Update: International Geology Review, v. 40, p. 375-402

Axen, G.J, 1998, The Caliente Enterprise Zone, southeastern Nevada and southwestern Utah, *in* Faulds, J.E., and Stewart, J.H., eds., Accommodation Zones and Transfer Zones: The Regional Segmentation of the Basin and Range Province: Boulder, Colorado, Geological Society of America Special Paper 323, p. 181-194.

Axen, G.J., Taylor, W.J., and Bartley, J.M., 1993, Space-time patterns of the onset of extension and magmatism, southern Great Basin, Nevada, Utah, and California: Geological Society of America Bulletin, v. 105, p. 56-76.

Axen, G.J., Wernicke, B.P., Skelly, M.F., and Taylor, W.J., 1990, Mesozoic and Cenozoic tectonics of the Sevier thrust belt in the Virgin River Valley area, southern Nevada, *in* Wernicke, B.P., ed., Basin and Range Extensional Tectonics Near the Latitude of Las Vegas, Nevada, Geological Society of America Memoir 176, p. 123-153.

Bartley, J.M., 1989, Changing Tertiary extension directions in the Dry Lake Valley area, Nevada, and a possible dynamic model, *in* Garside, L.J., and Shaddrick, D.R., eds., Compressional and extensional structural styles in the northern Basin and Range: Seminar proceedings: Reno, Nevada Petroleum Society and the Geological Society of Nevada, p. 35-39.

Bartley, J.M., Axen, G.J., Taylor, W.J., and Fryxell, J.E., 1988, Cenozoic tectonics of a transect through eastern Nevada near 38° N latitude, *in* Weide, D.L., and Faber, M.L., eds., This Extended Land; Geological Journey in the Southern Basin and Range: Las Vegas, Nevada, University of Nevada-Las Vegas, Geological Society of America Field Trip Guidebook, p. 1-20.

Bartley, J.M. and Taylor, W.J., 1992, Barrier network model for Basin and Range faulting: American Association of Petroleum Geologists Bulletin, v. 105, p. 416.

Bennett, R.A., Davis, J.L., and Wernicke, B.P., 1999, Present-day pattern of Cordilleran deformation in the western United States: Geology, v. 27, p. 371-374.

Best, M.G., and Christensen, E.H., 1991, Limited extension during peak Tertiary volcanism, Great Basin of Nevada and Utah: Journal of Geophysical Research, v. 96, p. 13509-13528.

Best, M.G., Christiansen, E.H., Deino, A.L., Gromme, C.S., and Tingey, D.G., 1995, Correlation and emplacement of a large, zoned, discontinuously exposed ash flow sheet: $^{40}Ar/^{39}Ar$ chronology, paleomagnetism, and petrology of the Pahranagat Formation, Nevada: Journal of Geophysical Research, v. 100, p. 24,593-24,609.

Best, M.G., Scott, R.B., Rowley, P.D., Swadley, W.C., Anderson, R.E., Gromme, C.S., Harding, A.E., Deino, A.L., Christensen, E.H., Tingey, D.G., and Sullivan, K.R., 1993, Oligocene-Miocene caldera complexes, ash-flow sheets, and tectonism in the central and southeastern Great Basin, *in* Lahren, M.M., et al., eds., Crustal Evolution

of the Great Basin and Sierra Nevada: Reno, Nevada, University of Nevada-Reno, Guidebook: p. 285-311.

Birrell, A.D., 1994, Digital mosaic of the western United States, copyrighted image: http://birrell.org/andrew/reliefMaps/301052020v2.jpg.

Blackwell, D.D., 1983, The role of heat in the development of energy and mineral resources in the northern Basin and Range province: Geothermal Resources Council Special Report 13, p. 81-93.

Block, L., and Royden, L., 1990, Core complex geometries and regional scale flow in the lower crust: Tectonics, v. 9, p. 557-567.

Bohannon, R.G, 1984, Nonmarine sedimentary rocks of Tertiary age in the Lake Mead region, southeastern Nevada and northwestern Arizona: U.S. Geological Survey Professional Paper 1259, 72 p.

Bohannon, R.G., and Parsons, T., 1995, Tectonic implications of post-30 Ma Pacific and North American relative plate motions: Geological Society of America Bulletin, v. 107, p. 937-959.

Buck, W.R., 1988, Flexural rotation of normal faults: Tectonics, v. 7, p. 959-973.

Byers, F.M., Barnes, H., Poole, F.G., and Ross, R.J., 1961, Revised subdivision of Ordovician system at the Nevada Test Site and vicinity, Nevada: U.S. Geological Survey Professional Paper 424-C, p. C106-C109.

Cakir, M., and Aydin, A., 1990, Deformation around the intersection of the Las Vegas shear zone and the Lake Mead fault system, SE Nevada: Geological Society of America Abstracts with Programs, v. 22, p. A96.

Cakir, M., Aydin, A., and Campagna, D.J., 1998, Deformation pattern around the conjoining strike-slip fault systems in the Basin and Range, southeast Nevada: The role of strike-slip faulting in basin formation and inversion: Tectonics, v. 17, p. 344-359.

Campagna, D.J, and Aydin, A., 1991, Tertiary uplift and shortening in the Basin and Range; the Echo Hills, southeastern Nevada: Geology, v. 19, p. 485-488.

Camilleri, P.A., 1996, Evidence for Late Cretaceous–early Tertiary (?) extension in the Pequop Mountains, Nevada: Implications for the nature of the early Tertiary unconformity, *in* Taylor, W.J. and Langrock, H., eds., Cenozoic Structure and Stratigraphy of Central Nevada: Nevada Petroleum Society 1996 Field Conference Volume, p. 19-28.

Chamberlain, A.K. and Warme, J.E., 1996, Devonian sequences and sequence boundaries, Timpahute Range, Nevada, *in* Longman, M.W., and Sonnenfeld, M.D.,

eds., Paleozoic Systems of the Rocky Mountain region: Rocky Mountain Section, Society for Sedimentary Geology, p. 63-84.

Compton, R.R., 1985, Geology in the Field, John Wiley & Sons, Inc., 398 p.

Dahlstrom, C. D. A., 1969, Balanced Cross Sections: Canadian Journal of Earth Sciences, v. 6, p. 743-757.

Davis, G.H., 1980, Structural characteristics of metamorphic core complexes, southern Arizona, *in* Critteden, J., Coney, P.J., and Davis, G.H., eds., Cordilleran Metamorphic Core Complexes: Geological Society of America Memoir 153, p. 913-929.

Dohrenwend, J.C., Schell, B.A., Menges, C.M., Moring, B.C., and McKittrick, M.A., 1996, Reconnaissance photogeologic map of young (Quaternary and late Tertiary) faults in Nevada, *in* Singer, D.A., ed., Analysis of Nevada's Metal-Bearing Mineral Resources: Nevada Bureau of Mines and Geology Open-File Report 96-2, scale 1:1,000,000.

Dokka, R.K., and Ross, T.M., 1995, Collapse of southwestern North America and the evolution of early Miocene detachment faults, metamorphic core complexes, the Sierra Nevada orocline, and the San Andreas fault system:Geology, v. 13, p. 1075-1078.

Duebendorfer, E.M., Beard, L.S., and Smith, E.I., 1998, Restoration of Tertiary deformation in the Lake Mead regions, southern Nevada: The role of strike-slip transfer faults, *in* Faulds, J.E., and Stewart, J.H., eds., Accommodation Zones and Transfer Zones: The Regional Segmentation of the Basin and Range Province: Boulder, Colorado, Geological Society of America Special Paper 323, p. 127-148.

Duebendorfer, E.M. and Black, R.A., 1992, Kinematic role of transverse structures in continental extension: An example from the Las Vegas Valley shear zone, Nevada: Geology, v. 20, p. 1107-1110.

Duebendorfer, E.M., Sewall, A.J., and Smith, E.I., 1990, The Saddle Island detachment system; An evolving shear zone in the Lake Mead area, Nevada, *in* Wernicke, B.P., ed., Basin and Range Extensional Tectonics Near the Latitude of Las Vegas, Nevada, Geological Society of America Memoir 176, p. 77-97..

Duebendorfer, E.M., and Simpson, D.A., 1994, Kinematics and timing of Tertiary extension in the western Lake Mead area: Geological Society of America Bulletin, v. 106, p. 1057-1073.

Eaton, G.P., 1982, The Basin and Range Province: Origin and tectonic significance: Annual Review of Earth and Planetary Sciences, v. 10, p. 409-440.

Ekren, E.B., Bucknam, R.C., Carr, W.J., Dixon, G.L., and Quinlivan, W.D., 1976, East-trending lineaments in central Nevada: U.S. Geological Survey Professional Paper 986, 19 p.

Ekren, E.B., Orkild, P.P., Sargent, K.A., and Dixon, G.L., 1977, Geologic map of Tertiary rocks, Lincoln County, Nevada: U.S. Geological Survey Miscellaneous Investigations Series, Map I-1041, scale 1:250,000.

Faulds, J.E., Feuerbach, D.L., Miller, C.F., and Smith, E.I., 2001, Cenozoic evolution of the northern Colorado River extensional corridor, southern Nevada and northwest Arizona: Pacific Section of the American Association of Petroleum Geologists Publication GB 78 (also Utah Geological Association Publication 30), p. 239-272.

Faulds, J.E., Geissman, J.W., and Mawer, C.K., 1990, Structural development of a major extensional accommodation zone in the Basin and Range province, northwestern Arizona and southern Nevada: Implications for kinematic models of continental extension, *in* Wernicke, B.P., ed., Basin and Range Extensional Tectonics Near the Latitude of Las Vegas, Nevada, Geological Society of America Memoir 176, p. 37-76.

Faulds, J.E., and Varga, R.J., 1998, The role of accommodation zones and transfer zones in the regional segmentation of extended terranes, *in* Faulds, J.E., and Stewart, J.H., eds., Accommodation Zones and Transfer Zones: The Regional Segmentation of the Basin and Range Province: Boulder, Colorado, Geological Society of America Special Paper 323, p. 1-45.

Gawthorpe, R.L., and Hurst, J.M., 1993, Transfer zones in extensional basins: their structural style and influence on drainage development and stratigraphy: Journal of the Geological Society, London, v. 150, p. 1137-1152.

Grabb, R.F., 1994, Extensional tectonics and petroleum accumulations in the Great Basin, *in* Schalla, R.A., and Johnson, E.H., eds., Oil Fields of the Great Basin: Nevada Petroleum Society, p. 41-55.

Groshong, R. H., Jr., 1994, Area balance, depth to detachment and strain in extension: Tectonics, v. 13, p. 1488-1497.

Guth, P.L., 1990, Superposed Mesozoic and Cenozoic deformation, Indian Springs Quadrangle, southern Nevada, *in* Wernicke, B.P., ed., Basin and Range Extensional Tectonics Near the Latitude of Las Vegas, Nevada, Geological Society of America Memoir 176, p. 237-250.

Harding, A.E., Scott, R.B., Mehnert, H.H., and Snee, L.W., 1995, Evidence of the Kane Springs Wash caldera in the Meadow Valley Mountains, southeastern Nevada, *in* Scott, R.B. and Swadley, W.C., eds., Geologic Studies in the Basin and Range–

Colorado Plateau Transition in Southeastern Nevada, Southwestern Utah and Northwestern Arizona, 1992: U.S. Geological Survey Bulletin 2056-A, p. 135-179.

Henry, C.D., Kunk, M.J., Muehlberger, W.R., and McIntosh, W.C., 1997, Igneous evolution of a complex laccolith-caldera, the Solitario, Trans-Pecos Texas: Implications for calderas and subjacent plutons: Geological Society of America Bulletin, v. 109, p. 1036-1054.

Horton, T.W., 2004, Neogene topographic evolution of the central Basin and Range province: Geological Society of America Abstracts with Programs, v. 36, p. 36.

Hudson, M.R., Rosenbaum, J.G., Gromme, C.S., Scott, R.B., and Rowley, P.D., 1998, Paleomagnetic evidence for counterclockwise rotation in a broad sinistral shear zone, Basin and Range province, southeastern Nevada and southwestern Utah, *in* Faulds, J.E., and Stewart, J.H., eds., Accommodation Zones and Transfer Zones: The Regional Segmentation of the Basin and Range Province: Boulder, Colorado, Geological Society of America Special Paper 323, p. 149-180.

Humphreys, E.D., 1995, Post-Laramide removal of the Farallon slab, western United States: Geology, v. 23, p. 987-990.

Jayko, A.S., 1990, Shallow crustal deformation in the Pahranagat area, southern Nevada: *in* Wernicke, B.P., ed., Basin and Range extensional tectonics near the latitude of Las Vegas, Nevada, Geological Society of America Memoir 176, p. 213-236.

Johnson, J.G., Sandberg, C.A., and Poole, F.G., 1991, Devonian lithofacies of the western United States, *in* Cooper, J.D., and Stevens, C.H., eds., Paleozoic paleogeography of the Western United States – II: Pacific Section, Society for Sedimentary Geologists, v. 97, p. 83-105.

Jones, C.H., Unruh, J.R., and Sonder, L.J., 1996, The role of gravitational potential energy in active deformation in the southwestern United States: Nature, v. 381, p. 37-41.

Jones, C.H., Wernicke, B.P., Farmer, G.L., Walker, J.D., Coleman, D.S., McKenna, L.W., and Perry, F.V., 1992, Variations across and along a major continental rift: an interdisciplinary study of the Basin and Range province: Tectonophysics, v. 213, p. 57-96.

Kerr, H. G., and White, N., 1994, Application of an automatic method for determining normal fault geometries: Journal of Structural Geology, v. 16, p. 1691–1709.

Lachenbruch A.H. and Sass, J.H., 1978, Models of extending lithosphere and heat flow in the Basin and Range province, *in* Smith, R.B. and G.P. Eaton, eds., Cenozoic Tectonics and Regional Geophysics of the Western Cordillera, Geological Society of America Memoir 152, p. 209-250.

Lipman, P.W., 1984, The roots of ash flow calderas in western North America: Windows into the tops of granitic batholiths: Journal of Geophysical Research, v. 89, p. 8801-8841.

Liu, M., 2001, Cenozoic extension and magmatism in the North American cordillera: the role of gravitational collapse: Tectonophysics, v. 342, p. 407-433.

Mabey, D.R., Zietz, I., Eaton, G.P., and Kleinkopf, M.D., 1978, Regional magnetic patterns in part of the Cordillera in the Western United States, *in* Smith, R.B., and Eaton, G.P., eds., Cenozoic Tectonics and Regional Geophysics of the Western Cordillera: Geological Society of America Memoir 152, p. 93–106

Marrett, R., and Allmendinger, R.W., 1990, Kinematic analysis of fault-slip data: Journal of Structural Geology, v. 12, p. 973-986.

Michel-Noel, G., Anderson, R.E., and Angelier, J., 1990, Fault kinematics and strain partitioning of a Neogene extensional fault system in southeastern Nevada, *in* Wernicke, B.P., ed., Basin and Range Extensional Tectonics Near the Latitude of Las Vegas, Nevada, Geological Society of America Memoir 176, p. 155-180.

Miller, E.L, Gans, P.B., and Garing, J., 1983, The Snake Range decollement: An exhumed mid-Tertiary ductile-brittle transition: Tectonics, v. 2, p. 239-263.

Morley, C.K., Nelson, R.A., Patton, T.L., Munn, S.G., 1990, Transfer zones in the East African rift system and their relevance to hydrocarbon exploration in rifts: The American Association of Petroleum Geologists Bulletin, v. 74, p. 1234-1253.

Nunns, A.G., 1991, Structural restoration of seismic and geologic sections in extensional regimes: American Association of Petroleum Geologists Bulletin, v. 75, p. 278-297.

Nutt, C., 1996, Cretaceous(?) to early Oligocene sedimentary and volcanic rocks at Alligator Ridge, Buck Mountain-Bald Mountain area, central Nevada, *in* Taylor, W.J., and Langrock, H., eds., Cenozoic Structure and Stratigraphy in Central Nevada: 1996 Field Conference Volume, Nevada Petroleum Society Inc., Reno, p. 13-18.

Overtoom, G.J., and Bartley, J.M., 1996, Kinematic evidence for mid-Tertiary north-south extension across the western Blue Ribbon lineament, east-central Nevada, *in* Taylor, W.J., and Langrock, H., eds., Cenozoic Structure and Stratigraphy of Central Nevada: 1996 Field Conference Volume, Nevada Petroleum Society Inc., Reno, p. 41-50.

Poole, F.G. and Sandberg, C.A., 1991, Mississippian paleogeography and conodont stratigraphy of the western United States, *in* Cooper, J.D., and Stevens, C.H., eds., Paleozoic Paleogeography of the Western United States – II: Pacific Section, Society for Sedimentary Geology, v. 97, p. 107-136.

Prodehl, C., 1970, Seismic refraction study of crustal structure in the western United States: Geological Society of America Bulletin, v. 81, p. 2629-2646.

Proffett, J.M., Jr., 1977, Cenozoic geology of the Yerington district, Nevada, and implications for the nature and origin of Basin and Range faulting: Geological Society of America Bulletin, v. 88, p. 247-266.

Prothro, L.B and Drellack Jr., S.L., 1997, Review and reconnaissance of the hydrogeology of Tertiary sedimentary rocks in the vicinity of Frenchman Flat, Nevada Test Site, Bechtel Nevada Report, DOE/NV/11718-155.

Reheis, M.C., 1993, Neogene tectonism from the southwestern Nevada volcanic field to the White Mountains, California–Part. II. Late Cenozoic history of the southern Fish Lake Valley fault zone, Nevada and California, *in* Lahren, M.N., Trexler, J.H., Jr., and Spinosa, C., eds., Crustal Evolution of the Great Basin and Sierra Nevada: Cordilleran/ Rocky Mountain Section, Geological Society of America Guidebook, Department of Geological Sciences, University of Nevada, Reno, p. 370-382.

Reheis, M.C., and Sawyer, T.L., 1997, Late Cenozoic history and slip rates of the Fish Lake Valley, Emigrant Peak, and Deep Springs fault zones, Nevada and California: Geological Society of America Bulletin, v. 109, p. 280-299.

Rey, P., Vanderhaeghe, O., and Teyssier, C., 2001, Gravitational collapse of the crust: definition, regimes and modes: Tectonophysics, v. 342, p. 435-449.

Rowland, S.M, Parolini, J.R., Eschner, E., McAllister, A.J., and Rice, J.A., 1990, Sedimentologic and stratigraphic constraints on the Neogene translation and rotation of the Frenchman Mountain structural block, Clark County, Nevada, *in* Wernicke, B.P., ed., Basin and Range Extensional Tectonics Near the Latitude of Las Vegas, Nevada, Geological Society of America Memoir 176, p. 99-122.

Rowley, P.D., 1998, Cenozoic transverse zones and igneous belts in the Great Basin, Western United States; their tectonic and economic implications: *in* Faulds, J.E., and Stewart, J.H., eds., Accommodation Zones and Transfer Zones: The Regional Segmentation of the Basin and Range Province: Boulder, Colorado, Geological Society of America Special Paper 323, p. 125-228.

Rowley, P. D. and G. L. Dixon, 2001, The Cenozoic evolution of the Great Basin area: Pacific Section of the American Association of Petroleum Geologists Publication GB 78 (also Utah Geological Association Publication 30), p. 169-188.

Rowley, P.D., Lipman, P.W., Mehnert, H.H., and Lindsey, D.A., and Anderson, J.J., 1978, Blue Ribbon lineament, an east-trending structural zone within the Pioche mineral belt of southwestern Utah and eastern Nevada: U.S. Geological Survey Journal of Research, v. 6, p. 175-192.

Rowley, P.D., Nealey, L.D., Unruh, D.M., Snee, L.W., Mehnert, H.H., Anderson, R.E., and Gromme, C.S., 1995, Stratigraphy of Miocene ash-flow tuffs in and near the Caliente caldera complex, southeastern Nevada and southwestern Utah, *in* Scott, R.B. and Swadley, W.C., eds., Geologic studies in the Basin and Range–Colorado Plateau transition in southeastern Nevada, southwestern Utah and northwestern Arizona: U.S. Geological Survey Bulletin 2056-A, p. 42-87.

Rowley, P.D., and Shroba, R.R., 1991, Geologic Map of the Indian Cove Quadrangle, Lincoln County, Nevada: U.S. Geologic Survey, Geologic Quadrangle Map GQ-1701, 1:24,000 scale.

Rowley, P.D., Shroba, R.R., Simonds, F.W., Burke, K.J., Axen, G.J., and Olmore, S.D, 1994, Geologic map of the Chief Mountain Quadrangle, Lincoln County, Nevada: U.S. Geologic Survey, Geologic Quadrangle Map GQ-1731, 1:24,000 scale.

Sandru, J.M., and Taylor, W.J., 2003, Cenozoic extension and strike slip tectonics in the Mount Irish Range, Nevada; changes in stress fields through time: Geological Society of American Abstracts with Programs, v. 35, p. 26.

Scott, R.B., Gromme, C.S., Best, M.G., Rosenbaum, J.G., and Hudson, M.R., 1995, Stratigraphic relations of Tertiary volcanic rocks in central Lincoln County, southeastern Nevada, *in* Scott, R.B. and Swadley, W.C., eds., Geologic Studies in the Basin and Range–Colorado Plateau Transition in Southeastern Nevada, Southwestern Utah and Northwestern Arizona: U.S. Geological Survey Bulletin 2056-A, p. 5-41.

Sengor, A.M., and Burke, K., 1978, Relative timing of rifting and volcanism on Earth and its tectonic implications: Geophysical Research Letters, v. 5, p. 419-421.

Severinghaus, J. and Atwater, T., 1990, Cenozoic geometry and thermal state of the subducting slabs beneath western North America, *in* Wernicke, B.P., ed., Basin and Range extensional tectonics near the latitude of Las Vegas, Nevada, Geological Society of America Memoir 176, p. 1-22.

Smith, R.B., and Arabasz, W.J., 1991, Seismicity of the Intermountain seismic belt, *in* Slemmons, D.B., Engdahl, I.R., Zoback, M.L., and Blackwell, D.D., eds., Neotectonics of North America: Geological Society of America Decade Map Volume 1, p. 185-228.

Smith, R.B., and Sbar, M.L., 1974, Contemporary tectonics and seismicity of the western United States with emphasis on the Intermountain seismic belt: Geological Society of America Bulletin, v. 85, p. 1205-1218.

Snow, J.K., and Wernicke, B.P., 2000, Cenozoic tectonism in the central Basin and Range: Magnitude, rate, and distribution of upper crustal strain: American Journal of Science, v. 300, p. 659-719.

Sonder, L.J. and Jones, C.H., 1999, Western United States extension: How the west was widened: Annual Review of Earth and Planetary Science, v. 27, p. 417-462.

Spell, T.L., Smith, E.I., Sanford, A. and Zanetti, K.A., 2001, Systematics of xenocrystic contamination: Preservation of discrete feldspar populations at McCullough Pass Caldera revealed by $^{40}Ar/^{3}9Ar$ dating, Earth and Planetary Science Letters, v. 190/3-4, p. 153-165.

Spera, F., 1980, Thermal evolution of plutons: A parameterized approach: Science, v. 201, p. 299-301.

Sterner, R., 1995, Digital elevation tiles of Nevada, Idaho, and Oregon, copyrighted images: http://fermi.jhuapl.edu/states/states.html.

Stewart, J.H., 1978, Basin-Range structure in western North America – A review, *in* Smith, R.B., and Eaton, G.P., eds., Cenozoic Tectonics and Regional Geophysics of the Western Cordillera: Geological Society of America Memoir 152, p. 1-31.

Stewart, J.H., 1980, Geology of Nevada, a discussion to accompany the geologic map of Nevada: Nevada Bureau of Mines and Geology Special Publication 4, 136 p.

Stewart, J.H., 1998, Regional characteristics, tilt domains, and extensional history of the late Cenozoic Basin and Range province, western North America, *in* Faulds, J.E. and Stewart, J.H., eds., Accommodation Zones and Transfer Zones: The Regional Segmentation of the Basin and Range Province, Geological Society of America Special Paper 323, p. 47-74.

Stewart, J.H., Morre, W.J., and Zietz, I., 1977, East-west patterns of Cenozoic igneous rocks, aeromagnetic anomalies, and mineral deposits, Nevada and Utah: Geological Society of America Bulletin, v. 88, p. 67-77.

Switzer, D.D., 1996, The geology and structure of the northern Hiko Range, Lincoln County, Nevada [M.S. thesis]: Las Vegas, University of Nevada, 129 p.

Taylor, W.J., 1990, Spatial and temporal relations of Cenozoic volcanism and extension in the North Pahroc and Seaman ranges, eastern Nevada, *in* Wernicke, B.P., ed., Basin and Range extensional tectonics near the latitude of Las Vegas, Nevada, Geological Society of America Memoir 176, p. 181-194.

Taylor, W.J., 2002, Extensional transverse and transfer faults, Timpahute and Mount Irish ranges, southern Nevada: Geological Society of America Abstracts with Programs, v. 34, p. 248.

Taylor, W.J. and Bartley, J.M., 1992, Prevolcanic extensional Seaman breakaway fault and geologic implications for eastern Nevada and western Utah: Geological Society of America Bulletin, v. 104, p. 255-266.

Taylor, W.J., Bartley, J.M., Fryxell, J.E., Schmitt, J.G., and Vandervoot, D.S., 1993, Tectonic style and regional relations of the central Nevada thrust belt, *in* Lahren, M.N., Trexler, J.H., Jr., and Spinosa, C., eds., Crustal Evolution of the Great Basin and Sierra Nevada: Cordilleran/ Rocky Mountain Section, Geological Society of America Guidebook, Department of Geological Sciences, University of Nevada, Reno, p. 57-96.

Taylor, W.J., Bartley, J.M., Lux, D.L., and Axen, G.J., 1989, Timing of Tertiary extension in the Railroad Valley–Pioche transect, Nevada: Constraints from $^{40}Ar/^{39}Ar$ ages of volcanic rocks: Journal of Geophysical Research, v. 94, p. 7757-7774.

Taylor, W. J., Bartley, J.M., Martin, M.W., Geissman, J.W., Walker, J.D., Armstrong, P.A., and Fryxell, J.E., 2000, Relations between hinterland and foreland shortening: Sevier orogeny, central North American Cordillera: Tectonics, v. 19, p. 1124-1143.

Taylor, W.J., and Switzer, D.D., 2001, Temporal changes in fault strike (to 90°) and extension directions during multiple episodes of extension: An example from eastern Nevada: Geological Society of America Bulletin, v. 113, p. 743-759.

Thatcher, W., Foulger, G.R., Julian, B.R., Svarc, J., Quilty, E., and Bawden, G.W., 1999, Present day deformation across the Basin and Range province, western United States: Science, v. 282, p. 1714-1718.

Thenhaus, P.C., and Barnard, T.P, 1998, Insights from Quaternary relations for segmentation of the Great Basin by regional, transverse accommodation zone, *in* Faulds, J.E., and Stewart, J.H., eds., Accommodation Zones and Transfer Zones: The Regional Segmentation of the Basin and Range Province: Boulder, Colorado, Geological Society of America Special Paper 323, p. 229-239.

Tschanz, C.M., and Pampeyan, E.H., 1970, Geology and mineral deposits of Lincoln County, Nevada: Nevada Bureau of Mines and Geology Bulletin 73, 188 p.

U.S. Geological Survey, 1999, Public review draft; digital cartographic standard for geologic map symbolization (PostScript implementation): Open-File Report 99-430.

Wdowinski, S., and Axen, G.J., 1992, Isostatic rebound due to tectonic denudation: A viscous flow model of the layered lithosphere: Tectonic, v. 11, p. 303-315.

Wells, M.L., 1992, Kinematics and timing of sequential deformations in the eastern Raft River Mountains, *in* Wilson, J.R., ed., Field guide to geologic excursions in Utah and adjacent areas of Nevada, Idaho, Utah, and Wyoming: Utah Geologic Survey Miscellaneous Publication 92-93, p. 59-78.

Wells, M.L., Dallmeyer, R.D., and Allmendinger, R.W., 1990, Late Cretaceous extension in the hinterland of the Sevier thrust belt, northwestern Utah and southern Idaho: Geology, v. 18, p. 929-933.

Wells, M.L., Hoisch, T.D., Peters, M.T., Miller, D.M., Wolff, E.D., and Hanson, L.M., 1998, The Mahogany Peaks fault, a Late Cretaceous-Paleocene (?) normal fault in the hinterland of the Sevier orogen: Journal of Structural Geology, v. 106, p. 623-634.

Wendt, I. and Carl, C., 1991, The statistical distribution of the mean squared weighted deviation: Chemical Geology, v. 86, p. 275-285.

Wernicke, B., 1981, Low-angle normal faults in the Basin and Range province: Nappe tectonics in an extending orogen: Nature, v. 291, p. 645-648.

Wernicke, B. Axen, G.J., and Snow, J.K., 1988, Basin and Range extensional tectonic at the latitude of Las Vegas, Nevada: Geological Society of America Bulletin, v. 100, p. 1738-1757.

Wernicke, B. and Axen, G.J., 1988, On the role of isostasy in the evolution of normal faults: Geology, v. 16, p. 848-851.

Wernicke, B., 1992, Cenozoic extensional tectonics of the U.S. Cordillera, *in* Burchfield, B.C., Lipman, P.W., and Zoback, M.L., eds., The Cordilleran orogen: Conterminous U.S.: Boulder, Colorado, Geological Society of America, Geology of North America, v. G-3, p. 553-582.

Williams, N.D., 2000, A transverse fault in an extended terrane, the Currant Summit fault, Nevada [M.S. thesis]: Las Vegas, University of Nevada, 104 p.

VITA

Graduate College
University of Nevada, Las Vegas

Tandis S. Bidgoli

Local Address:
1441 Dorothy Ave., #4
Las Vegas, Nevada 89119

Home Address:
2070 Mountain Blvd.,
Oakland, CA 94611

Degrees:
Bachelor of Science, Geology, 2002
San Francisco State University

Special Honors and Awards:
UNLV, Graduate College, GREAT Assistantship, 2004
UNLV, Graduate and Professional Student Association Poster Award, 2004
Bernada E. French, Geoscience Scholarship, 2003 and 2004
American Association of Petroleum Geologists, Grants-In-Aid, 2003
Geological Society of America, Student Research Grant, 2003
UNLV, Graduate and Professional Student Association, Research Grants, 2003
Geological Society of America, Cordilleran Section, Student Paper Award, 2002
Association for Woman Geoscientists, Outstanding Student Award, 2002
SFSU, College of Science and Engineering, Outstanding Project Award, 2002

Publications:
Bidgoli, T.S. and Taylor, W.J., 2004, The role of transverse faults in Great Basin extension: Transfer faults or N-S extension?: Geological Society of America Abstracts with Programs, v. 36, p. 424.

Bidgoli, T.S., Fossett, E., Knudsen, T.R., Kubart Dano, R.K., McEwan, D.J., and Taylor, W.J., 2003, Surface rupture, paleoseismology, and seismic hazard assessment of the Holocene California Wash Fault, southern Nevada:

Implications for risk to the greater Las Vegas area: Geological Society of America Abstracts with Program, v. 35, p. 476.

Bidgoli, T. and Grove, K., 2002, Determining uplift rates and patterns from Quaternary marine terrace of the Point Reyes Peninsula, California: Geological Society of America Abstracts with Program, v. 34, p. 27.

Caskey, S.J., Domrose, C.J., Ford, E.W., Goebel, M.W., Smith, N.W., Bidgoli, T.S., and Scherer, A.M., 2002, Tectonic and isostatic deformation of latest Pleistocene shorelines, Dixie Valley: Geological Society of America Abstracts with Program, v. 34, p. 100.

Caskey, J., Ramelli, A.R., Ford, E.W., Domrose, C.J., Schneider, G., Goebel, M.W., Smith, N.W., Bidgoli, T.S., and Scherer, A.M., 2002, Tectonic and isostatic deformation of latest Pleistocene Lake Dixie shorelines, *in* Caskey, J., ed., Historical Faulting, Chronostratigraphy, and Paleoseismicity of the Central Nevada Seismic Belt: Friends of the Pleistocene, Pacific Cell, Fieldtrip Guidebook, 114 p.

Thesis Title: The Role of Transverse Fault in Great Basin Extension: Transfer Faults or N-S-Extension?

Thesis Examination Committee:

Chairperson, Dr. Wanda J. Taylor, Ph. D.
Committee Member, Dr. Michael L. Wells, Ph. D.
Committee Member, Dr. Andrew Hanson, Ph. D.
Graduate Faculty Representative, Dr. J. Abiodun Elegbede, Ph. D.

NOTE TO USERS

Oversize maps and charts are microfilmed in sections in the following manner:

LEFT TO RIGHT, TOP TO BOTTOM, WITH SMALL OVERLAPS

This reproduction is the best copy available.

UMI

PLATE 1. GEOLOGIC

DESCRIPTION OF MAP UNITS

In the following descriptions, I use the combined stratigraphic nomenclature of Byers et al. (1961), Tschanz and Pampeyan (1970), and Best et al. (1993). Phenocryst percentages are based on modal analyses from thin sections. The exceptions are the lower cooling unit of the Monotony Tuff and Hiko Tuff, for which phenocrysts percentages are estimated from hand samples. Ages for volcanic tuffs are from Best et al. (1993). The exception is tuff of Hancock Summit dated by this study (Appendix II).

Qa — Alluvium (Quaternary) — Unconsolidated active stream channel and wash deposits; light yellow-brown to grayish-orange silt, sand, gravel, pebbles, and small boulders; poorly sorted; angular to subrounded; clasts include Paleozoic carbonates and quartz sandstone, volcanic rocks and jasperoid.

Qc — Colluvium (Quaternary) — Unconsolidated rock fall and slope wash deposits; pebble to large boulder sized; angular to sub angular; derived from adjacent slopes and cliffs.

Qva — Fan young (Quaternary) — Alluvial fan and stream channel deposits; granule to large cobble size clasts within a light tan-brown coarse sand and silt matrix; dominantly small pebble size clasts; angular; poorly consolidated; poorly sorted; poorly stratified. Dominantly volcanic clasts (~75%); some Paleozoic carbonate and sandstone clasts. Recognizable clasts of tuff of Hancock Summit, Shingle Pass Tuff and Monotony Tuff. Fan surfaces have numerous small channels; poor soil, desert pavement, and desert varnish development. Vegetation consists of sparse desert scrub, yucca, and junipers.

Qfy — Volcanic alluvium (Quaternary) — Granule to large cobble size clasts within a reddish-orange to tan-brown to light pink coarse sand and silt matrix; clasts are angular to subrounded, poorly consolidated and poorly sorted volcanic clasts derived from nearby units.

Qfi — Intermediate fan (Quaternary) — Alluvial fan and stream channel deposits; pebble to boulder sized clasts; dominantly coarse pebble gravel within a light yellowish-brown very fine sand and silt matrix; subrounded; poorly sorted; moderately to poorly consolidated; poorly to moderately stratified. Dominantly Paleozoic carbonate, quartz sandstone, and black chert; little to no volcanic clasts. Recognizable clasts of the Eureka Quartzite and Ely Springs Dolomite. Stage I carbonate soil. Fan surfaces have poor desert pavement development. Vegetation consists of patchy desert scrub, small junipers and small pines.

Qfo — Older fan (Quaternary) — Alluvial fan and stream channel deposits; granule to small boulder size clasts within yellow-tan to orange-brown fine sand and silt matrix; dominantly small pebble size clasts; sub angular to subrounded; moderately consolidated; poorly sorted; moderately stratified. Dominantly Paleozoic carbonate and quartz sandstone clasts; minor Tertiary volcanic and sedimentary rock clasts. Recognizable clasts of Eureka Quartzite, Sevy Dolomite, freshwater limestone, and Shingle Pass Tuff. Stage II soil carbonate. Fan surfaces are mostly planar; some bar and swale topography. Moderate to weak desert pavement development; weak desert varnish on some clasts. Vegetation consists of sparse desert scrub and scattered junipers.

QTo — Older fan gravels (Quaternary and/ or Tertiary (?)) — Dissected alluvial fan and fan remnant deposits; granule to large boulder sized clasts; dominantly small pebbles sized clasts; subangular to subrounded; well-consolidated; poorly to moderately well sorted; poor to moderate stratification. Dominantly Paleozoic carbonate clasts (>75%); some jasperoid and minor volcanic clasts. Recognizable clasts of the Pogonip

GIC MAP OF THE MOUI

LINCOLN C

T

nd Pampeyan
ne exceptions
ed from hand
by this study

low-brown to
unded; clasts

oulder sized;

clasts within
gular; poorly
ic carbonate
onotony Tuff.
development.

tan-brown to
poorly sorted

sized clasts;
subrounded;
ly Paleozoic
f the Eureka
rt pavement

clasts within
angular to
ic carbonate
ble clasts of
onate. Fan
t pavement
nd scattered

sits; granule
subrounded;
ly Paleozoic
the Pogonip
Av horizon
opment and

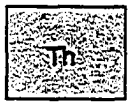

Hiko Tuff (Miocene) — 18.5 Ma rhyolitic ash-flow tuff; light-gray, brown-gray and tar medium-gray, pink-gray to buff fresh; crystal rich; poorly to moderately compacted; poorly t welded; jointed. Unit contains ~30-40% phenocrysts, including: quartz (~10%), sanidin plagioclase (~50%), biotite (~15%), and amphibole (~1-3%). Lithic fragments (~5%); pumice (~5 moderately resistant, rounded hills and cliffs. Contacts are sharp. Exposed thickness is ~180 to 670 ft).

Pahranagat Formation (early Miocene) — 22.6 Ma rhyolitic ash-flow tuff, pink to purple-gra lighter fresh, moderately crystal-rich, well-compacted, densely welded. Base of the unit contains vitrophyre, and 9 m of poorly welded surge (?) deposits, which can be divided into 3 flow units. unit is pink-brown weathering, buff to pink fresh, moderately-compacted, poorly-welded, lithic-fra 6 cm in diameter) and biotite-rich, reverse graded. Overlying is a buff-white thin (6-10 cm) laminated, upward coarsening (up to 1 mm in diameter) crystal- and lithic fragment-rich tuff. Upp (?) unit is a poorly compacted, moderately welded, lithic fragment (up to 2.5 cm in diameter) an reverse-graded deposit. Unit contains 6.3% phenocrysts, including: quartz (26.3%), sanic plagioclase (23.6%), biotite (7.8%) and hornblende (2.6%). Lithic fragments (5%), pumice-ri Form moderately resistant cliffs and ledges. Contact with overlying unit not exposed. Exposed 70 to 90 m (220 to 300 ft).

Shingle Pass Tuff (Ts—undivided lower and upper units or Tsu—upper cooling unit) (late O Rhyolitic ash-flow tuff, upper of two cooling units, separated by the tuff of Hancock Summit. 2 dark purple-brown to red-brown weathering, red-gray to purple-gray fresh, crystal-poor, wel densely welded. Unit contains ~2 m thick, dark gray to black vitrophyre near base, overlain by finely laminated, upward coarsening (up to 1 mm in diameter) crystal- and lithic fragment-ri deposit. Unit contains 7.8% phenocrysts, including: quartz (8.5%), sanidine (31.9%), plagiocl biotite (4.3%), and pyroxene (4.3%). Lithic fragments (5%) pumice (15%). Very resistant, forms m and steep slopes. Contacts are sharp. Exposed thickness is 70 to 120 m (230 to 400 ft).

Tuff of Hancock Summit (late Oligocene) — Rhyolitic ash-flow tuff; tan-gray, orange-gray ar weathering; tan to pink-gray fresh; crystal-rich; lithic-fragment-rich near base (~20%); poor t compacted; poorly welded near base; moderately welded towards top; jointed. 0.5 to 1 m thick, l gray vitrophyre near base of unit. Unit contains 18.5% phenocrysts including: quartz (do smokey) (40.5%), sanidine (31.5%), plagioclase (21.6%), and biotite (3.6%). Lithic fragment pumice (<5%). Forms moderately resistant, rounded cliffs and slopes. Contacts are sharp. Thi m (500 ft). Single crystal fusion of sanidines from this tuff yielded an $^{40}Ar/^{39}Ar$ weighted mean ag 0.15 Ma.

Shingle Pass Tuff (Ts—undivided lower and upper units or Tsl—lower cooling unit) (late O Rhyolitic ash-flow tuff, lower of two cooling units, separated by the Tuff of Hancock Summit. 26 light pink-gray to red-gray weathering, darker fresh, crystal-poor, moderately to well-compac welded. Red-brown to black, devitrified vitrophyre at base. Unit contains 8.3% phenocrysts, incl (14%), sanidine (28%), plagioclase (42%), pyroxene (2%) and olivine (2%). Lithic fragments

OUNT IRISH AND EAST
N COUNTY, NEVADA

By
Tandis Bidgoli
2003

rown-gray and tan weathering; compacted; poorly to moderately lz (~10%), sanidine (~15-25%), s (~5%); pumice (~5-10%). Forms hickness is ~180 to 200 m (600 to

, pink to purple-gray weathering, e of the unit contains a ~1 m thick ded into 3 flow units. Lowest flow orly-welded, lithic-fragment (up to vhite thin (6-10 cm) unit of finely agment-rich tuff. Uppermost surge 5 cm in diameter) and crystal rich, uartz (26.3%), sanidine (34.2%), ents (5%), pumice-rich (10–20%). ot exposed. Exposed thickness is

cooling unit) (late Oligocene) — Hancock Summit. 26.0 Ma tuff is sh, crystal-poor, well-compacted, ear base, overlain by 15-30 cm of and lithic fragment-rich surge (?) ine (31.9%), plagioclase (46.8%), ery resistant, forms moderate cliffs 30 to 400 ft).

gray, orange-gray and red-brown base (~20%); poor to moderately ed. 0.5 to 1 m thick, light brown to ncluding: quartz (dominantly var. 6%). Lithic fragments (10–25%), ntacts are sharp. Thickness ~150 ^{40}Ar weighted mean age of 26.78+/-

cooling unit) (late Oligocene) — Hancock Summit. 26.7 Ma tuff is rately to well-compacted, densely 3% phenocrysts, including: quartz

Tfl — Lacustrine limestone and conglomerate (late Oligocene) — Freshwater l pebble to cobble conglomerate. Limestone: light yellow-brown to light oran buff fresh, fine to medium grained, coarsely crystalline in places, fetid, algal cm) to massive freshwater limestone. Stromatolite mounds common. Intra intraclasts up to 3 cm in diameter, commonly 0.5 cm in diameter. Plana ranges from 5-40 cm. Limestone forms soft low-relief hills and moderatel beds consist of small pebbles to small cobbles within a medium yellow-l matrix; dominantly small pebble sized clasts; subrounded to rounded; p Dominantly Paleozoic carbonate and black chert clasts. Recognizable clast Limestone, Sevy Dolomite, and Pogonip Group. Conglomerate forms soft sharp. Thickness ~360 m (1200 ft.).

Tm — Monotony Tuff (lower cooling unit) (late Oligocene) — ~27.3 Ma dacitic identical, cooling units. Lower cooling unit is light-gray, tan-pink weathering; poorly to moderately compacted and welded. Unit contains ~20-40% (10-15%), sanidine (~10%), plagioclase (~50%), biotite (~20%), amphib Lithic fragments (~5%), pumice (1-5%). Forms weak, rounded outcrops. ~90 m (300 ft).

Tfl — Lacustrine limestone and conglomerate (Tertiary) — Freshwater lime orange-brown weathered, tan-brown to buff fresh, fine to medium grained, algal-laminated (lamina range from 1-3 cm) to massive freshwater limesto Indistiguishable from Tfl above, except by stratigraphic order.

Mc — Chainman Shale (Mississippian) — Siltstone, yellow-brown weathering, b fractured. Platy thin beds form nonresistant slopes and saddles. Contact Exposed thickness is ~53 m (175 ft).

Mj — Joana Limestone (Mississippian) — Limestone, medium blue-gray to light-gray fresh, medium to coarse-grained, thinly laminated, chert nodules common. Fossiliferous with abundant crinoids and bryozoans. Thick (> 1 and step-like slopes. Contact with overlying unit is sharp. Exposed thickn to 720 ft).

Mp — West Range Limestone/ Pilot Shale (Mississippian–Devonian) — Calcareo limestone, yellow gray to medium gray weathering, dark-gray fresl thin-bedded. Bed thickness ranges from 2 to 20 cm. Forms nonresistant contact is sharp. Exposed thickness is ~36 m (120 ft).

D EASTERN TIMPAHU
/ADA

omerate (late Oligocene) — Freshwater limestone interbedded locally with Limestone: light yellow-brown to light orange-brown weathered, tan-brown to d, coarsely crystalline in places, fetid, algal-laminated (lamina range from 1-3 tone. Stromatolite mounds common. Intraclast beds (5 to 30 cm thick) with ter, commonly 0.5 cm in diameter. Planar to wavy bedded, bed thickness ıe forms soft low-relief hills and moderately resistant ledges. Conglomerate o small cobbles within a medium yellow-brown to orange-brown sandy silt sized clasts; subrounded to rounded; poorly consolidated; poorly sorted. and black chert clasts. Recognizable clasts of Scotty Wash Quartzite, Joana Pogonip Group. Conglomerate forms soft, easily eroded saddles. Contacts ft.).

ıit) (late Oligocene) — ~27.3 Ma dacitic ash-flow tuff, lower of two, nearly ɔling unit is light-gray, tan-pink weathering; light-gray to buff fresh; crystal-rich; ɛd and welded. Unit contains ~20-40% phenocrysts, including: quartz gioclase (~50%), biotite (~20%), amphibole (1-5%), and pyroxene (~3%). (1-5%). Forms weak, rounded outcrops. Contacts are sharp. Thickness is

ɡlomerate (Tertiary) — Freshwater limestone: light yellow-brown to light own to buff fresh, fine to medium grained, coarsely crystalline in places, fetid, ɔm 1-3 cm) to massive freshwater limestone. Stromatolite mounds common. ɛxcept by stratigraphic order.

— Siltstone, yellow-brown weathering, brown-gray fresh, very fine-grained, ıonresistant slopes and saddles. Contact with overlying unit is not exposed. ft).

ı) — Limestone, medium blue-gray to medium brown-gray weathering, e-grained, thinly laminated, chert nodules (3 to 8 cm in diameter) and layers dant crinoids and bryozoans. Thick (> 1 m) bedded. Forms resistant cliffs h overlying unit is sharp. Exposed thickness ranges from 180 to 215 m (600

ıle (Mississippian–Devonian) — Calcareous siltstone, yellow-brown, and silty dium gray weathering, dark-gray fresh, very fine-grained, well-sorted, ɛs from 2 to 20 cm. Forms nonresistant slopes and saddles. Overlying unit ɛss is ~36 m (120 ft).

Dsi — Simonson Dolomite (Devonian) brown weathering, medium g stromatoporoid and "spaghetti" crinoids. Bed thickness ranges placed at base of yellow-brown 200 to 280 m (680 to 940 ft).

Do — Oxyoke Canyon Sandstone (D fresh, fine to coarse-grained s features common; fractured and resistant cliffs and steep slopes to 150 ft).

Dse — Sevy Dolomite (Devonian) — fine-grained, thinly laminated. W step-like slopes. Contact with 900 ft)

Sl — Laketown Dolomite (Silurian) – medium-brown fresh, medium-g near base, dominantly poorly be exposed. Exposed thickness ra

Oes — Ely Springs Dolomite (Ordovici fresh, medium to coarse graine appearance, fossiliferous. Calci Blocky cliff former. Upper conta (940 ft).

Oe — Eureka Quartzite (Ordovician) - gray to pink fresh; fine to mec locally; pervasively fractured; b and below. Contact with overlyir

Pogonip Group (Ordovician) — divided, from Valley Limestone using subdivisions of Byers used on cross sections

Opa — Antelope Valley Formation (Or weathering, medium gray to ligh mottled in places. Chert nod Receptaculites, corals, bryozoa overlying Eureka Quartzite is sh

Opg — Goodwin Limestone (Ordovician light purple-gray fresh, fine to m

MPAHUTE RANGES,

Dsi — Simonson Dolomite (Devonian) — Alternating beds of light and dark brown dolomite, light brown to chocolate brown weathering, medium gray to dark brown fresh, fine to medium grained, thinly laminated, local stromatoporoid and "spaghetti" fossil bioherms common near top. Other fossils include brachiopods and crinoids. Bed thickness ranges from 10 cm to 1 m. Forms steep step-like cliffs and slopes. Upper contact placed at base of yellow-brown weathering, nonresistant, thin-bedded, silty dolomite. Thickness ranges from 200 to 280 m (680 to 940 ft).

Oo — Oxyoke Canyon Sandstone (Devonian) — Sandstone, tan to red-brown weathering, buff white to light gray fresh, fine to coarse-grained silica-cemented quartz-sandstone. Cross-bedding, ripple marks and channel features common; fractured and brecciated near faults. Bed thickness ranges from 0.3 to 1.5 m thick. Forms resistant cliffs and steep slopes. Contact with overlying unit is sharp. Thickness ranges from 36 to 45 m (120 to 150 ft).

Dse — Sevy Dolomite (Devonian) — Dolomite, white to light gray weathering, medium to dark gray fresh, very fine-grained, thinly laminated. Well-bedded, bed thickness ranges from 40 to 80 cm. Forms moderate to steep, step-like slopes. Contact with overlying unit is sharp. Exposed thickness ranges from 225 to 270 m (750 to 900 ft)

Sl — Laketown Dolomite (Silurian) — Dolomite and silty dolomite, light to medium gray-brown weathering, tan to medium-brown fresh, medium-grained to moderately crystalline in places, fossil corals present. Thin-bedded near base, dominantly poorly bedded. Forms steep, step-like cliffs and slopes. Contact with overlying unit not exposed. Exposed thickness ranges from 72 to 210 m (240 to 700 ft).

Oes — Ely Springs Dolomite (Ordovician) — Dolomite and limestone, dark brown gray weathering, dark olive-gray fresh, medium to coarse grained, sugary texture, abundant chert nodules, bioturbation can give unit a mottled appearance, fossiliferous. Calcite-filled fractures and vugs common. Bed thickness ranges from 30 to 50 cm. Blocky cliff former. Upper contact placed at base of light gray, thin-bedded, silty dolomite. Thickness ~280 m (940 ft).

Oe — Eureka Quartzite (Ordovician) — Quartz sandstone; buff-white, orange to red-brown weathering; white, light gray to pink fresh; fine to medium grained; dominantly well-sorted and silica-cemented; calcite cemented locally; pervasively fractured; brecciated near faults; thick-bedded. Forms resistant cliffs with ledges above and below. Contact with overlying unit is sharp. Thickness ranges from 126 to 135 m (420-450 ft).

Pogonip Group (Ordovician) — divided, from base to top, into the Goodwin Limestone, Ninemile Formation, and Antelope Valley Limestone using subdivisions of Byers et al. (1961). Ninemile Formation is not exposed in map area. Op - undivided, used on cross sections

Opa — Antelope Valley Formation (Ordovician) — Limestone and silty limestone, medium gray to brownish gray weathering, medium gray to light blue-gray fresh, finely to moderately crystalline, massive to thinly laminated, mottled in places. Chert nodules and nodular layers, bioturbation, and fossils common. Fossils include Receptaculites, corals, bryozoans, and sponges. Bed thickness ranges from 8 to 40 cm. Contact with overlying Eureka Quartzite is sharp. Exposed thickness ~74 m (245 ft).

Opg — Goodwin Limestone (Ordovician) — Limestone and silty limestone, medium to dark purple-gray weathering to light purple-gray fresh, fine to medium grained. Brownish-orange silty layers and lenses, chert nodules (4 to 6 cm in diameter) and irregular layers and fossil hash common. Bed thickness ranges from 6 to 50 cm

QTo — Older fan gravels (Quaternary and/ or Tertiary (?)) — Dissected alluvial fan and fan remnant deposits; granul to large boulder sized clasts; dominantly small pebbles sized clasts; subangular to subrounded well-consolidated; poorly to moderately well sorted; poor to moderate stratification. Dominantly Paleozoi carbonate clasts (>75%); some jasperoid and minor volcanic clasts. Recognizable clasts of the Pogoni Group, Eureka Quartzite, Monotony Tuff and Shingle Pass Tuff. Unit contains a 4-6 cm thick Av horizo overlying a thick stage 4-5 carbonate soil. Fan surfaces have moderate desert pavement development an moderate desert varnish on quartz-rich clasts. Vegetation consists of sparse desert scrub, small juniper an pine trees.

QTg — Older stream gravels (Quaternary and/ or Tertiary (?)) — Stream channel deposit; granule to large cobb sized clasts; dominantly pebble sized clasts; subrounded to rounded; consolidated; poorly to moderately we sorted; moderately to well stratified. Dominantly Paleozoic carbonate clasts; some quartz sandstone clast Well cemented; stage 4-5 carbonate soil.

115° 30' 00"

37° 37' 30"

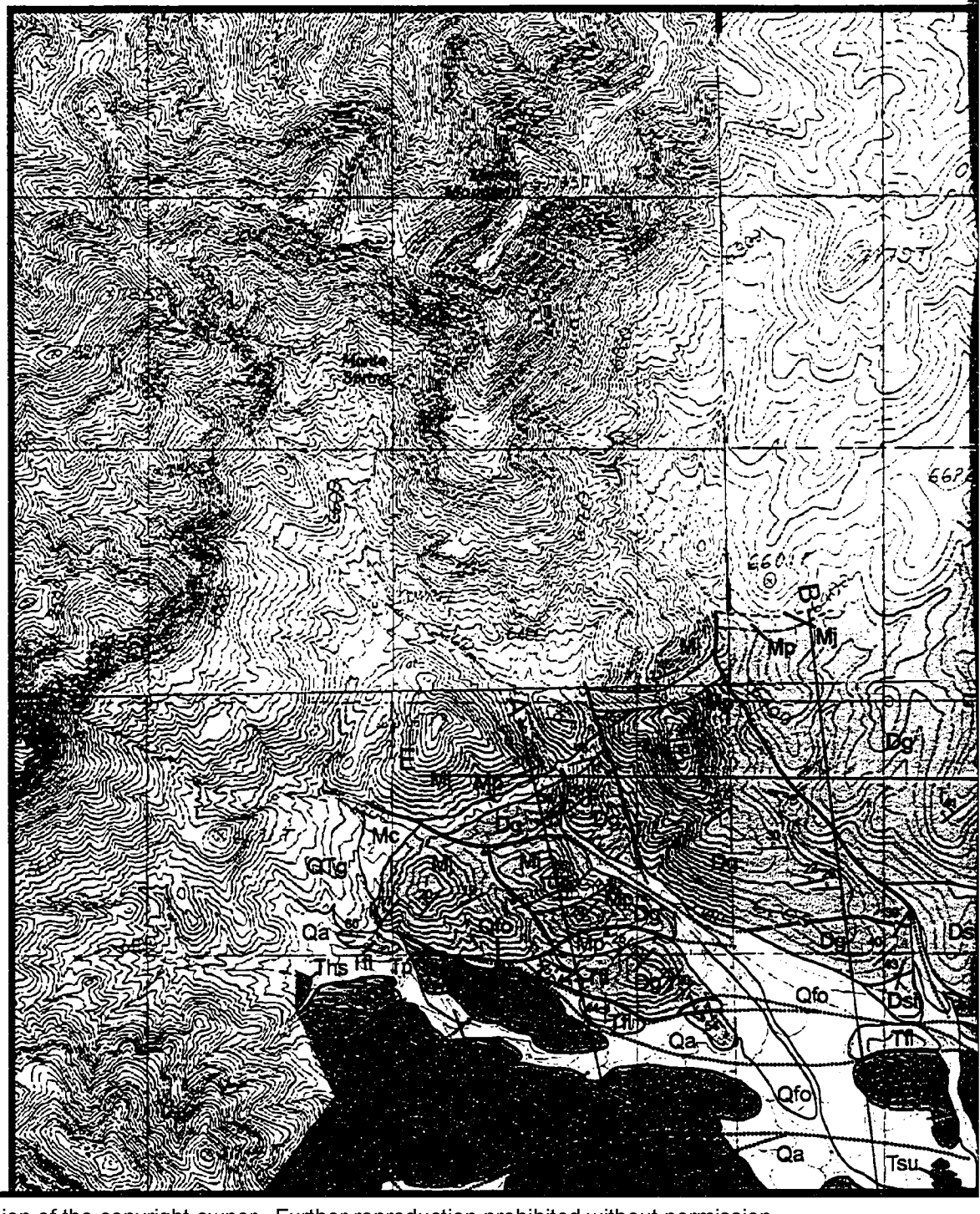

deposits; granule
to subrounded;
inantly Paleozoic
s of the Pogonip
thick Av horizon
development and
small juniper and

e to large cobble
o moderately well
sandstone clasts.

Tsl

Shingle Pass Tuff (Ts—undivided lower and upper units or Tsl—lower cooling unit) (late
Rhyolitic ash-flow tuff, lower of two cooling units, separated by the Tuff of Hancock Summit. 2
light pink-gray to red-gray weathering, darker fresh, crystal-poor, moderately to well-compa
welded. Red-brown to black, devitrified vitrophyre at base. Unit contains 8.3% phenocrysts, in
(14%), sanidine (28%), plagioclase (42%), pyroxene (2%) and olivine (2%). Lithic fragments
(~10%). Forms resistant cliffs and ledges. Contacts are sharp. Thickness is 45 to 245 m (150 to

Monotony Tuff (upper cooling unit) (late Oligocene) — ~27.3 Ma dacitic ash-flow tuff, upper
identical, cooling units. Light-gray, tan-yellow and orange-pink weathering, light- gray to buff fre
moderately compacted and welded. Unit contains 16.7% phenocrysts, including: quartz (
(24%), plagioclase (37%), biotite (14%), and pyroxene (2%). Lithic fragments (~5%); pumice
soft to moderately resistant, rounded outcrops. Contacts are sharp. Thickness is ~900 ft.

115° 27' 30"

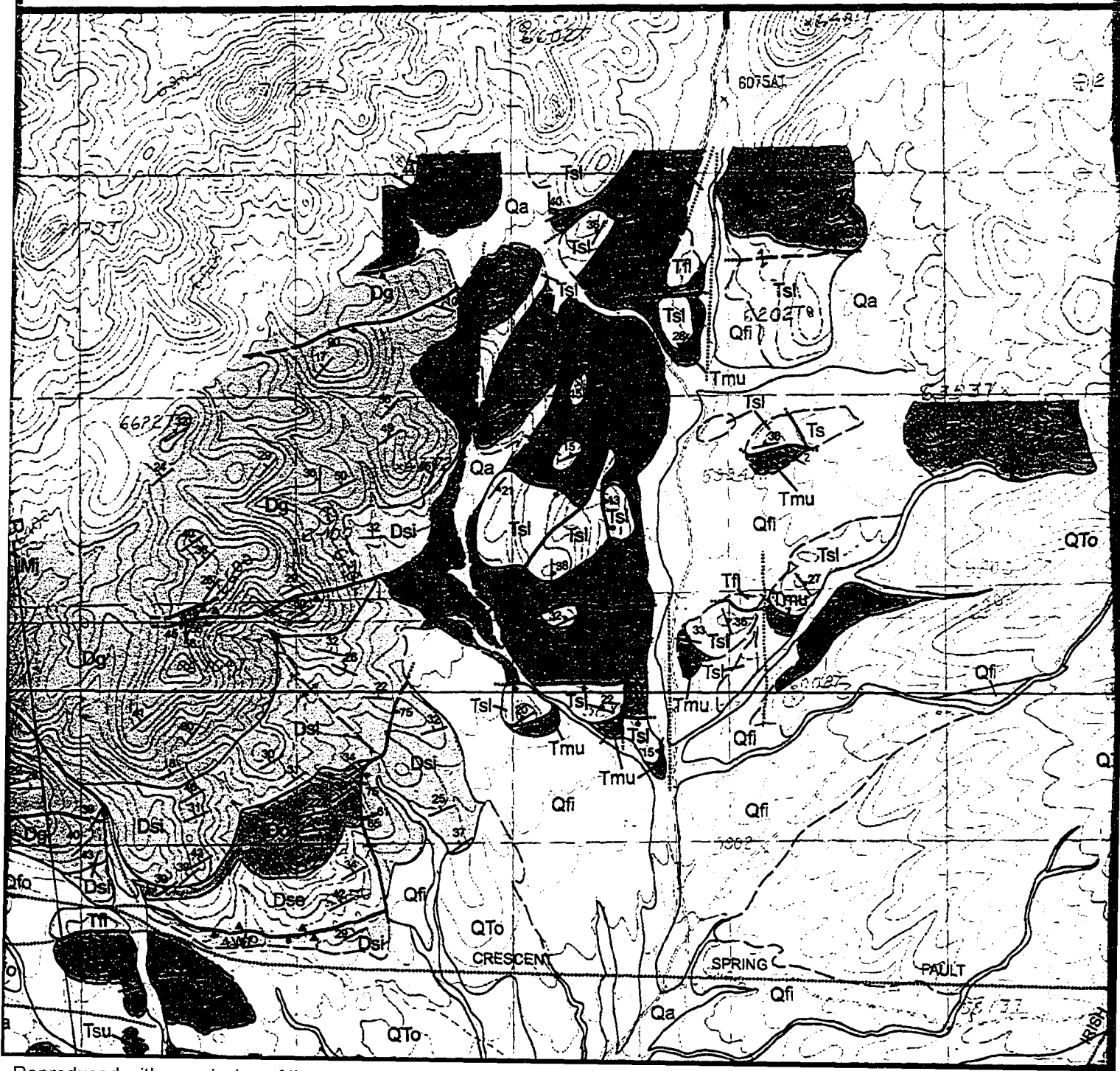

ver cooling unit) (late Oligocene) —
f of Hancock Summit. 26.7 Ma tuff is
derately to well-compacted, densely
s 8.3% phenocrysts, including: quartz
2%). Lithic fragments (~5%); pumice
s is 45 to 245 m (150 to 850 ft).

ic ash-flow tuff, upper of two, nearly
g, light- gray to buff fresh; crystal rich,
ts, including: quartz (12%), sanidine
ments (~5%); pumice (1-5%). Forms
kness is ~900 ft.

Mp

limestone, yellow gray to medium gray weathering, dark-gray fresh
thin-bedded. Bed thickness ranges from 2 to 20 cm. Forms nonresistant sl
contact is sharp. Exposed thickness is ~36 m (120 ft).

Dg

Guilmette Formation (Devonian) — Silty dolomite, sandy limestone and san
nonresistant, silty dolomite at base. Overlain by medium to dark gra
medium-grained limestone. Bioturbation and local stromatoporoid and "sp
Colonial corals, solitary corals, and brachiopods also common. Upper part
sandstone beds that are tan, orange to red-brown weathering; white to buff
well-sorted, silica-cemented; pervasively fractured and brecciated near fau
from 0.5 to 2 m. Forms resistant cliffs and step-like slopes. Contact with o
area. Exposed thickness ranges from 645 to 708 m (2150 to 2360 ft).

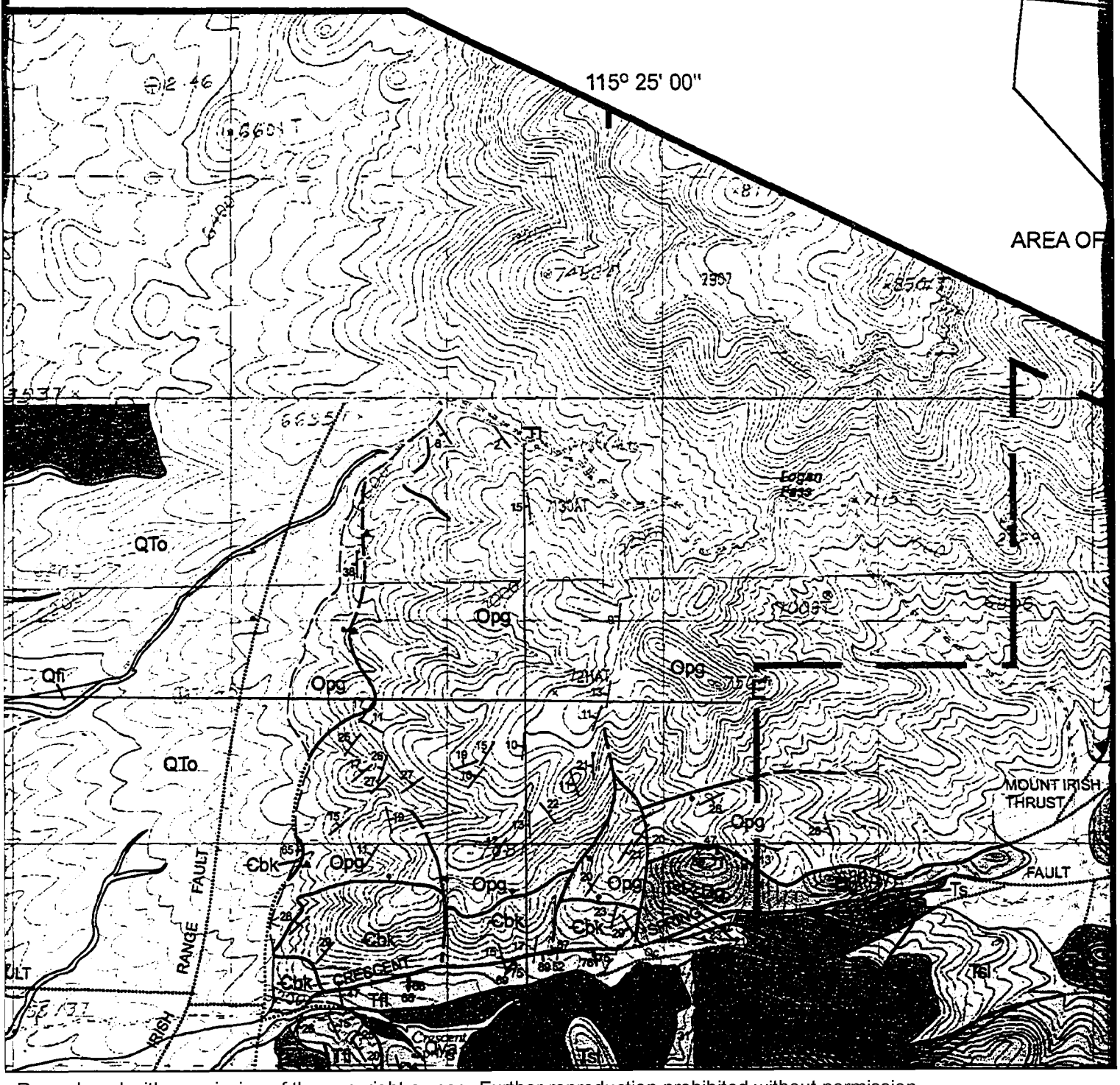

–Devonian) — Calcareous siltstone, yellow-brown, and silty
hering, dark-gray fresh, very fine-grained, well-sorted,
m. Forms nonresistant slopes and saddles. Overlying unit
ft).

sandy limestone and sandstone. Yellow-brown weathering,
by medium to dark gray weathering, dark gray fresh,
al stromatoporoid and "spaghetti" fossil bioherms common.
lso common. Upper part of unit contains numerous quartz
weathering; white to buff fresh; medium to coarse-grained;
and brecciated near faults. Overall, bed thickness ranges
e slopes. Contact with overlying unit is not exposed in map
m (2150 to 2360 ft).

overlying Eureka Quartzite is sharp. Exposed thickne

Opg

Goodwin Limestone (Ordovician) — Limestone and s
light purple-gray fresh, fine to medium grained. Brow
cm in diameter) and irregular layers, and fossil ha
Resistant cliff former. Contacts are not exposed. Exp

Cbk

Bonanza King Formation (Cambrian) — Alternating
dolomite, dark brown-gray to light blue-gray weathe
grained, thinly laminated. Chert nodules and n
Pervasively fractured and brecciated. Thick bedded,
overlying unit contacts are not exposed. Exposed thi

Contacts

Stratigraphic contact. Dashed where approximately located.

Normal fault. Dashed where approximately located, dotted where concealed. Ball and bar on down-thrown block, slip direction unknown.

Fault. Dashed where approximately located, dotted where concealed. Tick mark shows dip direction and magnitude. Arrow shows trend and plunge of lineation on fault surface.

45 70

Thrust fault. Dashed where approximately located, dotted where concealed. Sawteeth on upper plate, slip direction unknown

AREA OF MAP

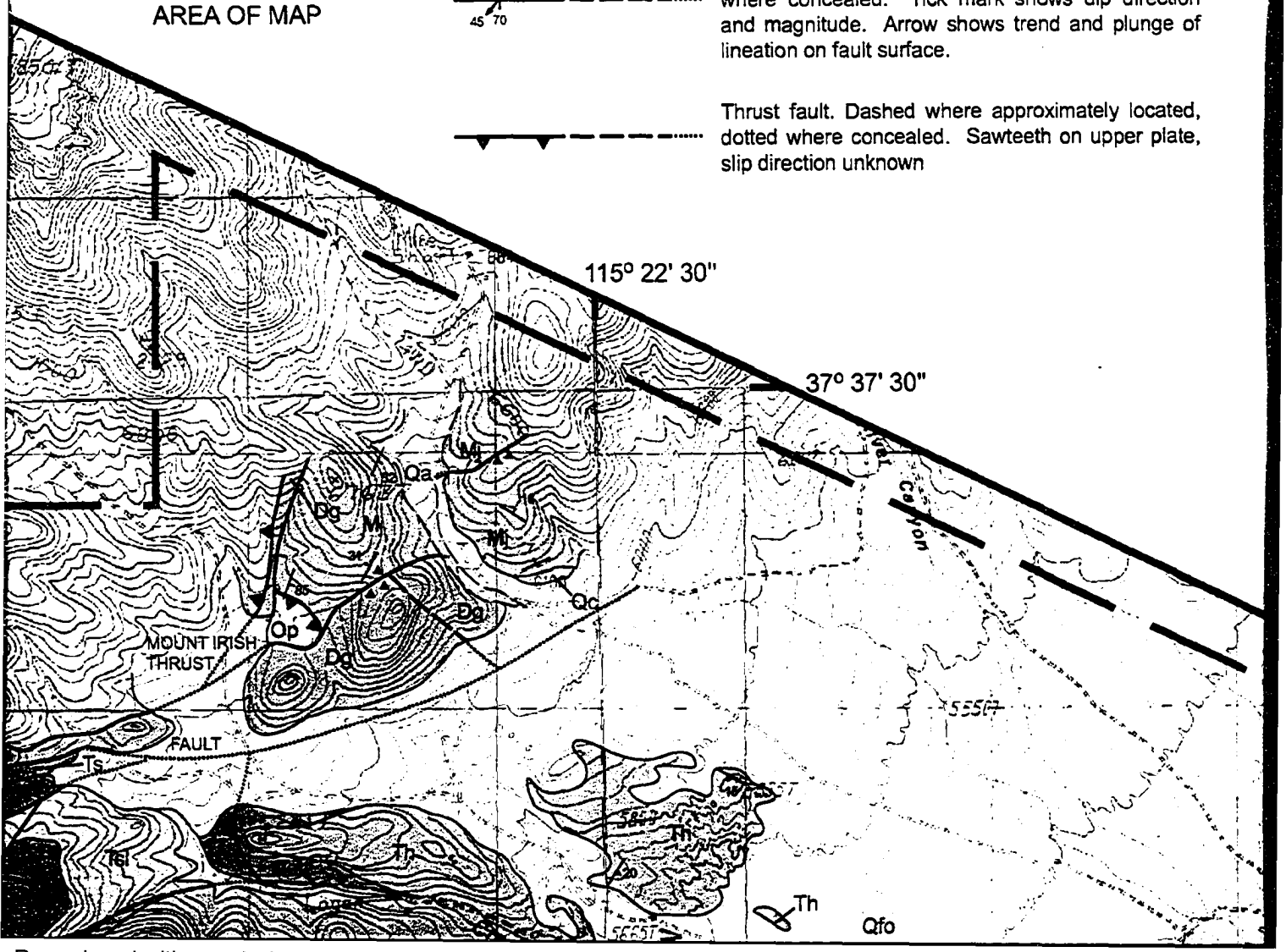

overlying Eureka Quartzite is sharp. Exposed thickness ~74 m (245 ft).

Goodwin Limestone (Ordovician) — Limestone and silty limestone, medium to dark purple-gray weathering to light purple-gray fresh, fine to medium grained. Brownish-orange silty layers and lenses, chert nodules (4 to 6 cm in diameter) and irregular layers, and fossil hash common. Bed thickness ranges from 6 to 50 cm. Resistant cliff former. Contacts are not exposed. Exposed thickness ranges from 135 to 150 m (450-500 ft).

Bonanza King Formation (Cambrian) — Alternating thick (>1 m) bands of light and dark gray limestone and dolomite, dark brown-gray to light blue-gray weathering, light gray to medium gray fresh, medium to coarse grained, thinly laminated. Chert nodules and nodular layers, bioturbation and fossil hash common. Pervasively fractured and brecciated. Thick bedded, forms steep resistant cliffs and ledges. Underlying and overlying unit contacts are not exposed. Exposed thickness ranges from ~60 to 150 m (200-500 ft).

Symbols

atigraphic contact. Dashed where approximately ated.

rmal fault. Dashed where approximately located, ted where concealed. Ball and bar on down-own block, slip direction unknown.

ult. Dashed where approximately located, dotted ere concealed. Tick mark shows dip direction d magnitude. Arrow shows trend and plunge of ation on fault surface.

rust fault. Dashed where approximately located, ted where concealed. Sawteeth on upper plate, direction unknown

15 Strike and dip of bedding

20 Strike and dip of compaction foliation

Tie line linking stratigraphic units

Syncline. Trend and plunge of the axial surface. Dashed where approximately located.

Anticline. Trend and plunge of the axial surface. Dashed where approximately located.

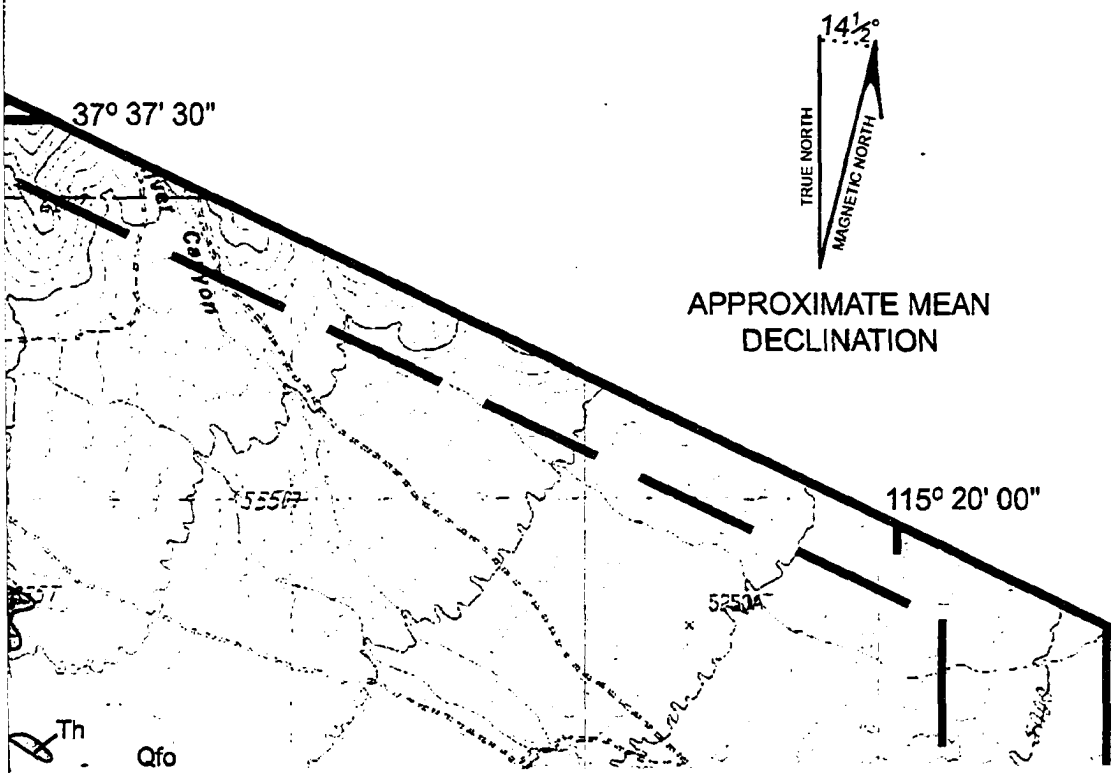

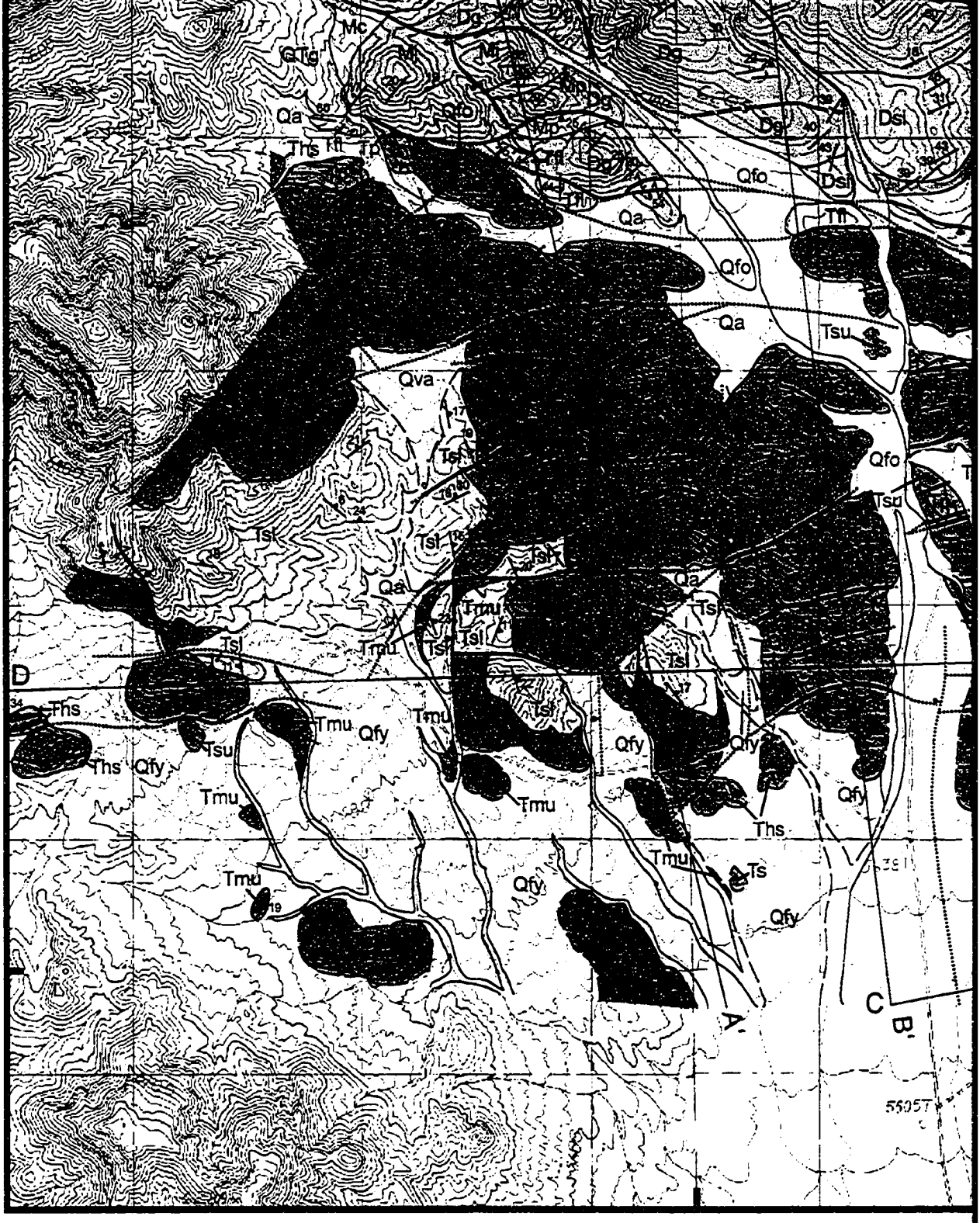

Data are placed onto portions of the Crescent Spring, Mount Irish, Mount Irish SE, Monte Mountain and Tempiute Mountain SE, USGS 7.5 minute quadrangle, topographic base maps.

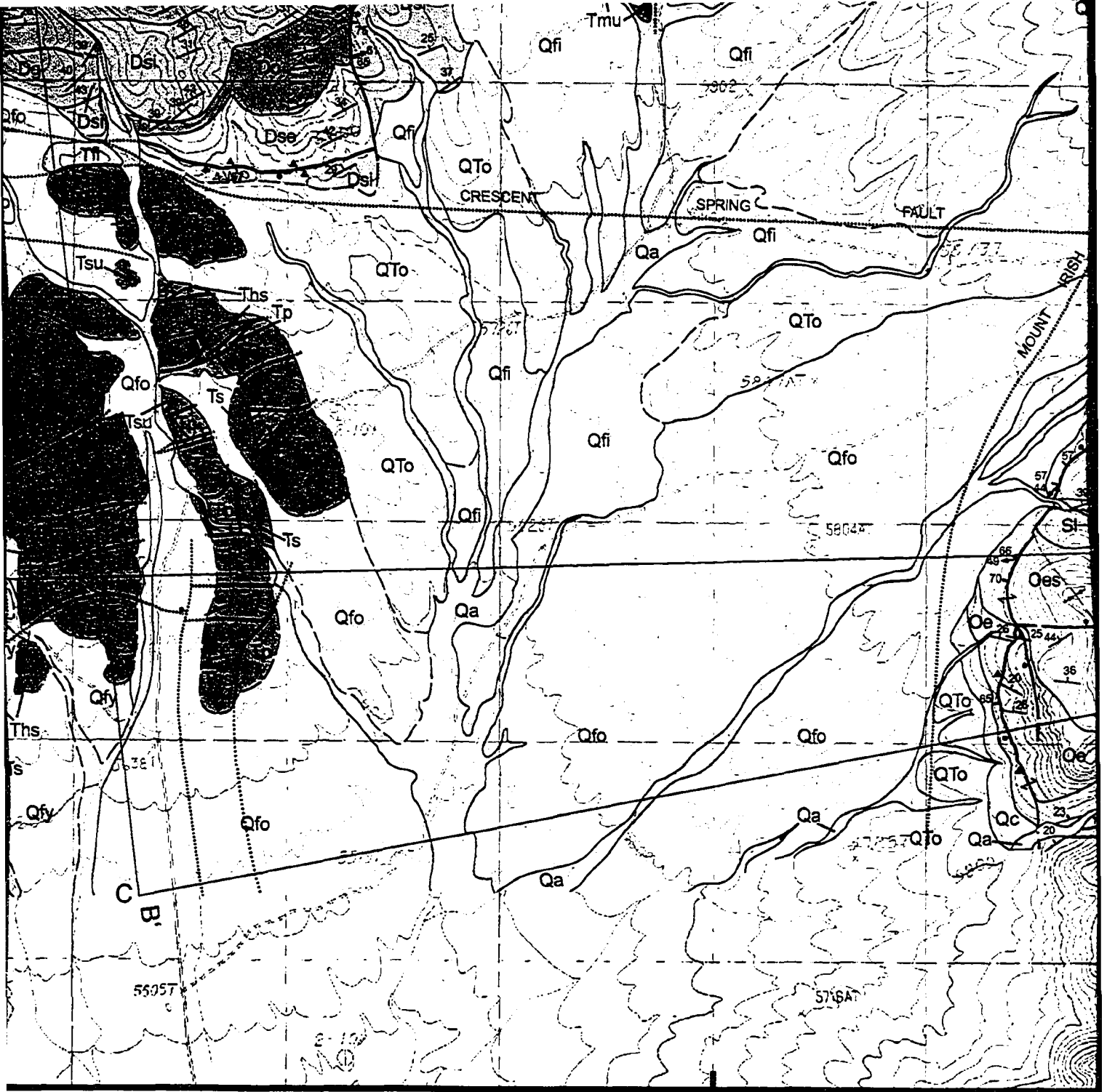

1 0.5

1000 0 100

1

CONTOU
NATIONAL GE

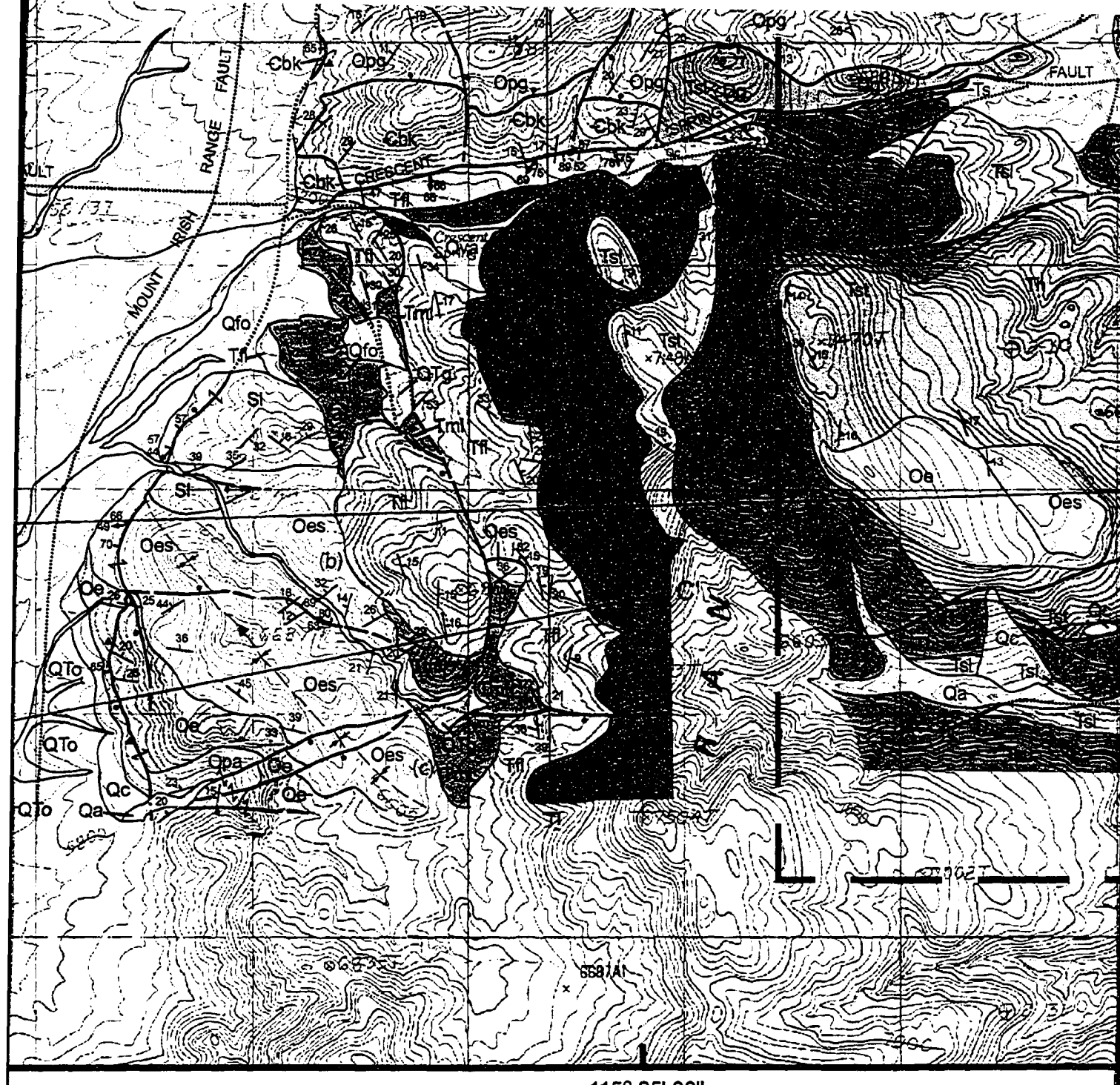

115° 25' 00"

SCALE 1:24,0000

0.5 0 1 MILE

1000 0 1000 2000 3000 4000 5000 6000 7000 FEET

1 0.5 0 1 KILOMETER

CONTOUR INTERVALS 20 AND 40 FEET
NATIONAL GEODETIC VERTICAL DATUM OF 1929

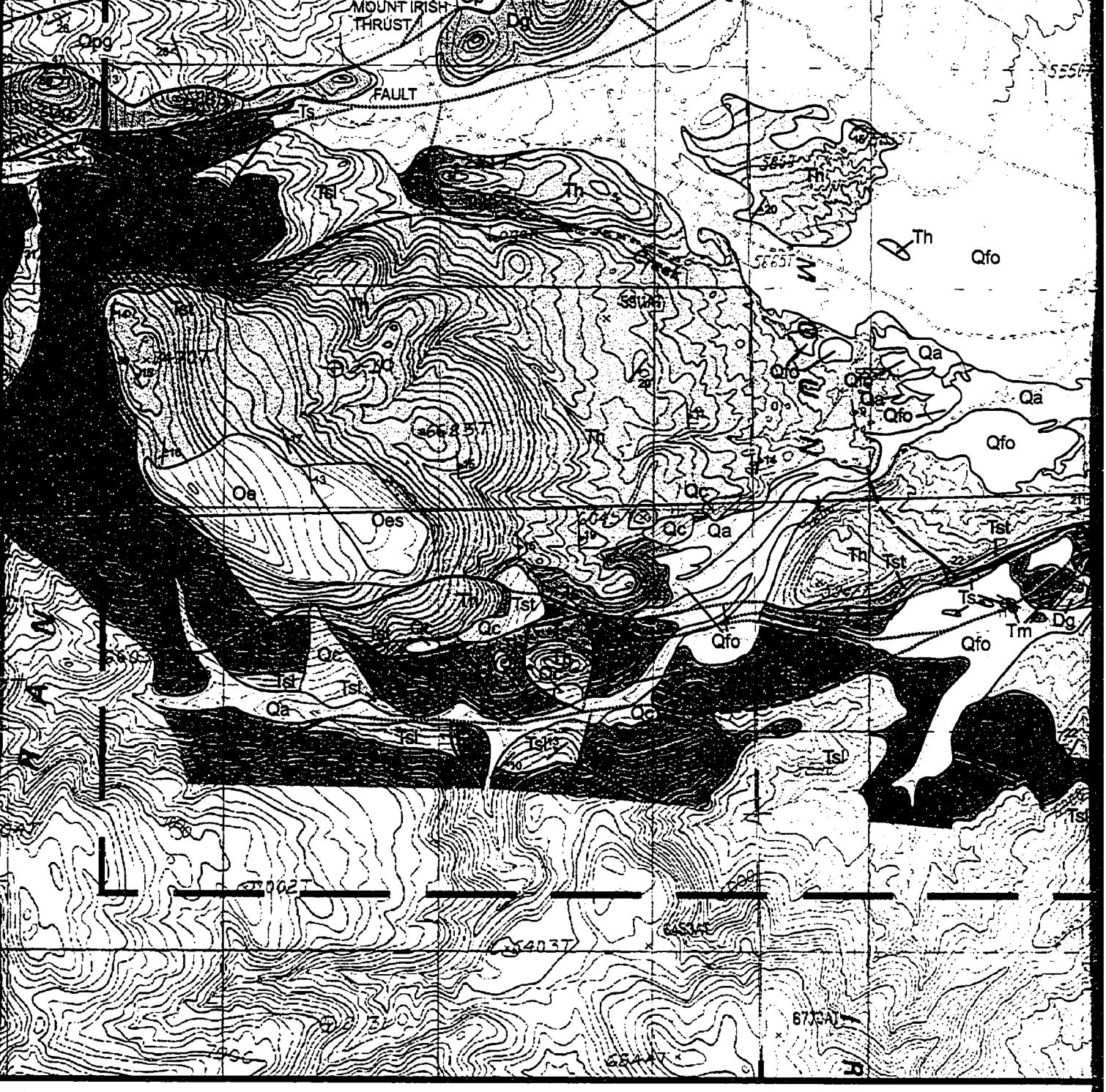

00"

115° 22' 30"

MILE

Supplement to:

Bidgoli, T.S., 2005, The role of transverse fa
faults or N-S extension? [M.S. thesis]: L

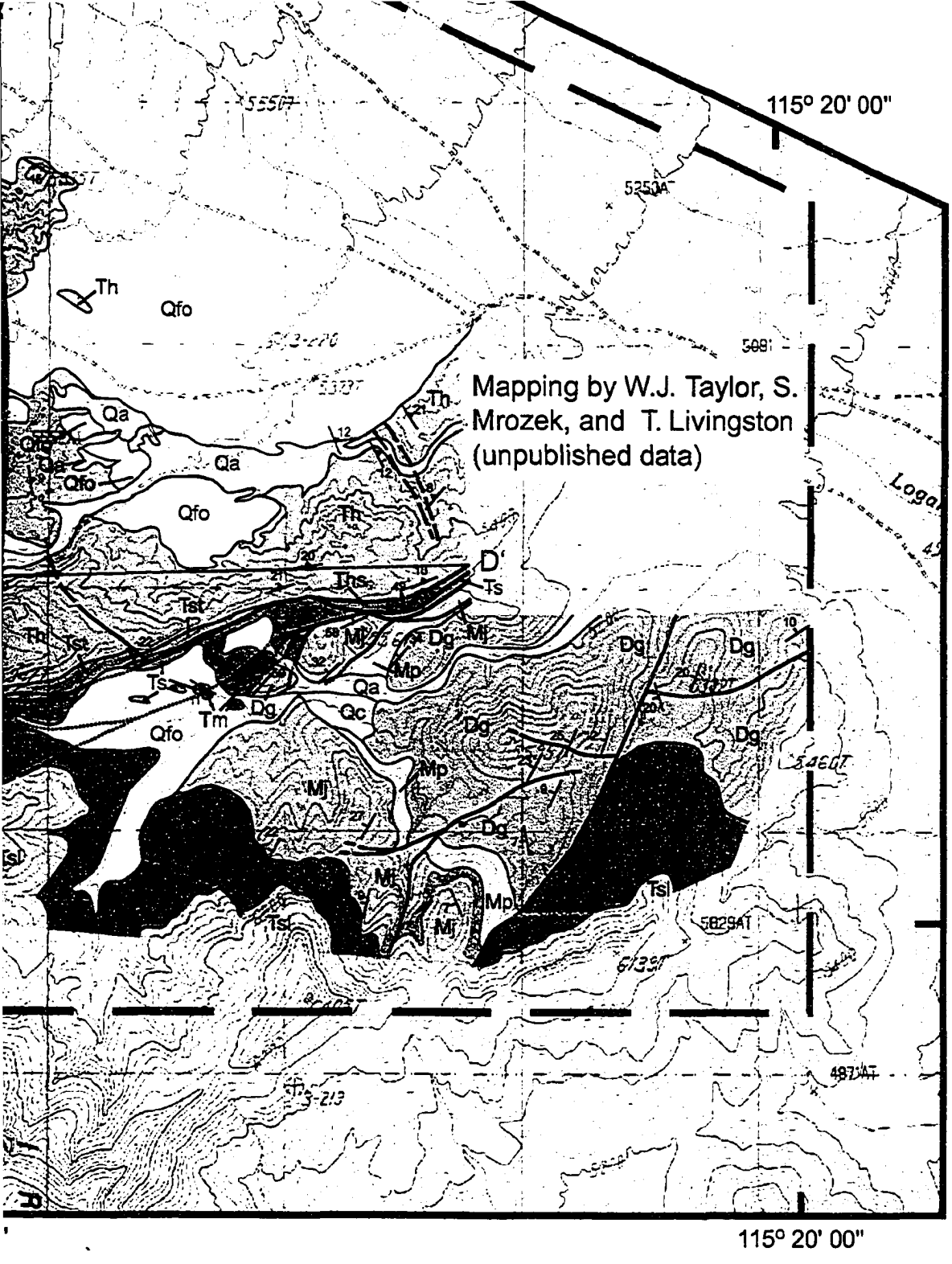

ble of transverse faults in Great Basin extension: Transfer on? [M.S. thesis]: Las Vegas, University of Nevada, 109 p.

PLATE 2. GEOLOGIC

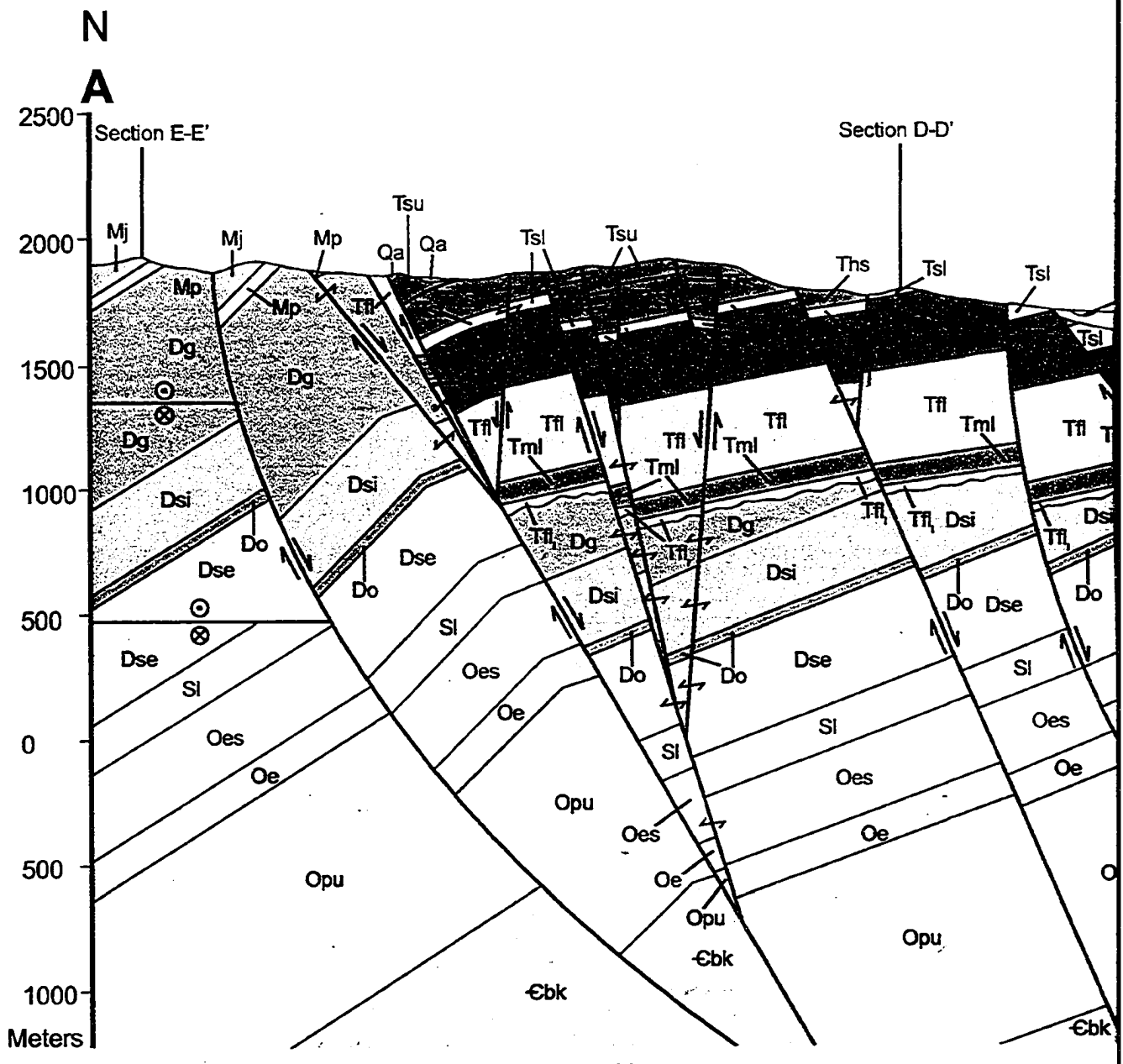

a. Deformed state cross-section A-A'.

W
D
2500

GIC CROSS SECTIONS

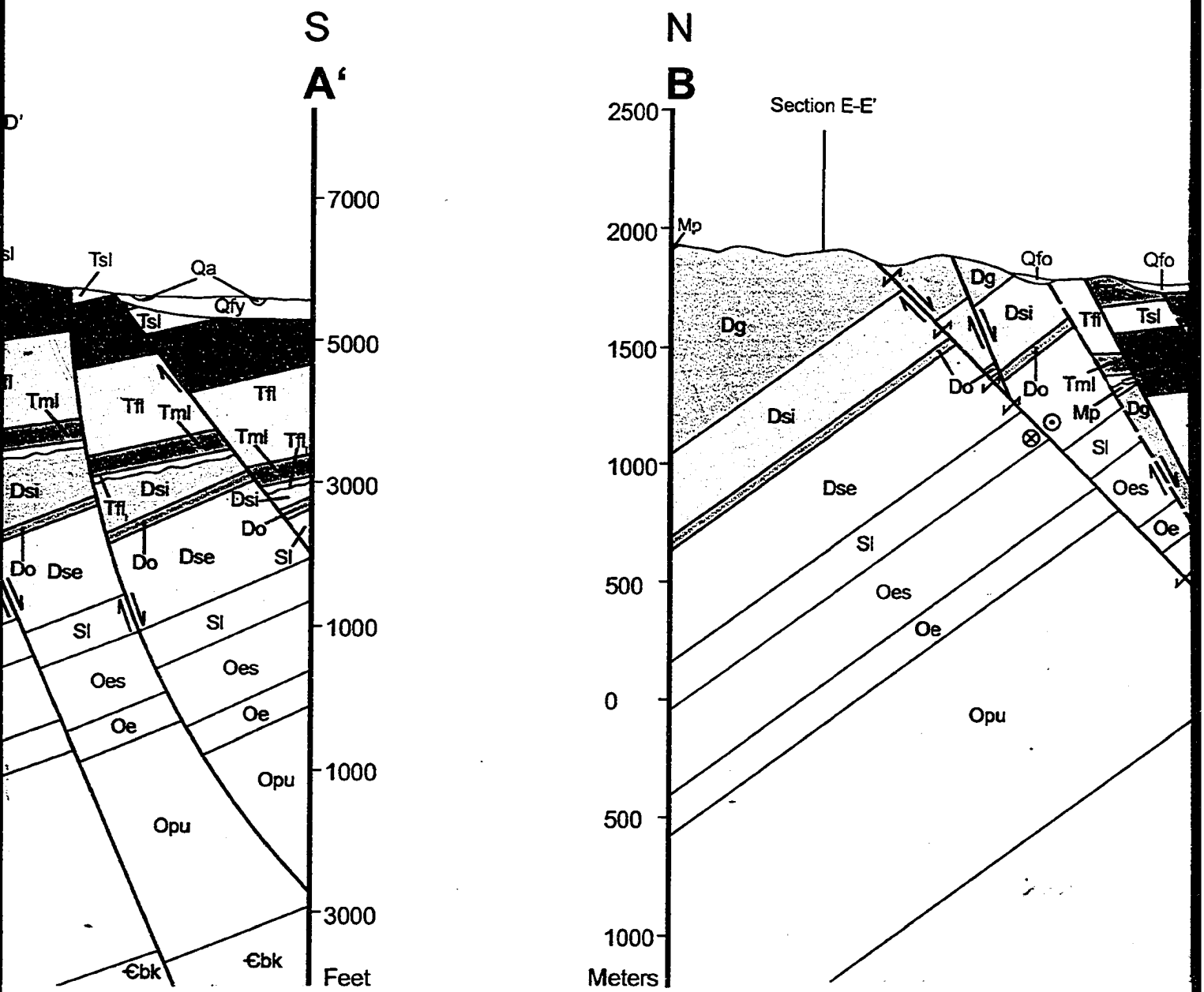

b. Deformed state cross-section B-B'

ONS

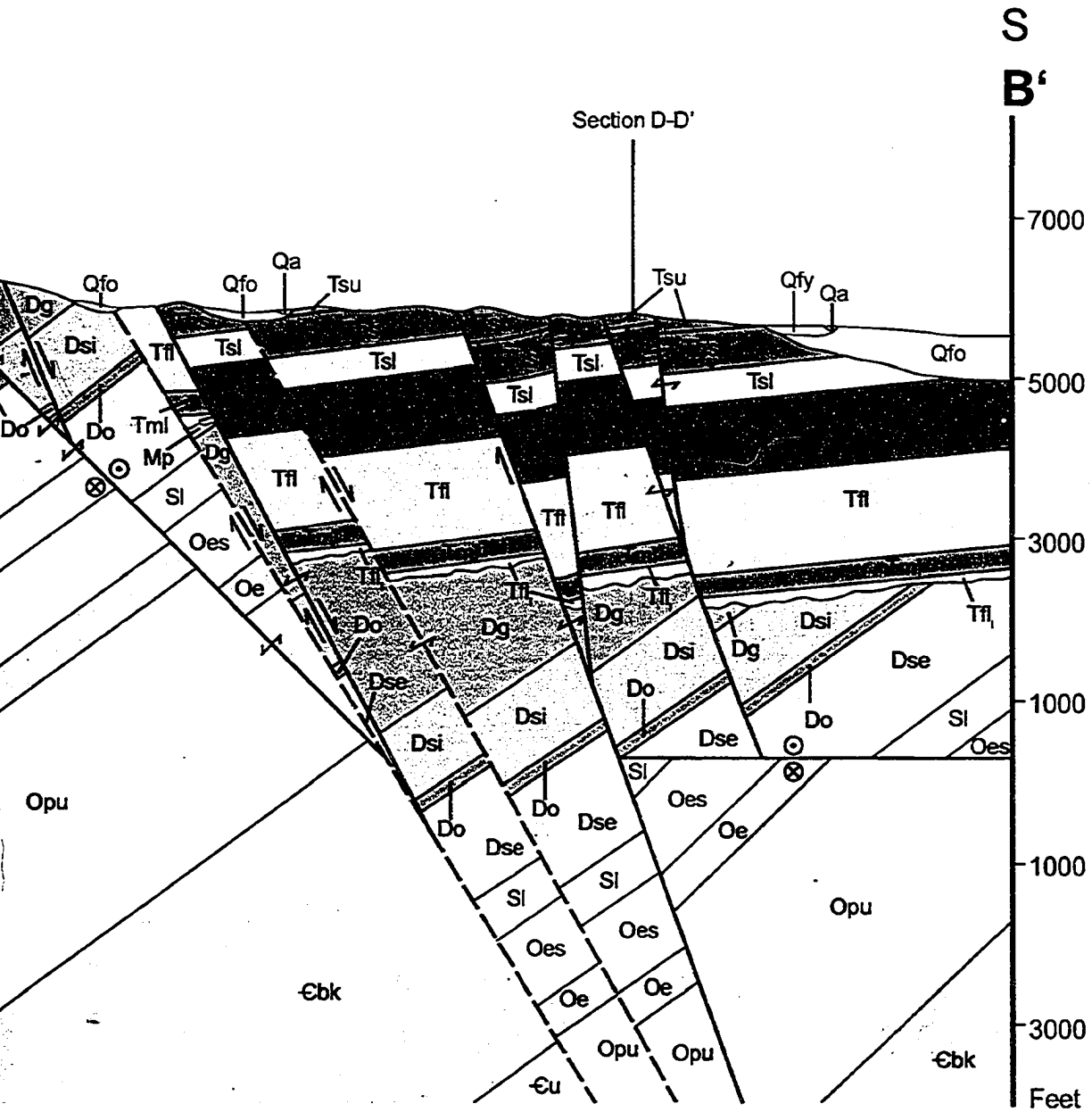

cross-section B-B'.

Section E-E'

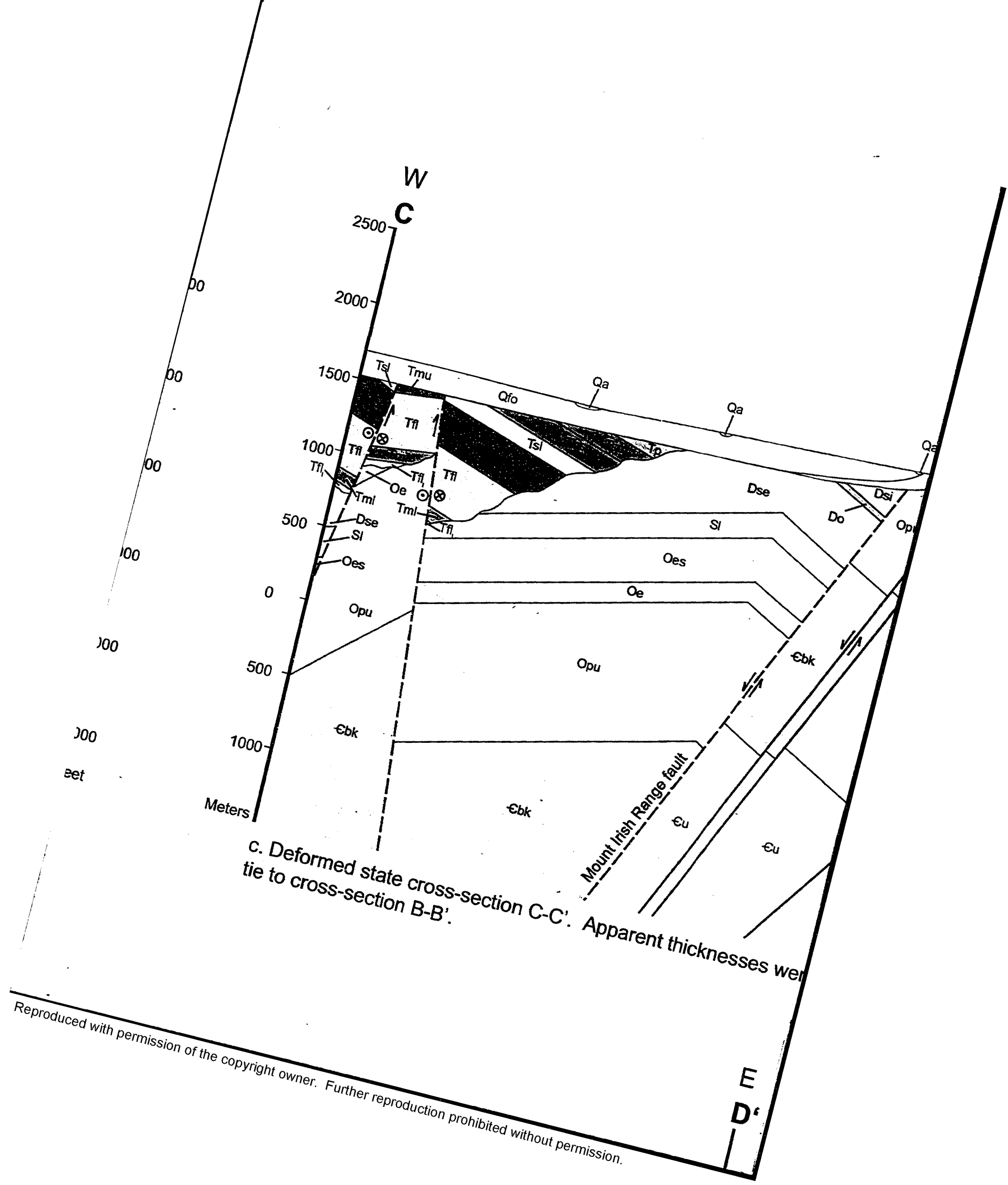

c. Deformed state cross-section C-C'. Apparent thicknesses wer
tie to cross-section B-B'.

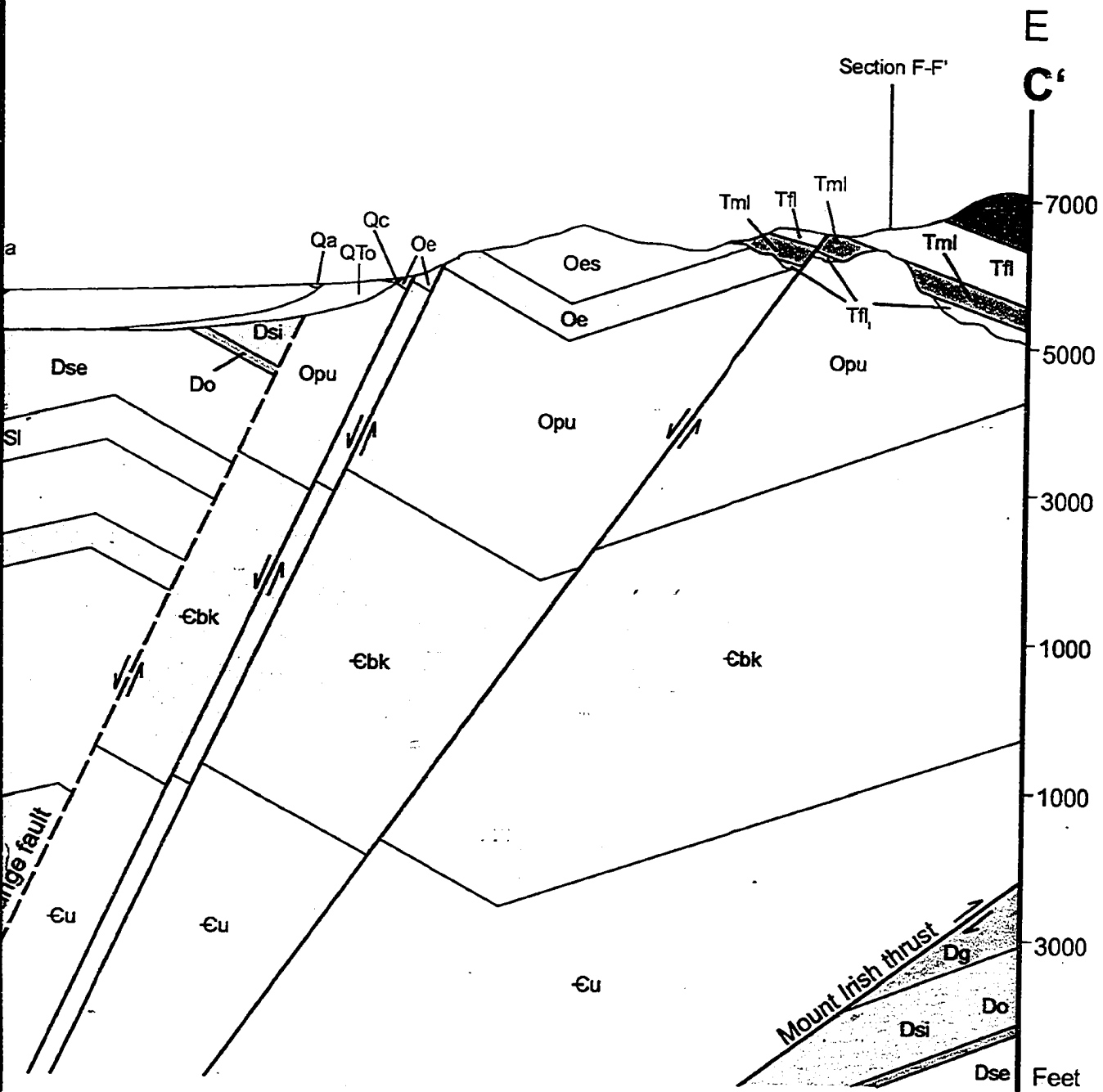

arent thicknesses were used in the west fault block in order to properly

E

D'

KEY

Qa Alluvium

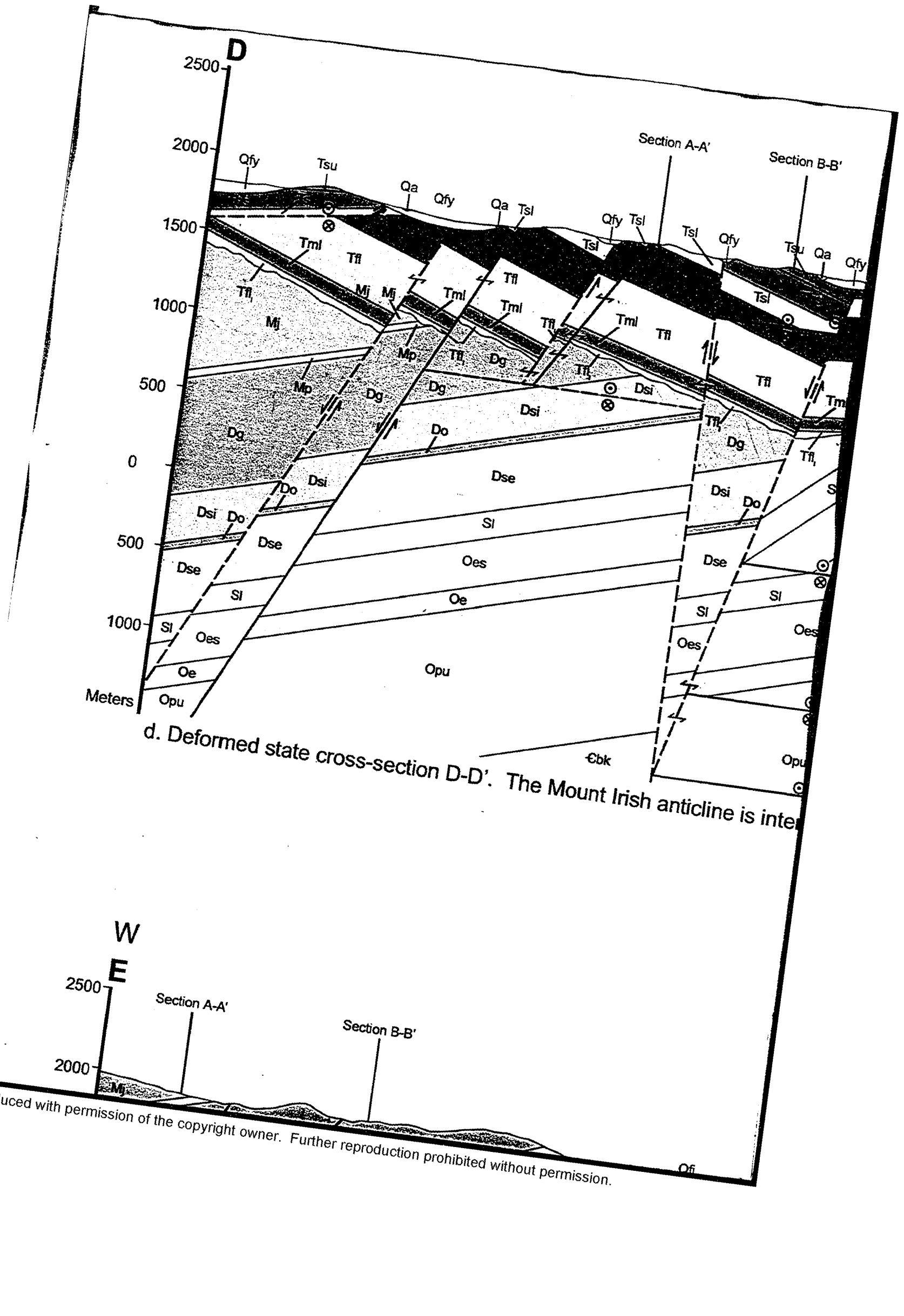

d. Deformed state cross-section D-D'. The Mount Irish anticline is inte

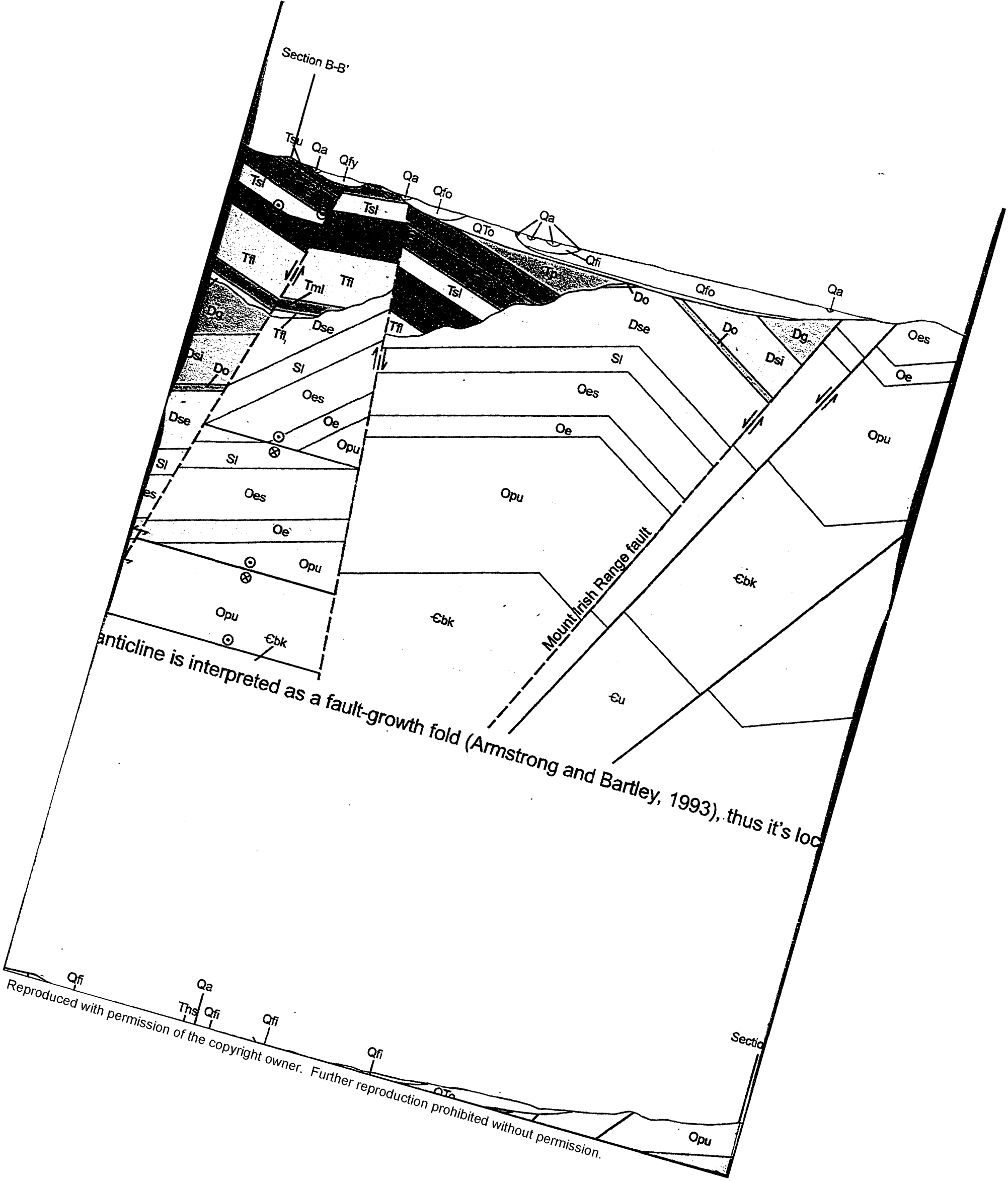

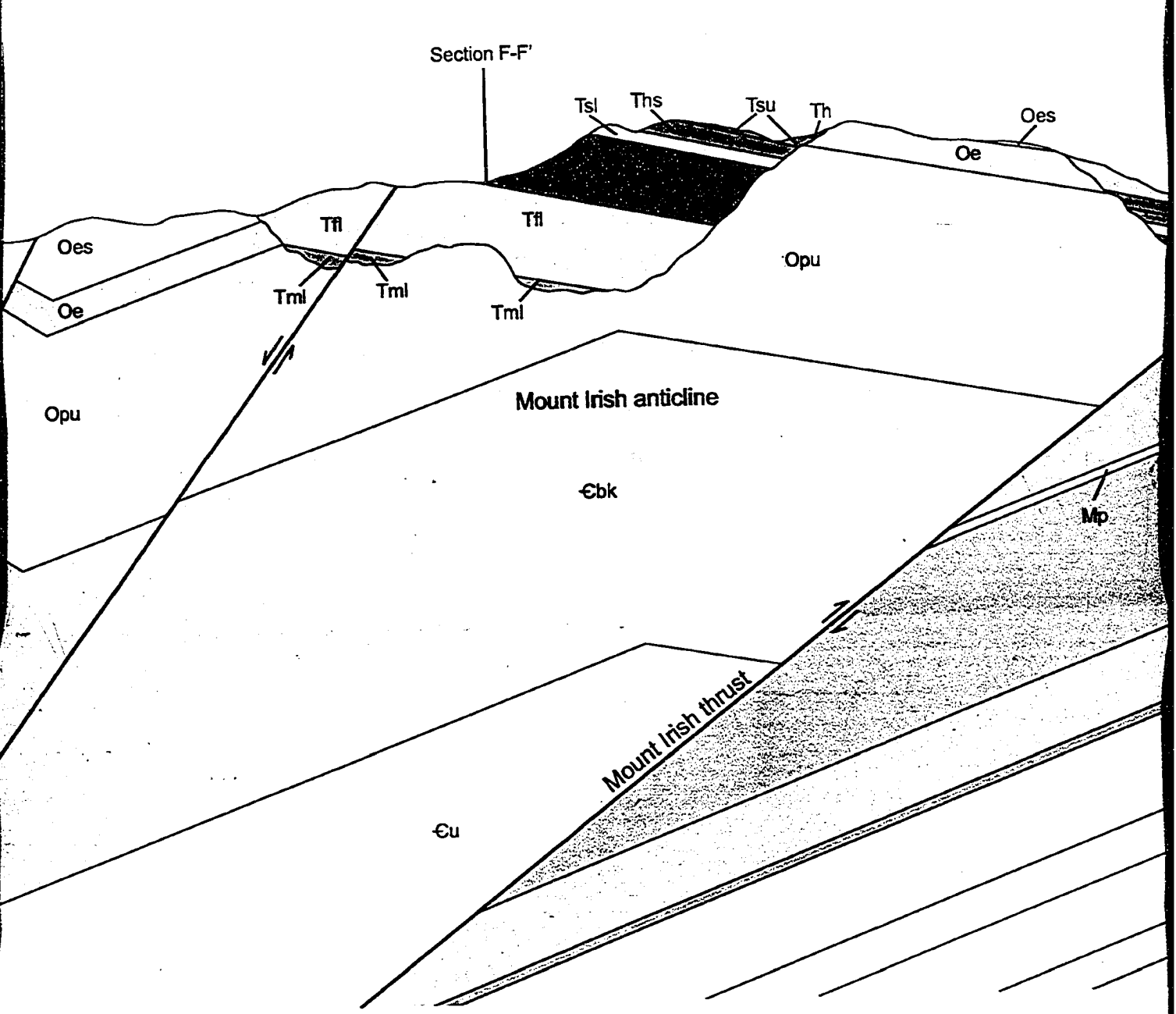

thus it's location does not correspond to a fault bend.

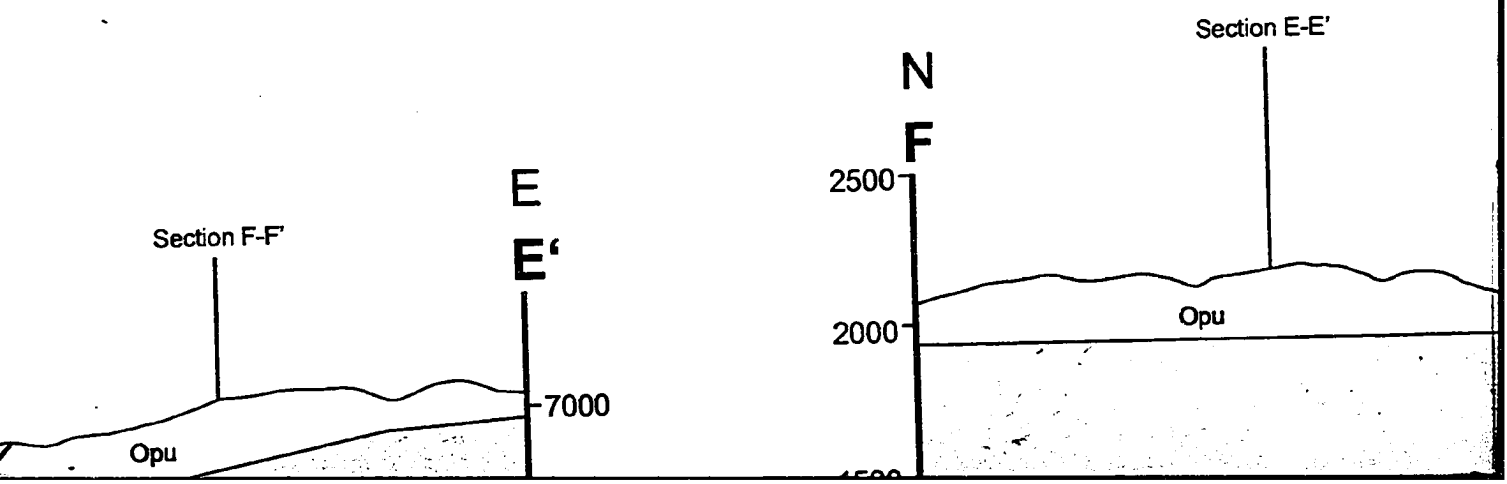

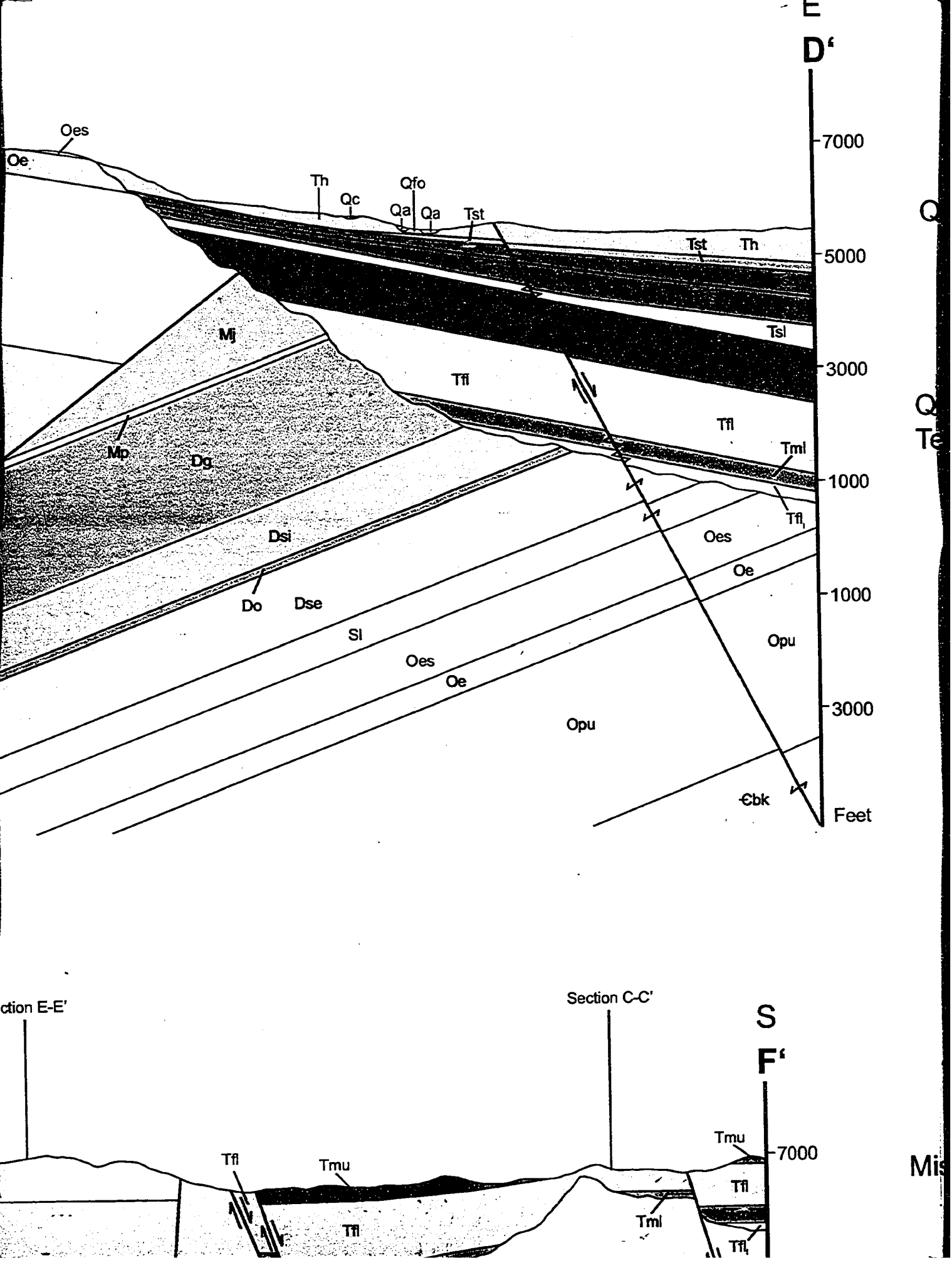

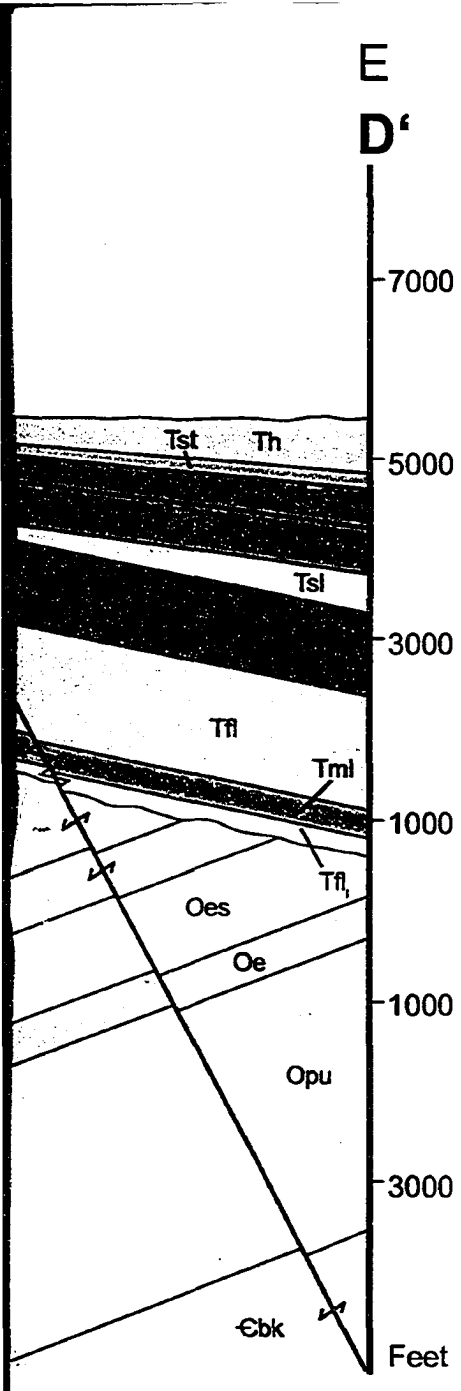

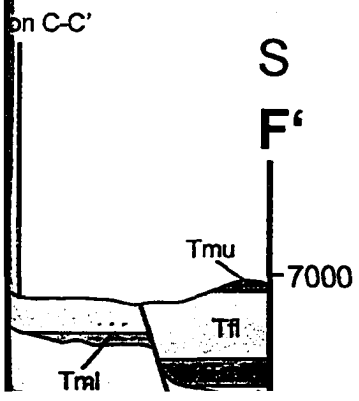

KEY

Quaternary	Qa	Alluvium
	Qc	Colluvium
	Qfy	Fan young
	Qfi	Intermediate fan
	Qfo	Older fan
Quaternary/ Tertiary	QTo	Older fan gravels
	Th	Hiko Tuff
	Tp	Paharangat Tuff
		Shingle Pass Tuff (Upper)
		Tuff of Hancock Summit
Tertiary	Tsl	Shingle Pass Tuff (Lower)
		Monotony Tuff (Upper)
	Tfl	Lacustrine limestone and conglomerate
		Monotony Tuff (Lower)
	Tfl1	Lacustrine limestone and conglomerate (Lower)
Mississippian	Mj	Joana Limestone
		West Range Limestone/

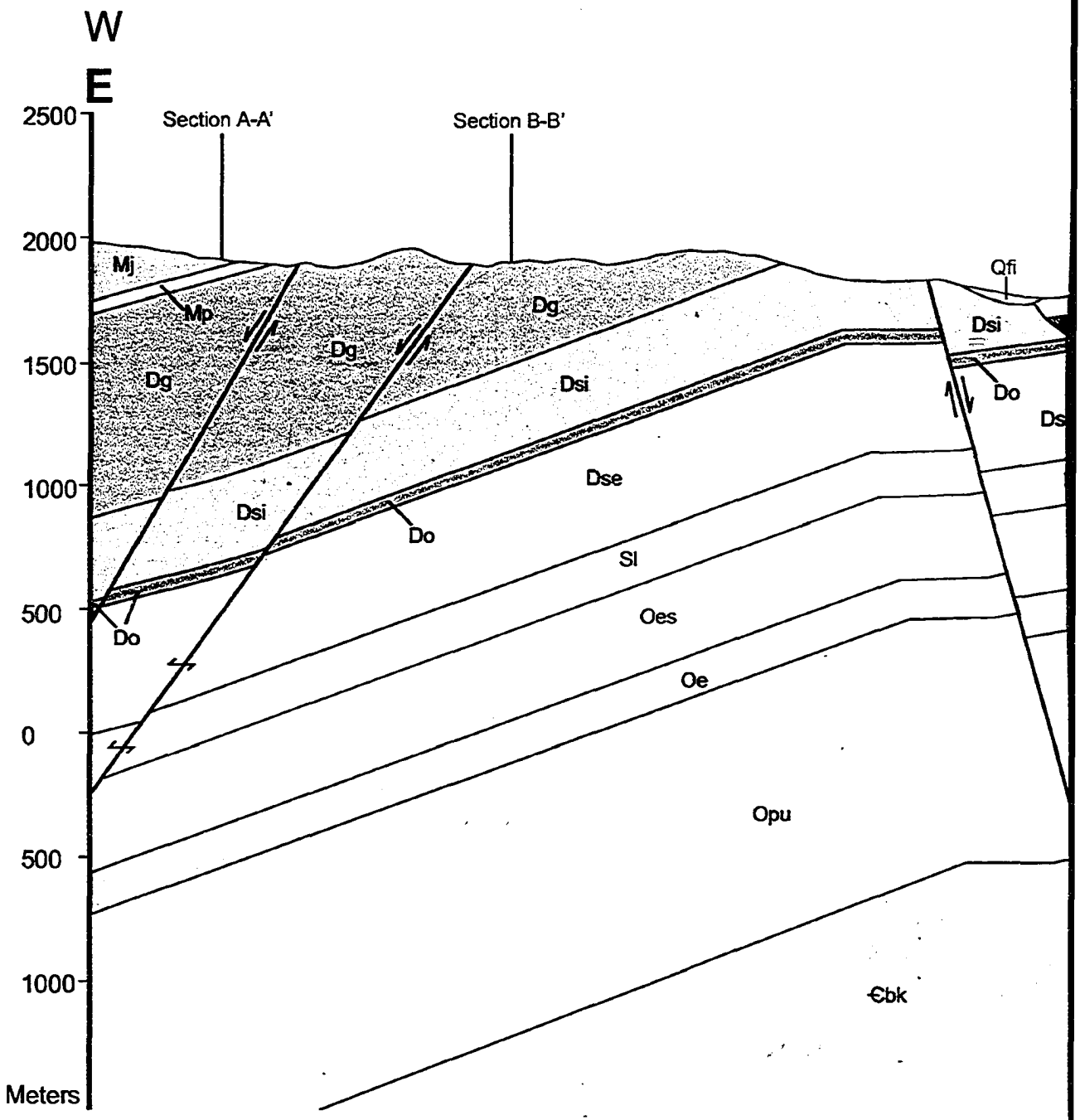

e. Deformed state cross-section E-E'. Apparent thicknesses were u
strike of the map units in that area.

Supplement to:

Bidgoli, T.S., 2005, The role of transverse faults in Great Basin ex
faults or N-S extension [M.S. thesis]: Las Vegas, University o

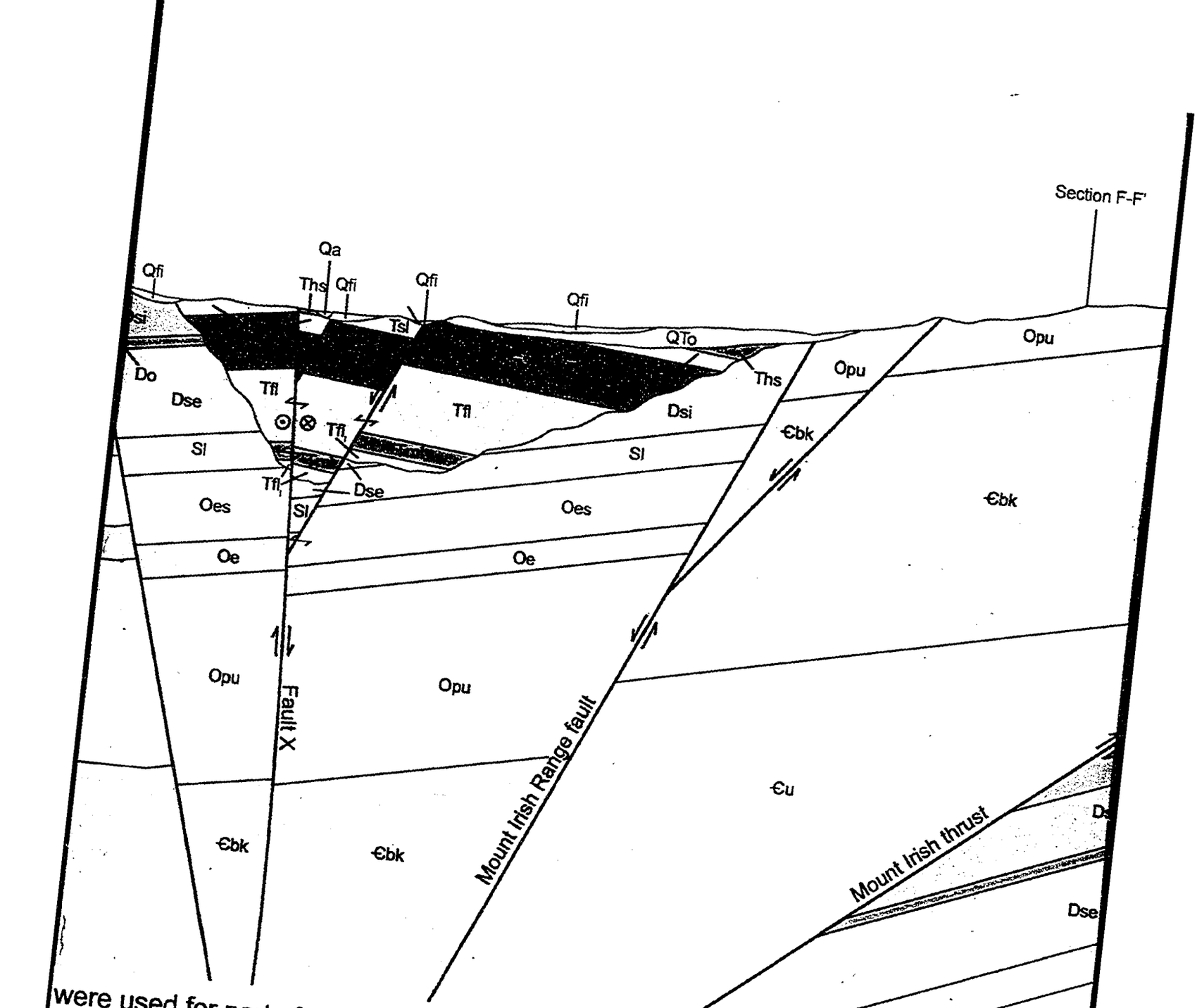

were used for part of the cross section west of fault "X" because the section line is para

sin extension: Transfer
rsity of Nevada, 109 p.

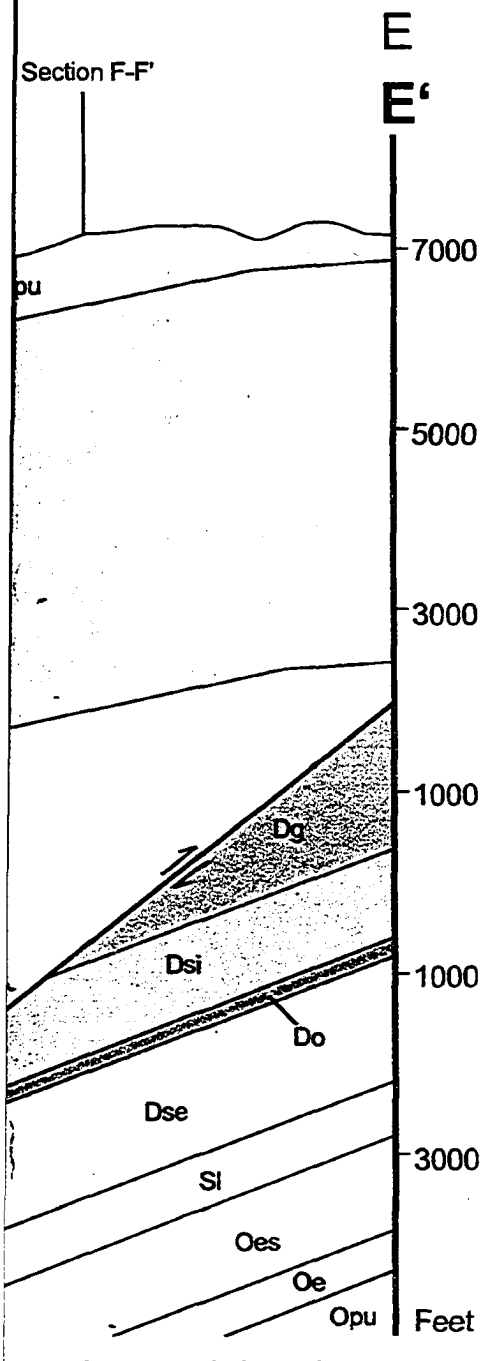

line is parallel to the

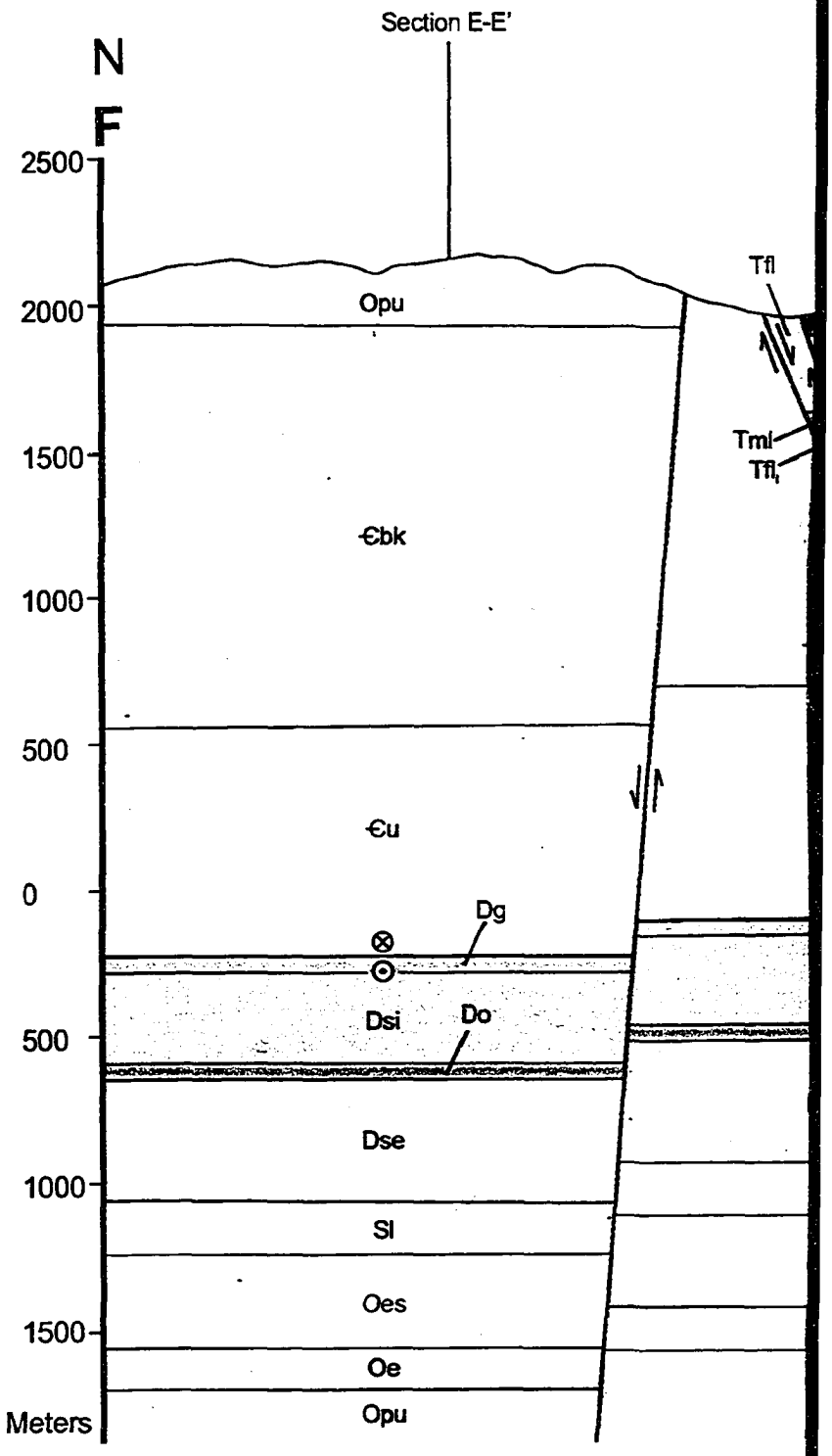

f. Deformed state cross-section F-F'. Ap
cross section because the section line is

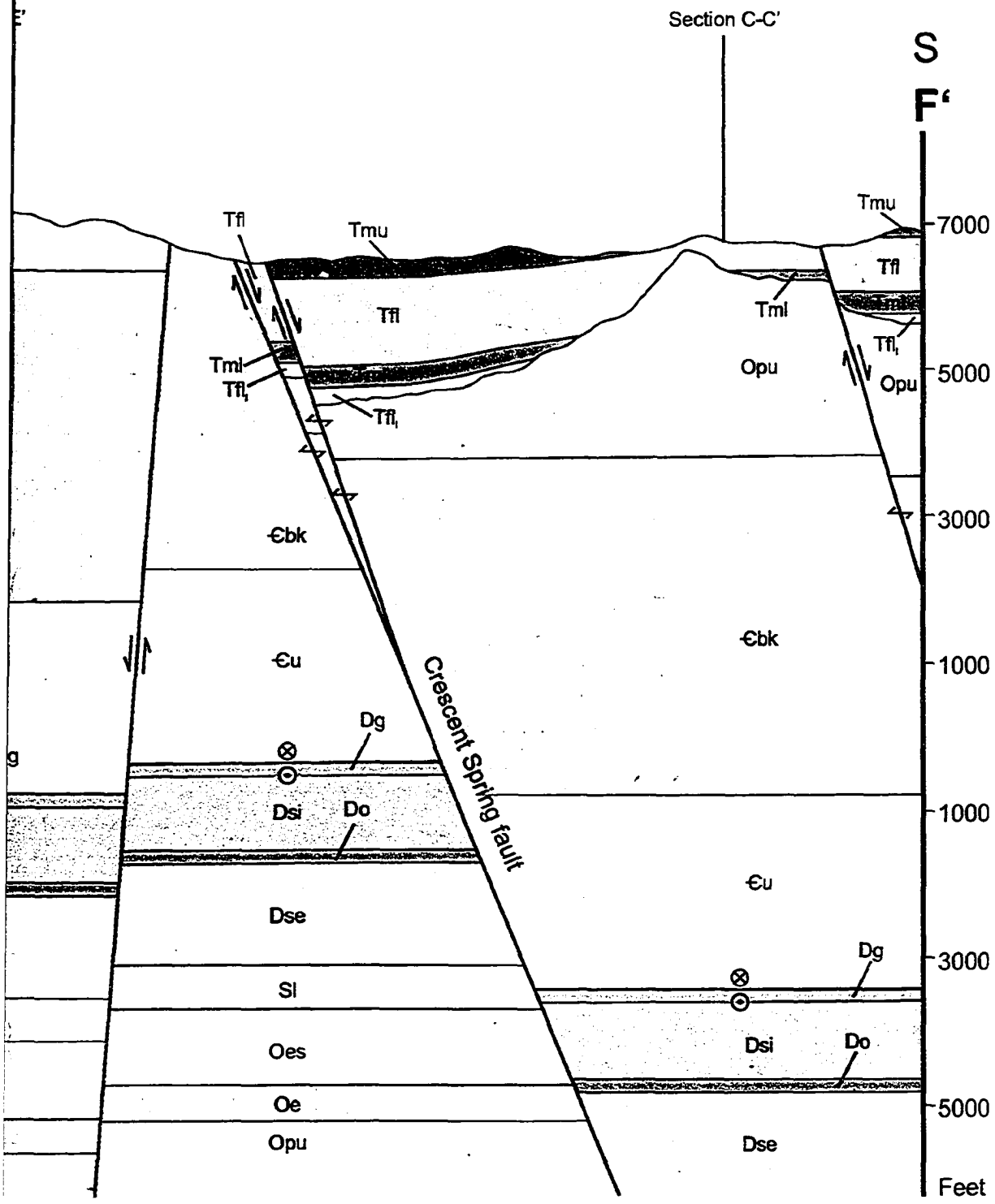

s-section F-F'. Apparent thicknesses were used to construct this
the section line is parallel to the strike of the map units.

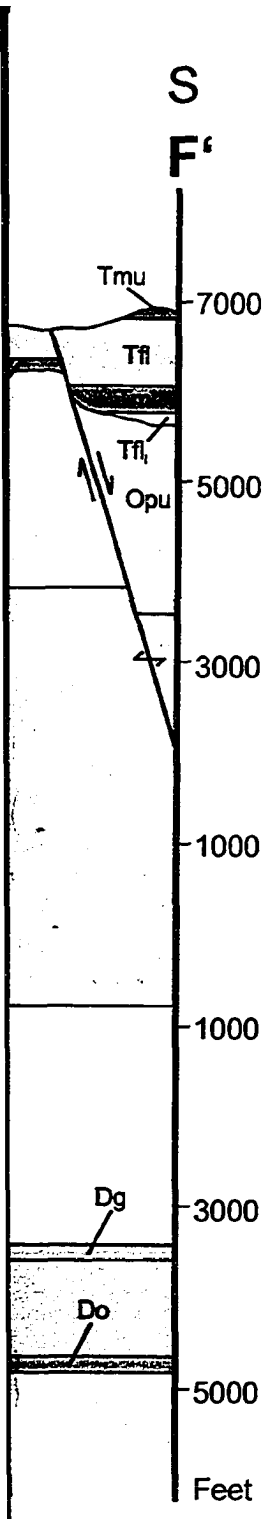

truct this

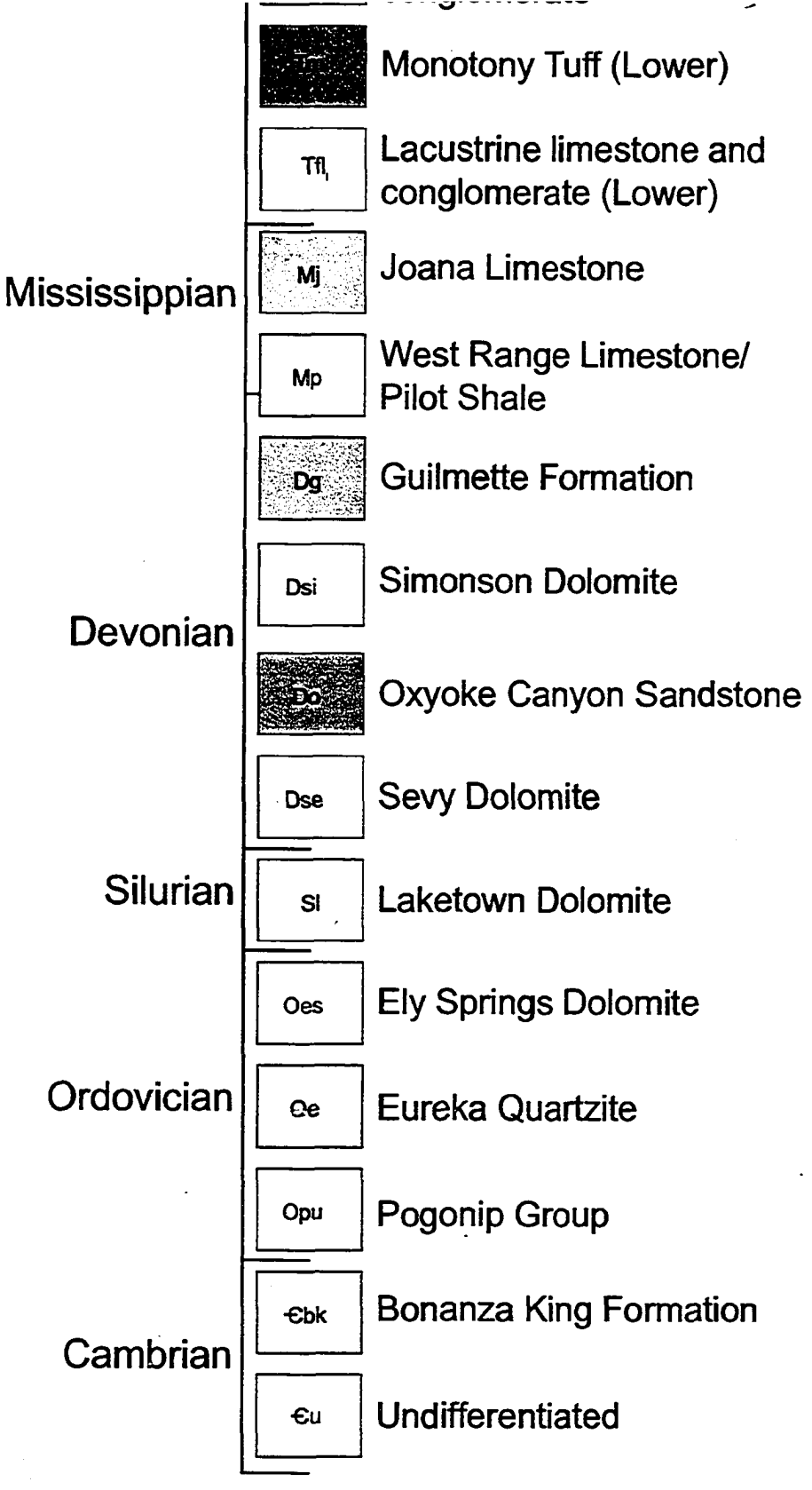

No Vertical Exaggeration